63

GUIDE TO PROCEDURES FOR ESTIMATING THE LIGHTNING PERFORMANCE OF TRANSMISSION LINES

Working Group 01 (Lightning)
of
Study Committee 33 (Overvoltages and Insulation Co-ordination)

October 1991

FOREWORD

During the past six years preparation of this report has been the major topic of discussion within Working Group 33.01 "Lightning", of Study Committee 33 "Overvoltages and Insulation Co-ordination" of CIGRE. The work presented in this document represents a consolidation of much of the analyses carried out within this Working Group over the last 10 years. The document itself has been reviewed extensively by the Working Group and represents the collective opinion of the members. At the time of preparation of this report, the members of the Working Group included the following:

A Eriksson	CH (Convenor)
L Dellera	IT (Secretary)
G Baldo	IT
C H Bouquegneau	BE
M Darveniza	AU
J Elovaara	FI
E Garbagnati	IT
C Gary	FR
I Grant	US
A Hileman	US
R Houlgate	GB
J Huse	NO
W Janischewskyj	CA
T Kawamura	JP
F Popolansky	CS
F Rühling	DE
K-H Weck	DE

The report itself was prepared by a specific editing team, in which the principal authors were:

A Eriksson	(Convenor)
L Dellera	
J Elovaara	
A Hileman	
R Houlgate	
J Huse	
K-H Weck	

CONTENTS

GUIDE TO PROCEDURES FOR ESTIMATING THE LIGHTNING PERFORMANCE OF TRANSMISSION LINES

by

Working Group 33.01 (Lightning)

1. INTRODUCTION

The primary aim of this guide is to apply modern knowledge about various aspects of the lightning discharge, including the striking process, the discharge parameters and the overvoltage disturbance mechanisms, as well as the related transmission line overvoltage response, in a set of practical engineering procedures, whereby the expected lightning performance of a line may be estimated with a reasonable degree of confidence.

The principal objective is the determination of the transmission line total outage rate due to lightning disturbances taking account both of backflashovers and shielding penetration flashovers. In order to maintain a simplified level of approach however, multiple-circuit/multi-phase flashovers are not considered in detail. The aim is to present the background understanding and modelling principles rather than extensively detailed or complex analytical procedures and thus discussion has been mainly confined to single-circuit flashovers.

Since a generalised approach is followed in presenting the overall modelling concepts involved, these guidelines may also readily be applied in addition to outage-rate calculations, to estimation of the incoming overvoltage surges into stations for station insulation co-ordination purposes, subject to the specific simplifications included. The work consolidated in this document has developed over about a 10-year period of activity within Working Group 33-01 (Lightning), and has also involved active collaboration with several other working groups, especially 33-06 and 33-07. In addition, informal co-operation has been maintained with the corresponding IEEE working group for the lightning performance of transmission lines, in order to ensure a consistent exchange of information.

Over the years, many lightning performance estimation procedures have in fact been presented in the technical literature. In many instances, however, such procedures have been based on certain simplifications or assumptions about the characteristics of the lightning disturbance process, which have since been established to have been inaccurate or incomplete due to the relative state of knowledge available at those times.

In certain instances, such published procedures have also been accompanied with comparative data on observed performance of sample lines, usually demonstrating good agreement with calculation, or, more particularly, such calculation procedures have included empirical adjustment of various constants such that good agreement with observation is achieved. In most such cases therefore, a measure of mutual compensation of various errors is present in such empirically adjusted estimation procedures.

The inclusion of such errors may still allow effective application of such calculations to lines of the type employed in the original empirical derivation, but leaves the calculations fundamentally inconsistent with contemporary knowledge about lightning overvoltage mechanisms.

Accordingly a basic objective within this guide is to avoid as far as possible any such empiricism and especially any such mutually self-compensating errors. Each important aspect of the lightning process, or the corresponding overvoltage and line-response mechanisms, will thus be dealt with relatively rigorously and independently. In each case, the relative state of modern understanding concerning that particular aspect will first be reviewed, leading to the presentation of appropriate engineering simplifications and approximations whereby that aspect may be effectively represented in practice. Wherever possible, appropriate sources of data and suitable substantiations in the modern literature will also be cited. Chapters 2, 3 and 4 are thus concerned with presenting the main background information on lightning climatology and on the parameters of the discharge - including the important statistical aspects - together with modern understanding of the lightning striking process and the related implications for transmission line shielding analyses.

A particular aim here is to avoid the subjectivity of several contemporary approaches - whereby "standard" but arbitrarily chosen "worst-case" lightning parameters (eg 300 kA strokes with 0.6 μs fronts) are specified for calculation purposes, but which often bear little relation to reality. The aim is rather to provide sufficient information concerning the practical range of lightning parameters and the relative stochastics of occurrence, such that calculations may be more objective and more realistically based - leading to more cost-effective designs.

Chapter 5 is a central chapter to the guide and comprises a review of modern modelling concepts. It is particularly in this area that previous estimation procedures have included empirical assumptions, or simplifications, which are not in line with modern understanding. Each important aspect of transmission line modelling is dealt with independently, involving a short review of the current knowledge, (backed up by the appropriate literature - including several Electra and CIGRE papers which have been published in the course of this work), together with presentation of suitable engineering representations which have proved convenient and effective in modern calculations.

Aspects dealt with thus include multi-conductor systems, tower modelling, earth electrode impulse response, non-standard lightning impulse insulation strength representation and impulse corona response.

Chapter 6 is essentially a tutorial chapter, in which the backflash mechanism is outlined, taking account, wherever appropriate, of the parameters and modelling aspects presented in the preceding chapters. The level of approach is aimed especially at simplified practical engineering calculations and includes simplified procedures for determining the incoming overvoltages to stations.

Throughout this document, the priority is to guide engineers toward appropriate simplifications, taking correct account of the relative sensitivities

involved, whereby practical calculations may be facilitated, and where a degree of accuracy in estimation suitable for normal engineering applications may reasonably be expected. In addition however, an attempt has been made to provide sufficient detail, including also the appropriate references, such that those engineers wishing to carry out more sophisticated dynamic computations may also be suitably guided as to the choice of reference parameters and representation of the important interrelated physical processes.

Concurrent with the preparation of this guide document, Working Group 33-01 also initiated a program for assembling representative practical transmission line lightning performance data, with a view to carrying out a series of comparative calculations, both simplified and sophisticated, based upon the information and procedures presented in this guide. The overall aim of this latter phase of the work is to demonstrate the validity of the general approach and the relative sensitivity of several of the modelling aspects involved. Sample results are included in Chapter 6 for illustrative purposes. Completion of these analyses would take several years however, and such results will thus only be available at a later stage.

By way of a guide to this report, Figure 1 provides a simple flow-diagram which illustrates the principal steps that could be followed in carrying out a simplified estimation of the total outage rate of a transmission line due to lightning and shows the main relationships to the various sections of the report.

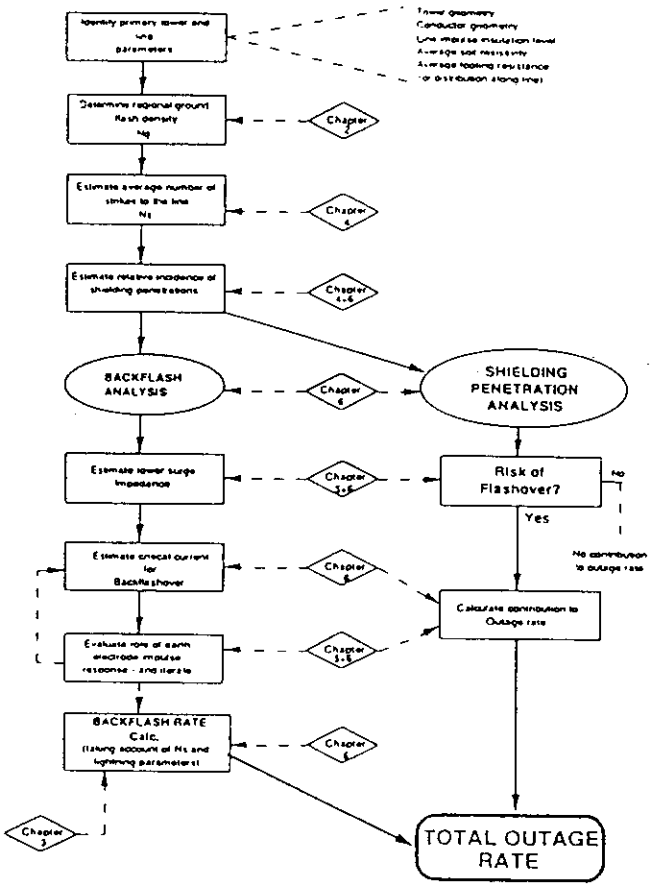

Fig 1 - Steps in simplified estimation of the total lightning outage rate for a transmission line (in relation to the chapters of this report).

2. LIGHTNING CLIMATOLOGY

2.1 Introduction

The phenomenology of lightning involves the frequency of lightning flashes observed over large spatial and time scales - including determination of the maximum and average flashing rates per unit area, as well as variations in flash characteristics with location, time of year, and storm type. Accumulation and consolidation of such data allows description of the lightning climatology for any particular region of engineering concern. The aim is to relate these data both to past observations and to predictions of the lightning performance of power systems (eg. [1,2]).

The purpose of this brief review is to summarise the broad range of observation techniques currently used, and to note the possible lightning climatological data available for practical calculation purposes.

In most engineering applications where lightning disturbances may be of importance, it is usually sufficient (if not unavoidable due to the lack of better data), to base regional climatology upon average quantities. However, since thunderstorm occurrence and lightning incidence are usually also stochastic in character, it is necessary to establish such average indices (and preferably their dispersion as well), over comparatively long periods of analysis. This in turn frequently presents problems of reliable measurement and consistent long- term data acquisition.

The extent to which a meaningful lightning climatology may thus be available for any particular region (i.e. for engineering purposes), is therefore dependent upon the nature and availability of useful data. At present, this varies considerably throughout the various regions of the world.

2.2 Measurement Possibilities

Historically, most of the available information on lightning characteristics has been obtained from localised ground-based observations. It has only been over the past 10-15 years, with the advent of satellite observations, that preliminary global data have been acquired which illustrate diurnal, latitudinal and seasonal variations in lightning activity across the world [3].

Such data are still rudimentary - due to limitations of spatial resolution and the sensitivity of the optical sensors generally employed. In addition, measurements of this type have as yet only been carried out over a few seasons. Nevertheless, preliminary trends may be identified [4]:

- the majority of global thunderstorm activity is concentrated over the land areas (subject to local and seasonal variations)

- irrespective of season, global lightning activity generally peaks over the late afternoon to dusk period (local times).

- there is a pronounced latitudinal variation in global activity, as a function of season, peaking over the respective regional summer months, but with significant levels of activity still being observed in winter regions.

- analysis of lightning flashing rates over the year indicate a global average rate lying in the range of

50/100 up to about 300 flashes per second, depending upon whether optical or radio-based methods of satellite observation were employed.

2.3 Ground-based observations

In general, the majority of lightning flashes are intracloud, and only a relatively small proportion of flashes reach the ground. Since most engineering problems associated with lightning relate to ground flashes, the latter have been the principal focus of ground-based observations - and are also the main concern of this document. It is sufficient therefore, to note that the ratio of cloud to ground flashes, N_c/N_g, varies considerably over the globe - ranging from a high of over 6 in the tropics, to about 2 in near-polar latitudes [5].

The primary requirement in most engineering analyses is the number of lightning strikes per unit time per unit area, or regional ground flash density (usually expressed as an annual average, N_g). Several important alternative bases of observation have been, or are currently applied in characterising regional ground flash activity:

2.3.1 Thunderstorm day (keraunic level) (T_d)

This is still perhaps the most widely available index of average regional lightning activity (with data having traditionally been assembled in many parts of the world for many years). Although of limited engineering value due to the poor correlation between the occurrence of storms and the actual regional ground flash density, when no other data are available, the keraunic level may be used as a guide to the relative activity in any particular region (as presented in 2.3.3 below).

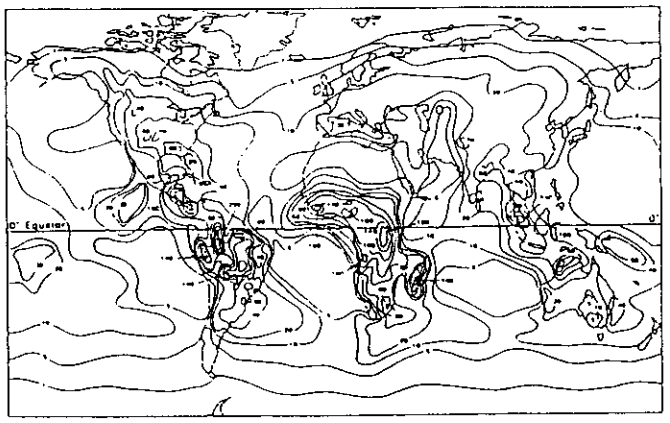

Fig 2 - World map of keraunic level (World Meteorogical Organisation, 1956).

Figure 2 illustrates the global distribution of the annual number of thunderstorm days, [6], while Figure 3 demonstrates how rigorous monitoring of this particular parameter may be applied to produce a detailed map for a specific region [7].

2.3.2 Thunderstorm duration (T_h)

Thunderstorm duration data have also been acquired in several regions of the world (eg [8]). While broad variations are still evident (i.e. statistical, seasonal and regional), comparative analyses indicate that there is a positive correlation between storm duration h (hours) and ground flash density - which can be approximated as [9,10];

$$N_g \approx 0.05\ h \quad \text{flashes km}^{-2}\ \text{year}^{-1}$$

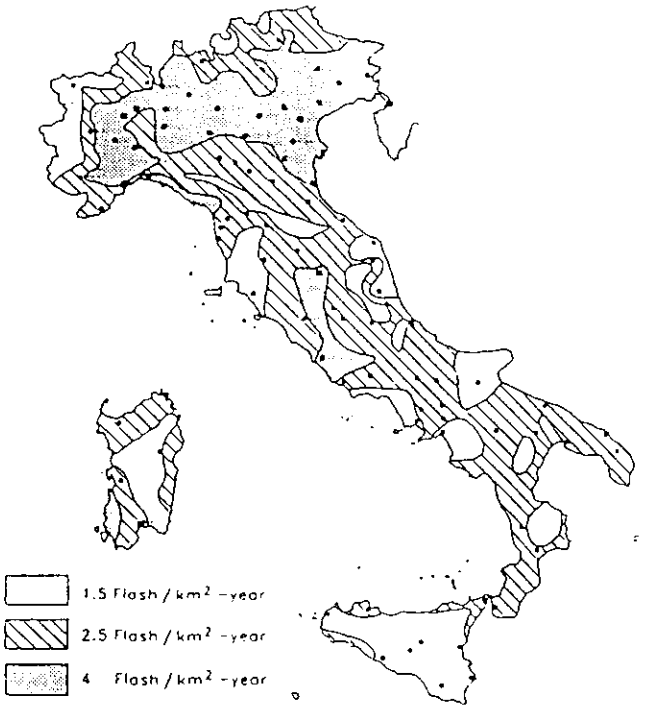

Fig 3 - Annual lightning flash density of Italy.

Figure 4 illustrates application of thunderstorm duration data to the derivation of regional variations in approximate ground flash density over the United States [10].

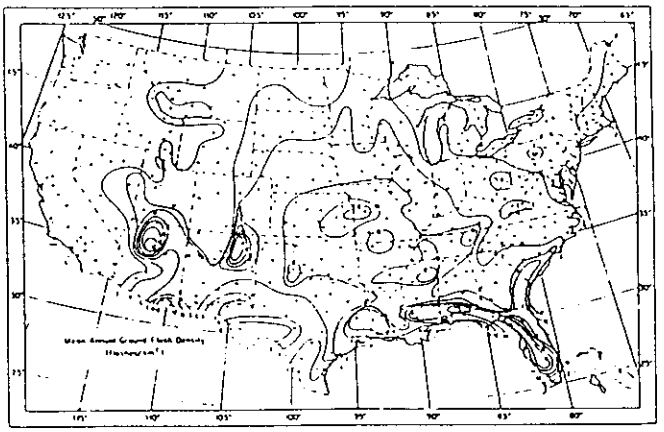

Fig 4 - USA annual lightning flash density estimates based on thunderstorm annual duration [10].

2.3.3 Lightning Flash Counters

These instruments have had a long history of development, calibration and evaluation, notably within the CIGRE forum [11]. Until recently, most of the specific information available on ground flash density has been acquired through the application of flash counters in various countries. Provided a rigorous basis of calibration and ground flash discrimination is available, flash counters may be readily applied over a suitable period of time to determine regional variations in average ground flash density and even its dispersion, if sufficient data are collected [12,13].

Figure 5 illustrates the collated results of such measurements, as applied over a large scale, and over more than 10 years, in South Africa [14]. Regional variations in N_g from less than 1 to more than 12 flashes /km^2/yr, are apparent on a comparatively small geographic scale. Analysis of the dispersion in annual observations of N_g at any one location, indicates that this may be approximated by a normal distribution having an average standard deviation given by [15].

$$S_{ng} \approx 0.32\ N_g$$

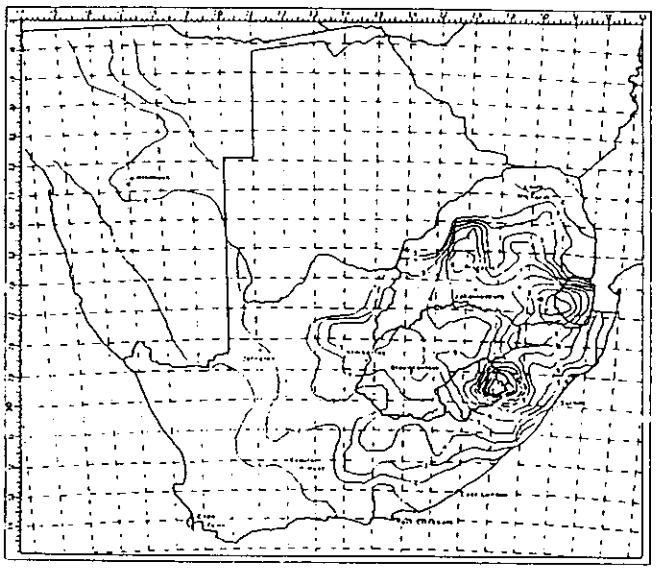

Fig 5 - Regional variations in mean lightning ground flash density in South Africa (1975 - 1986).

Analysis of the correlations amongst such annual registrations of thunderstorm day, T_d, and regional ground flash density N_g, drawn from some 60 stations distributed over South Africa, over a period of 6 years, yields the approximation [12];

$$N_g = 0.04\ T_d^{1.25}$$

In the absence of directly measured ground flash density data, this relation may be used to estimate N_g from available thunderstorm-day data.

2.3.4. Lightning Location Systems

The development of automatic lightning location systems over the past 10 years has greatly facilitated ground-based analyses of lightning characteristics and activity. Two main types are currently being applied to such measurements;

- gated wideband magnetic direction-finding systems
- time-of-arrival lightning location systems

Although still requiring careful calibration of their discrimination characteristics, such systems have a long effective range (up to about 400 km), and, when combined into a network of stations with on-line processing and data acquisition, are capable of providing extensive information over large areas, including both regional and seasonal variations in lightning characteristics [16,17].

Preliminary comparisons amongst data acquired from such location systems in various parts of the world (including Canada, Norway, US East Coast, Japan and South Africa) have indicated several consistent trends in lightning characteristics [18,19];

- the majority of ground flashes are of negative polarity (about 90% averaged over a year)

- regions experiencing winter thunderstorms also experience a pronounced increase in the occurrence of positive ground flashes during winter (typically over 50 % of all ground flashes during such storm periods, as in [17]).

- negative ground flashes are more often of multi-stroke character, but with a tendency toward more single-stroke flashes during the winter months

- positive flashes are predominantly single-stroke

- the distributions of recorded peak magnetic field amplitudes appear to be similar in various parts of the world. When calibrated against the median of the CIGRE reference current peak amplitude distribution [20], only about 5% or less of negative flashes involve currents in excess of 100 kA. Positive flashes appear to involve higher amplitude peak currents (median value around 45 kA), with a small prospect still of attaining peak values higher than about 200 kA (approx. 1%).

Automatic lightning location systems also allow analysis of short-term variations in ground-flash flashing rates, over areas of immediate storm activity [21]. Over the short term (5 - 30 minutes), in areas having an N_g range of 6 - 12 km^2/year, mean flashing rates of the order of 4 - 10 per 1000 sq.km/min could typically be encountered across local areas of about 1000 - 2000 sq.km. Over longer periods of observation (ie. typical storm durations of 1 - 3 hours), and over larger areas, (1500 - 4000 sq.km), the average flashing rates could reduce to about 0,5 per 1000 sq.km/min. Comparable observations of average intervals between flashes within local areas have also been recorded earlier, using simpler methods of registration [22].

As a general comment from an engineering point of view, the prospects of any one particular square kilometre being struck even once, in the vicinity of an active storm, are relatively low, (typically around 1-10%/storm in areas with N_g in the range of 6 -12).

2.4 Availability of lightning climatological data

Based on the information reported to WG 33-01, relatively detailed lightning ground flash density data have been acquired, or are currently still being accumulated, in the countries listed in the following table 1:

	Flash Counters	Location Systems
Argentina	X	
Australia (Queensland)	X	X
Austria	X	
Belgium	X	
Brazil (Minas Gerais)	X	X
Canada	X	X
Czechoslovakia	X	
England	X	X
Federal Republic of Germany	X	X
France	X	
Finland	X	X
Holland	X	X
Italy	X	
Japan	X	X
Mexico	X	
Norway	X	X
Rumania	X	
South Africa	X	X
Sweden	X	
Switzerland		X
USA (East Coast especially)	X	X
USSR (selected regions)	X	

The periods of time over which such data have been assembled, however, and the corresponding areas of geographic coverage, vary considerably from case to case.

3. LIGHTNING PARAMETERS

3.1 Introduction

The lightning flash is categorised by the polarity of the cloud charge and the direction of propagation of the flash leader. Hence there are four categories of lightning flash to ground in which the developed leader is followed by a return-stroke current impulse, namely:

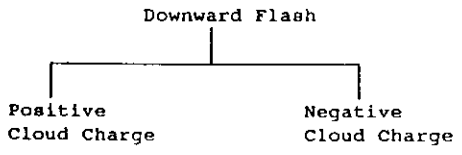

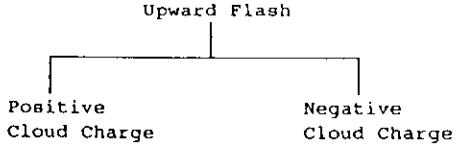

On average, [20] at least 90% of downward flashes are of negative polarity, with some 45-55% of flashes comprising only one stroke. Multiple stroke flashes seldom involve more than 10 strokes (less than 5%), and generally average three strokes per flash, typically at intervals of less than 50 ms per stroke.

Upward flashes occur mainly from very tall structures or mountain-top installations. The majority of transmission line structures are of only moderate height (typically less than 60-100 m) and will not in general be subject to upward flashes [32]. This report therefore concentrates mainly on downward flashes and although it is recognised that positive ground flashes are experienced in varying degrees (typically 10% or less) in different climatic regions of the world and seasons of the year, the report largely focuses upon the more prevalent negative discharge.

Available data on lightning parameters and waveshape characteristics have been previously reported [20]. This report concentrates upon those parameters particularly required for lightning performance studies, and updates earlier information where appropriate.

The lightning flash may contain several lightning strokes whereby the first stepped-leader/return-stroke sequence is followed in short succession by a series of one or more subsequent strokes. Each stroke comprises a dart-leader and return-stroke sequence that generally follows the breakdown path of the first stroke. Lightning protection systems for transmission lines must therefore be capable of withstanding the effects of a series of lightning strokes to the same location within a short period of time. Each lightning stroke is considered an ideal current source of infinite source impedance and the parameters contained within the incident impulse current waveshape determine the transmission network response. These waveshape-parameters include the peak-current amplitude (crest value), time to crest, steepness and duration. Also of importance are the polarity, time interval and number of incident strokes within each lightning flash.

3.2 Waveshapes

The waveshape of negative downward stroke discharges measured at San Salvatore have previously been analyzed and comprehensively summarised [20,23]. In the earlier analysis, the front characteristics were defined in terms of the maximum rate of rise of current. The wavefront characteristics were studied in more detail in the later publication, and several additional parameters were introduced as defined in Figure 6. Note that the statistical parameters based on the 10% intercepts will consistently be less reliable than the 30% values, due to the use of a 2kA reference level for measurements. For engineering purposes therefore, the 30% based parameters should generally be used, as indicated in the following sections. The frequency distribution of these additional impulse front parameters is summarised in Table 2, assuming a log-normal distribution of variables, where the general equation for the probability density for any particular parameter x is given by

$$f(x) = \frac{1}{(2\pi)^{\frac{1}{2}}\,\beta x}\, e^{-(z^2/2)}$$

where $$z = \frac{\ln (x/M)}{\beta}$$

M is the median parameter value and β is the slope parameter or logarithmic standard deviation (base e). The mean value of any parameter may then be expressed as

$$\mu = M \exp (\beta^2/2)$$

For example the median value of the tail is 77.5 μs but the average or mean is 91.5 μs.

Table 2

Parameters of Log-Normal Distribution

for Negative Downward Flashes

Parameter	First Stroke		Subsequent Stroke	
	M	ß	M	ß
Front, μS				
$t_{d10} = T_{10}/0.8$	5.63	0.576	0.75	0.921
$t_{d30} = T_{30}/0.6$	3.83	0.553	0.67	1.013
Steepness, kA/μS				
S_m, Maximum	24.3	0.599	39.9	0.852
S_{10}, at 10%	2.6	0.921	18.9	1.404
$S_{10/90}$, 10-90%	5.0	0.645	15.4	0.944
$S_{30/90}$, 30-90%	7.2	0.622	20.1	0.967
Crest Current, kA				
I_I, Initial	27.7	0.461	11.8	0.530
I_F, Final	31.1	0.484	12.3	0.530
Initial/Final	0.9	0.230	0.9	0.207
Tail, t_h, μS	77.5	0.577	30.2	0.933
Charge, Q_I, C	4.65	0.882	0.938	0.882
$\int i^2\,dt$, $(kA)^2s$	0.057	1.373	0.0055	1.366
Inter Stroke Interval, ms			35	1.066

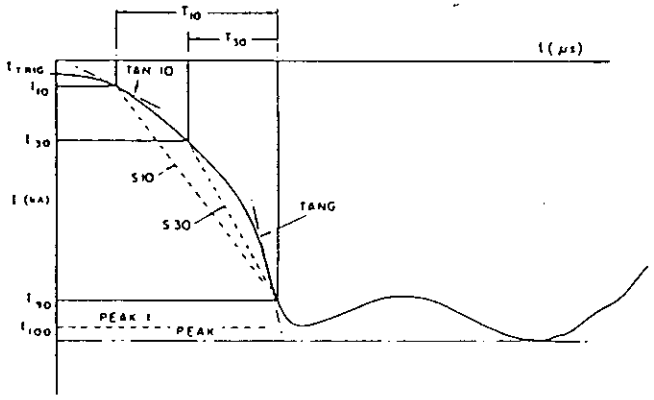

Fig 6 - Definition of front parameters for a lightning current impulse of negative polarity.

Normalisation of digitised records of first and subsequent stroke discharges have yielded the median impulse current characteristics shown in Fig 7. The median wave tails (times to half value) associated with these events are 77.5 μs (first stroke) and 30.2 μs (subsequent stroke), respectively.

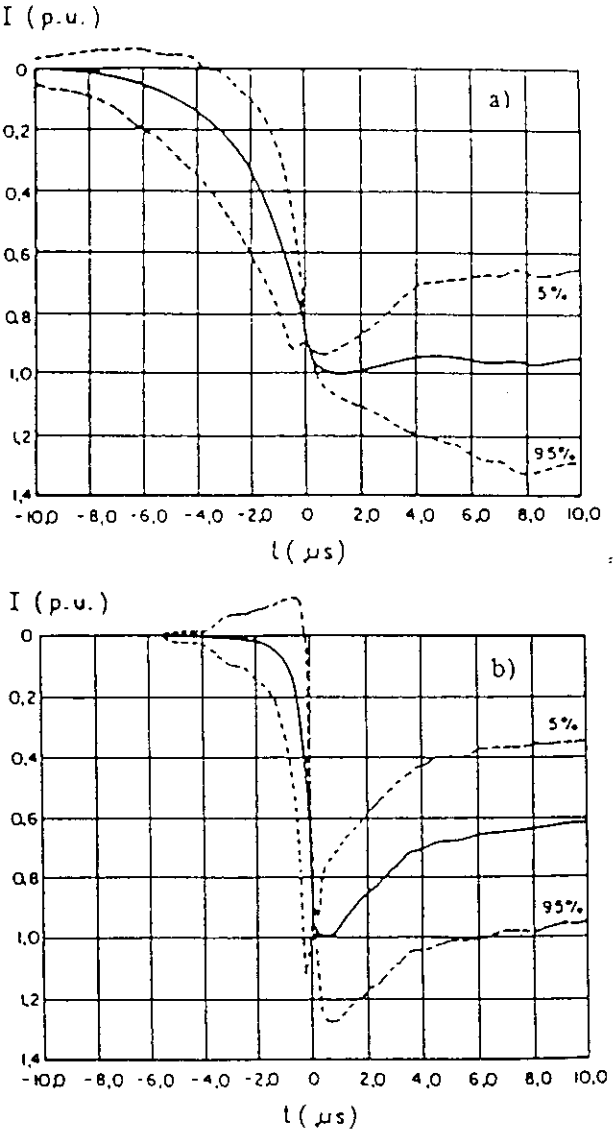

Fig 7 - Median impulse current front shapes.

a) First strokes

b) Subsequent strokes

The waveshapes of positive stroke discharges are all derived from limited measurements of single-stroke upward flashes [23]. Positive peak currents are larger than negative peak currents (see 3.3). The positive impulses, however, are slower than negative impulses with mean time to crest, time to half value and steepness ($^{dI}/_{dt}$) max, of about 22μs, 250 μs and 2.4 kA/μs, respectively.

3.3 Crest Value of Stroke Current

(a) Negative first stroke

The original study of the frequency distribution of peak current amplitudes for negative downward flashes to structures less than 60 m in height, was derived from 338 observations from various regions of the world. [20]. New data from the South African 60 m mast and 11 kV distribution project [12] have been incorporated into the original "global" sample - yielding 408 observations. The resultant frequency distribution is shown in Figure 8 with a median

amplitude of approximately 33 kA. No values within the total sample have exceeded 200 kA and the one percentile level is approximately 130 kA with five strokes exceeding 100 kA.

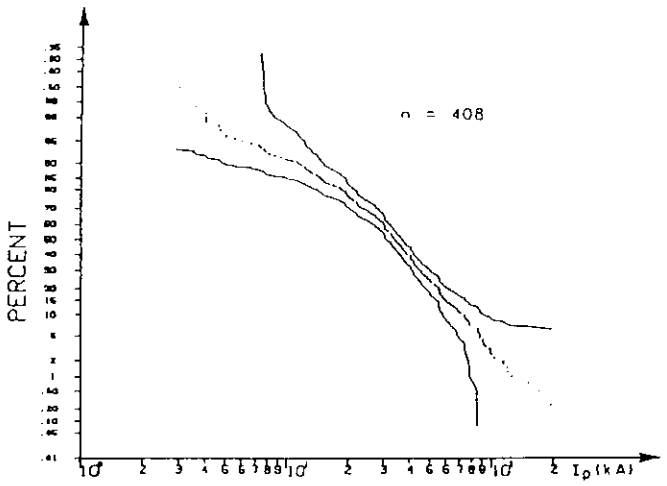

Fig 8 - Cumulative frequency distribution of lightning current amplitudes for negative downward flashes.

The distribution may be represented by a log-normal approximation as defined above, with the following parameters:

$$M = 31.1 \text{ kA}$$

$$\beta = 0.484$$

As previously noted [20], in such a log-normal representation, the measured distribution may be better approximated by two straight lines drawn through the measured data, as shown in Figure 9, that conveniently group the data, approximately, into shielding failure and backflash domains, respectively, and may be expressed in terms of the following log-normal parameters:

Parameter	Shielding Failure Domain (I < 20kA)	Backflash Domain (I > 20kA)
M	61	33.3
β	1.33	0.605

The shielding-failure domain comprises peak current amplitudes less than 20 kA and the backflash domain comprises those currents above 20 kA.

An alternative and simpler representation is that suggested by J G Anderson [24], and adopted by the IEEE [25] where

$$p(I) = \frac{1}{1 + (I/31)^{2.6}}$$

The distribution is shown in Figure 10 and follows the trend of the CIGRE two-line distribution comparatively well, except at the extremes, where the observed confidence limits are in any case quite wide (see Figures 8 and 9).

It is recommended that either of the above forms of distribution is adopted, as convenient for simplified calculation purposes, to represent the distribution of peak-current amplitudes for negative downward flashes in the normal range of structure heights.

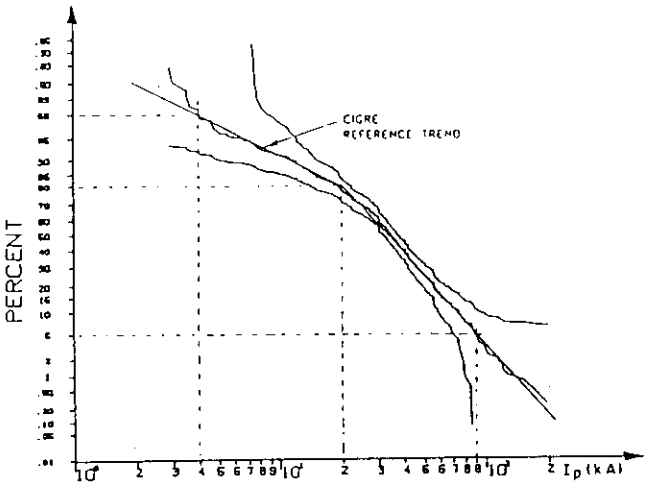

Fig 9 - CIGRE approximation to the measured distribution of negative lightning current amplitudes.

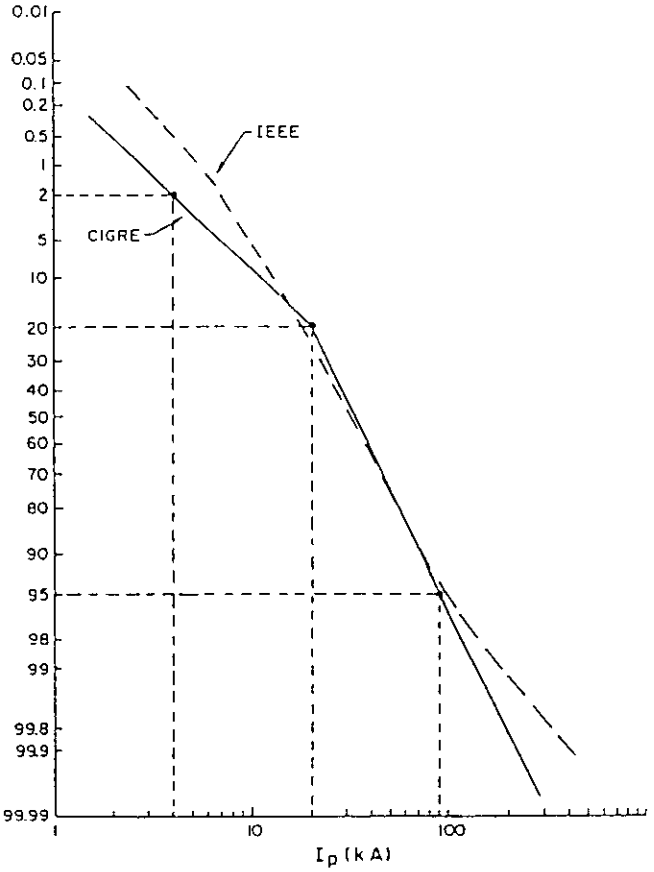

Fig 10 - Reference distributions for negative lightning current amplitudes.

(b) Negative following strokes

In general, there are no correlations between first and subsequent-stroke peak amplitudes, although subsequent strokes tend to be significantly lower in amplitude, attaining on average only about 40% of the first stroke peak.

Within the shielding-failure domain of flash peak currents, however, the available data suggest about a 12% probability of subsequent strokes having larger

amplitudes than the associated first stroke with factors up to 200% having been observed (eg, subsequent stroke of 24 kA for 12 kA first stroke) [26].

No subsequent-stroke amplitudes in excess of 80 kA have been observed within the available sample of records for negative downward flashes. The resultant frequency distribution may be approximated by a log-normal representation with the parameters

M = 12.3 kA

β = 0.53

(c) Positive Strokes

Typically, less than 10% of the total number of lightning flashes to ground are of positive polarity. The limited number of direct lightning current recordings does not permit a clear separation between upward and downward flashes. In consequence there is no comprehensive source of data available on impulse characteristics for positive downward flashes. The combined data base for all positive flashes from Italian and Swiss results [27] is shown in Figure 11 together with the CIGRE reference distribution for negative first strokes. Positive-flash current amplitudes are generally greater than those for the negative distribution. This trend is confirmed in comparative lightning field-change data from several large lightning-location projects [16,18], where the peak signal strengths for positive flashes, except for small discharges, are considerably higher than those for negative flashes. If the return-stroke velocity is similar for both polarities, then the peak currents for positive flashes are typically 1.6 to 2 times the peak currents for negative flashes, for median amplitude signals.

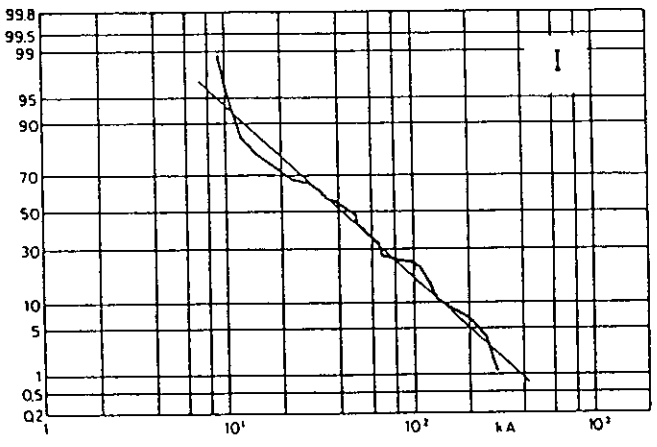

Fig 11 - Example of distribution for positive lightning current. Derived from Italy and Switzerland data.

The proportion of positive to negative flashes is higher in autumn/winter. However, in most regions the majority of all flashes occur during summer months. Until more data become available for the parameters of positive flashes, it is accordingly suggested that these events be disregarded in normal lightning-performance studies. Their relative incidence is generally low enough not to be of major concern, except perhaps on very tall structures (H > 200 m), or in those regions experiencing frequent winter thunderstorms.

3.4 Time to Crest

(a) Negative first stroke

The front durations t_d measured between 2 kA and the first peak of current for negative first strokes are compared below with "front times" derived from T_{10} and T_{30} parameters from Table 2.

First-Stroke Front Duration	% Cases Exceeding Tabulated Value		
	95%	50%	5%
t_d μs	1.8	5.5	18
$t_{d10}=T_{10}/0.8$ μs	2.2	5.6	14
$t_{d30}=T_{30}/0.6$ μs	1.5	3.8	10

Median front durations from t_d and t_{d10} distributions are almost identical although the dispersion is slightly reduced for t_{d10}. The t_{d30} front times are lower because of the generally concave shape of first-stroke current impulses. For practical calculation purposes, it is recommended that the parameter t_{d30} be adopted.

(b) Negative following strokes

Front-times of negative following strokes are generally much shorter than those of first strokes as shown below:

Following-Stroke Front Duration	% Cases Exceeding Tabulated Value		
	95%	50%	5%
t_d μs	0.2	1.1	4.5
$t_{d10}=T_{10}/0.8$ μs	0.1	0.8	3.5
$t_{d30}=T_{30}/0.6$ μs	0.2	0.7	3.0

Smaller disparity between the front-duration distributions indicated above are due to the reduced front concavity of subsequent negative strokes.

For practical calculation purposes, it is recommended that the parameter t_{d30} be adopted.

3.5 Steepness

(a) Negative first stroke

Steepness parameters for negative first strokes are summarised below:

Following-Stroke Front Duration	% Cases Exceeding Tabulated Value		
	95%	50%	5%
$S_{10/90}$ kA μs^{-1}	1.7	5.0	14
$S_{30/90}$ kA μs^{-1}	2.6	7.2	20
S_m kA μs^{-1}	9.1	24	65

$S_{10/90}$ and $S_{30/90}$ may be regarded as average steepness parameters while S_m represents the maximum rate of rise of current on the wavefront. High

values of steepness occur for only short durations of the wavefront, which explains the large difference in average and maximum steepness parameters.

For practical calculation purposes, it is recommended that the parameters $S_{30/90}$ and S_m be adopted.

Steepness parameter distributions may also each be represented by a log-normal approximation (see Table 2).

(b) Negative following strokes

Although the crest values of subsequent strokes are generally lower than first-stroke amplitudes, the respective steepness parameters (in contrast) are significantly higher, and exhibit wider dispersion as shown below.

Following-Stroke Front Duration	% Cases Exceeding Tabulated Value		
	95%	50%	5%
$S_{10/90}$ kA μs^{-1}	3.3	15	72
$S_{30/90}$ kA μs^{-1}	4.1	20	99
S_m kA μs^{-1}	10	40	162

The distributions of the steepness parameters for following strokes are all essentially similar to each other (see Table 2), implying a significantly less pronounced degree of concavity of the wavefront, compared with those of first strokes.

For practical calculation purposes, it is recommended that the parameters $S_{30/90}$ and S_m be adopted.

3.6 Duration (Time to Half Value)

Stroke durations measured at San Salvatore have previously been defined as the time interval between 2 kA on the wavefront and the point on the wavetail where the current amplitude has fallen to 50% of its crest value [20,23]. This data, shown in the table below, is adequate for line-performance studies where the tail of the current impulse is of minor importance.

Stroke Duration t_h	% Cases Exceeding Tabulated Value		
	95%	50%	5%
Negative first stroke	30μs	77.5μs	200μs
Negative following stroke	6.5μs	30.2μs	140μs

3.7 Multiple Strokes

The incidence of multiple-stroke flashes varies considerably both by region and by season of the year. On average, approximately 45% of negative downward flashes contain only one stroke [20], although during winter months the percentage may increase to approximately 80% [18]. The mean number of strokes per flash is 3 and fewer than 5% of downward negative flashes involve more than 10 strokes per flash, typically separated by less than 50 ms between strokes. The inter-stroke time interval may be represented by a log-normal approximation (see Table 2). There does not appear to be a correlation between the inter-stroke time interval and the peak current amplitude of the stroke. The duration of a negative downward flash is represented by a median M of 200 ms and dispersion ß of 0.69.

More than 90% of positive flashes, as observed in lightning-location projects, are single-stroke [18]. The limited number of direct lightning current impulse recordings of positive flashes are all of single strokes [27].

3.8 Correlations and Derived Statistics

In many system lightning-performance studies, the most important lightning waveshape parameters are those relating the wavefront (or steepness) to the peak amplitude.

The observed correlation coefficients between the crest currents and front times and front steepnesses are presented in Table 3. The brackets denote those coefficients which are below the critical values at the five percent level of significance.

Table 3

Correlation Coefficients between Front Parameters and Initial and Final Peak Current Amplitudes

	T_{10}	t_d	S_{10}	$S_{10/90}$	$S_{30/90}$	S_m
First Stroke						
I_I	0.40	0.40	0.47	(0.12)	(0.19)	0.43
I_F	0.33	0.33	0.45	(0.06)	(0.17)	0.38
Subsequent Strokes						
I_F	(0.15)	(0.00)	(0.05)	0.31	0.23	0.56

() denote those coefficients that are below the critical values at the 5% level of significance

Using these correlation coefficients and the statistics presented in Table 2, other statistics which may be useful in lightning performance studies can be derived. The derived statistics for the first and subsequent strokes, presented in Tables 4 and 5, are in terms of the median, M, and the slope parameter or logarithmic standard deviation (base "e"), ß, for the log-normal distribution. These derived statistics are:

1. $t_m = I_F/S_m$ defined as the minimum equivalent front or time-to-crest

2. Conditional distributions of S_m/I_F, t_m/I_F, I_F/t_m, t_d/I_F, and I_F/t_d where, in definition, x/y is the distribution of the random variable x given a specific and constant value of y.

For subsequent strokes (Table 5), the correlation coefficient as per Table 3 between t_d and I_F is zero. Also, the derived correlation coefficient between t_m and I_F is essentially zero. Therefore, the conditional distributions of t_m/I_F, t_d/I_F and I_F/t_F may be taken as equal to the single or marginal distributions of t_m, t_d and I_F respectively.

Table 4

Summarised Parameters of Log-Normal Representation for Characteristics of the First Negative Downward Strokes

Parameter	Range of Application			
	3 ≤ I ≤ 20 kA		I > 20 kA	
	M	ß	M	ß
I_F, Final Crest Current, kA	61.1	1.33	33.3	0.605
S_m, Max Front Steepness, kA/μs	24.3	0.599	24.3	0.599
t_{d30}, Max from 30/90%, μs	3.83	0.553	3.83	0.553
Derived Distribution				
$t_m = I_F/S_m$, Min Eq Front, μs	2.51	1.23	1.37	0.670
$S_m \mid I_F$, Conditional, kA/μs	$12.0\ I_F^{0.171}$	0.554	$6.50\ I_F^{0.376}$	0.554
$t_m \mid I_F$, Conditional, μs	$0.0834\ I_F^{0.828}$	0.554	$0.154\ I_F^{0.624}$	0.554
$I_F \mid t_m$, Conditional, kA	$25.2\ t_m^{0.962}$	0.597	$28.4\ t_m^{0.508}$	0.500
$t_{d30} \mid I_F$, Conditional, μs	$1.77\ I_F^{0.188}$	0.494	$0.906\ I_F^{0.411}$	0.494
$I_F \mid t_f$, Conditional, kA	$14.4\ t_f^{1.08}$	1.184	$17.2\ t_f^{0.492}$	0.540
Correlation Coefficients				
$\rho_c\ (t_d, I_F)$	0.45		0.45	
$\rho_c\ (t_m, I_F)$*	0.89		0.56	

* derived statistic

Table 5

Summarised Parameters of Log-Normal Representation for Characteristics of Subsequent Strokes

Parameters	M	ß
I_F, Crest Current, kA	12.3	0.530
S_m, Max Front Steepness	39.9	0.852
Derived Distributions		
$t_m = I_F/S_m$, Min Eq Front μs	0.308	0.708
$S_m \mid I_F$, Conditional, kA/μs	$4.17\ I_F^{0.900}$	0.706
$t_m \mid I_F$, Conditional, μs	$0.240\ I_F^{0.998}$	0.706
$I_F \mid t_f$, Conditional, kA	$13.1\ t_f^{0.0559}$	0.529
Correlation Coefficients		
$\rho_c(t_m, I_F)$*	0.0747	

* Derived statistic

3.9 Analytical Representation of the Current Shape

3.9.1 General

In accurate calculations of the lightning performance of equipment it may be necessary to simulate the concave front in the lightning stroke current representation. The fundamental requirement in such a simulation is that it provides:

- the correct amplitude of the current
- the highest steepness close to the peak amplitude (taken here as at I_{90})
- for first strokes the correct average steepness expressed as the front time passing through the 30% and the 90% values of the current. This front time must be larger than the current amplitude divided by the maximum steepness, thus resulting in the concave shape. For subsequent strokes this parameter may be neglected.

Many mathematical expressions may be suitable to fulfil these requirements and the one given here is only one proposal. Its disadvantage is that the current front and the current tail are not described by a single expression, but are separated into two parts, one describing the front up to 90% of the amplitude, the other, the amplitude range on the tail.

3.9.2 The Current Front

The current front of the first strokes can be expressed as

$$I = At + Bt^n$$

The basic assumption is that the current shape reaches the instant of maximum steepness (90% amplitude) at a time t_n dependent on the exponent n. In principle, both variables have to be evaluated by an iterative solution of the generalised equation.

$$(1-3x/2S_N)\ (1-x)^n = x(n-1)/2S_N + (1-3xn/2S_N)(1-x,$$

with

$$S_N = S_m\ t_f/I; \quad X_N = 0.6\ t_f/t_n$$

I : current amplitude
S_m : maximum steepness
t_f : front time

However, a sufficiently accurate solution is given by

$$n = 1+2(S_N-1)(2+1/S_N)$$

and

$$t_n = 0.6t_f \left[3S_N^2/(1+S_N^2) \right]$$

The constants then are:

$$A = \frac{1}{n-1} \left[0.9\ \frac{I}{t_n}\ .n - S_m \right]$$

$$B = \frac{1}{t_n^n\ (n-1)} \left[S_m.t_n - 0.9\ I \right]$$

For subsequent strokes the current front is given by:

$$I = S_m.t_f$$

3.9.3 The Current Tail

The fundamental requirements for the current tail are

- to have the maximum steepness at its beginning thus providing a steady transition from one part to the other

- to reach the correct amplitude value

- to describe the current tail. In order to avoid iterative procedures, the last requirement is not mathematically correctly fulfilled in the following proposal, but absolutely sufficient for practical purposes.

A suitable expression is

$$I = I_1 e^{-(t-t_n)/t_1} - I_2 e^{-(t-t_n)/t_2}$$

t_1, t_2 : time constants
I_1, I_2 : constants
t_h : time-to-half value

The constants are

$$t_1 = (t_h-t_n)/\ln 2$$

$$t_2 = 0.1I/S_m$$

$$I_1 = \frac{t_1.t_2}{t_1-t_2} \left[S_m + 0.9\frac{I}{t_2} \right]$$

$$I_2 = \frac{t_1.t_2}{t_1-t_2} \left[S_m + 0.9\frac{I}{t_1} \right]$$

3.9.4 Example

The average values of a first stroke are:

I	= 31	kA
S_m	= 26	kA/μs
t_f	= 3	μs
t_h	= 75	μs

For this current the following constants are derived:

front:
n = 8.29
A = 3.24 kA/μs
B = $3.65.10^{-5}$ kA/μs
t_n = 4.67 μs

tail:
T_1 = 105 μs
T_2 = 0.12 μs
I_1 = 31 kA
I_2 = 3.1 kA

The resulting current shape is shown in Fig 12

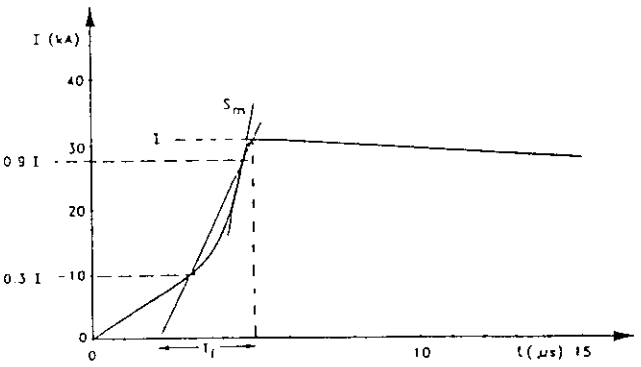

Fig 12 - Analytically derived lightning current impulse, showing the front parameters.

I : Impulse amplitude
S_m : Maximum rate of rise
t_f : Equivalent front duration

3.10 Comments on the Selection of Parameters

The downward negative flash is considered the most important discharge process that affects the lightning performance of transmission lines. It is therefore recommended that parameters describing the downward negative flash are used to calculate the lightning performance of lines, unless regional and/or seasonal differences are known to affect seriously the ratio of positive to negative flashes (typically 10%) at a particular location. Under such circumstances, more direct data should be sought to characterise the particular positive flashes, or published data on positive flashes should be utilised [23], [27].

For practical applications it is recommended that at least the probability distribution is used for the current amplitude, and the median value M (for the corresponding value of current) is used for the maximum steepness S_m, the front-time t_{d30} and the time-to-half value t_h. For more sophisticated calculations as in Monte Carlo procedures, the dispersion ß around this median value may also be included.

4. LIGHTNING STRIKE INCIDENCE AND TRANSMISSION LINE SHIELDING

4.1 Introduction

The purpose of this chapter is to provide suitable engineering procedures for two specific objectives;

- estimation of the incidence of lightning strikes to lines
- procedures for locating shield wires, such as to reduce to an acceptable level the risk of a flash terminating on a phase conductor and causing flashover of the line insulation.

In both instances, the procedures presented are based on consideration of the physical processes involved during the final stages of progression of a charged downwardly progressing lightning leader (usually assumed negative) in its approach to the earth, or toward structures such as a line or transmission tower. These complex processes and the role of structures have been extensively studied by a variety of workers over more than 50 years, ranging from the pioneering work of Schonland, Golde, Berger and Wagner, [28], to the contemporary studies still in progress (such as the work of Dellera and Garbagnati [29], and Eriksson [30,31]).

Over this period, a large number of analytical and empirical models have been postulated and applied to the practical problems of line design and lightning performance estimation, loosely collected under the term "Electrogeometric Modelling" (EGM). At various stages, attempts have also been made to relate or calibrate such estimations against practical service performance.

Despite this extensive background experience, given the complexities of the physical processes and the vagaries of lightning stochastics, there is yet no general consensus on appropriate analytical representation of the last stages of a lightning strike to a structure.

Against this however, by now there has also been wide practical experience with simplified EGM procedures in many operating transmission schemes, generally with satisfactory service performance. As a practical compromise therefore, taking account also of current discussions within both the related CIGRE and IEEE working groups (and the associated modern literature), this chapter summarises a simplified approach (based in part on a common version of the EGM), which is relatively easy to apply and which is generally conservative in relation to service reliability.

4.2 Background and Physical Concepts

Fundamental to EGM approaches is the concept of "striking distance"; originally considered as that critical distance between an object on the earth (or the earth) and a lightning leader, within which the leader must approach before the point of strike is determined.

More recently, based upon detailed observations of lightning strikes to instrumented research towers [23,27,32], it is now generally accepted that the final stages of a downward progressing lightning strike involve two critical aspects;

a) sufficiently close approach of at least one branch of the downward leader, to cause initiation of an upward rising connecting leader, through attainment of a critical electric field at the tip of the object being approached

b) successful completion of a process of interception between the downward and upward progressing leaders.

Both a) and b) are necessary conditions for termination of a strike upon a structure or a conductor, or even to the ground.

Nowadays, attainment of condition a) is more commonly regarded as corresponding to the "striking" distance - since the potential to strike is defined at this point - but this condition is no guarantee of an actual strike, as demonstrated by photographs of well developed upward leaders from structures, which have been provoked through the approach of charged downward leaders, but which have failed to intercept [32].

In reality, a descending lightning leader has a very large vertical extent (typically 5-10 km) and is also extensively branched both in the cloud and below, exhibiting on average 3-5 major branches between cloud base and ground. The extensive spatial distribution of charges across these various branches and the geometric extent of the leader structure, together determine the prevailing electric fields at ground level and in the vicinity of structures, such that the striking distance criterion can be attained at several independent points or structures upon the ground, during the approach of a leader. Field analyses readily show that it is this wide spatial distribution of charges (and their integration), that principally determine the striking distance, for a particular flash, rather than only the charges concentrated within the cloud.

The main problems lie in analytical description of the final interception phase (b), sometimes termed the "final jump" (although this may still involve several leader steps) and in consideration of the influence of structure geometry upon this process. The final interception, which may effectively involve "competition" amongst several relatively independently located upward leaders (ie giving rise to "root-branching") and the distance over which it takes place, is mainly determined through the local distribution of charge upon the nearest approaching branch element of the main leader, together with the development of the upward connecting leader and the local electric field distribution around the structure.

Various models setting out to represent this phase include especially the work of Dellera and his colleagues [29], and that of Eriksson [31,32], (both employing the "leader-progression" approach), and generally require quite complex analyses. The geometric volume around a structure within which this process of interception takes place, represents the "attractiveness" of the structure to lightning and may be expressed through either a "lateral distance" [29], or the "attractive radius" [30,31], depending upon the model involved; (in each case, valid for a particular value of leader charge, or the equivalent stroke current).

In terms of these concepts, analysis of protective effects, such as the role of shield wires, effectively thus requires analysis both of the striking distance D_s and of the geometric capture zone or attractive radius R_a. Invariably also, $D_s > R_a$

In many simplified EGM, however, no particular distinction is made between D_s and R_a. More usually, the "striking distance" terms employed in these EGM are intended to represent equivalent geometric zones of capture.

More generally, it is also evident that a structure will have a significant influence on both the striking distance and on the attractive radius, in the extent to which the structure geometry (especially its height) influences and further enhances the electric fields associated with the approaching leader charge distributions, thereby contributing to initiation of the upward leader and to its further development. This is thus another important aspect which as yet has not been satisfactorily taken into account in most of the simplified EGM applied in common practice, but which is taken into account in "leader progression" modelling.

A secondary problem is to relate either of these two distances to the prospective lightning stroke peak current amplitude, which has been the traditional basis of the many simplified EGM.

In reality, the physical processes are all charge driven and it would be more reasonable to relate the distances involved to the leader charge amplitudes and/or to their distributions. In practice however, this is not really feasible and it is necessary to seek a relation to the ensuing stroke current.

In the event of a strike, the resultant peak current is determined by the impulsive discharge of the closest leader elements alone, typically within some 200 - 1500 m return stroke propagation distance only, as may be readily estimated from consideration of return stroke parameters. This implies the prospect of relatively poor correlation between the striking distance (mainly macro-charge related) and the stroke current (mainly local charge related).

Nevertheless, despite these various problems and limitations, the simple EGM procedures depend essentially upon the joint premises of a lightning "striking distance" D_s, and of a functional relationship to the (prospective) return stroke peak current amplitude I, of the form;

$$D_s = AI^b \qquad (1)$$

where A and b are constants, normally determined through empirical calibration.

4.3 Estimation of Strike Incidence

Dellera and Garbagnati [29] have applied their dynamic leader progression model to analysis of the attractive effects of a variety of representative transmission line arrangements, yielding general curves of expected average strike incidence, in relation to line average height, as shown in Figure 13 (FLAT). This analysis also takes into account alternative topographical situations, such as lines, located either on the slopes or ridges of mountains (ie, SIDE or TOP).

Similarly, in an independent study [30], Eriksson derived a generalised expression for the average attractive radius on each side of a transmission line, based jointly upon a simplified leader progression model and upon analysis of the observed incidence of lightning strikes to a number of practical transmission lines, given by the equation:

$$R_a = 14\ H_T^{0.6} \quad \text{(meters)} \qquad (2)$$

where H_T = average tower height in m.

For estimation of the expected average incidence of strikes to a line therefore,

$$N_L = N_g\ (2\ R_a + b)\ /10 \quad \text{(strikes/100 km/year)} \qquad (3)$$

where N_g = regional ground flash density
b = line width in m

This expression is also plotted in Figure 13 and shows comparatively good agreement with the trend for FLAT situations - lying marginally higher, as would be expected for practical transmission situations which would generally involve a degree of elevated exposure. Dellera and Garbagnati have extended their analysis to demonstrate that the bulk of strokes to lines are likely to concentrate to the towers or to those sections in the span close to the towers. Only about 20-25% of strokes are likely to reach the central third of the span.

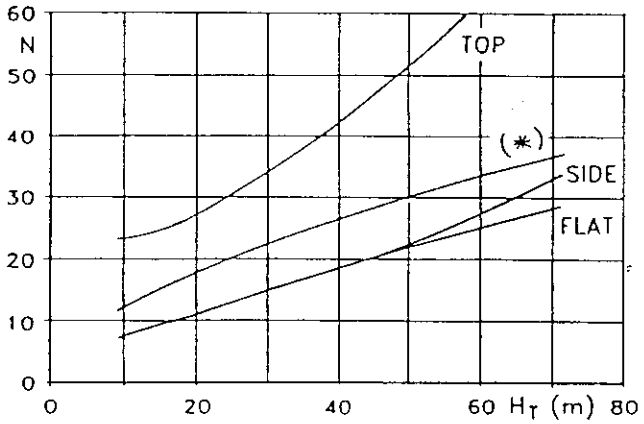

Fig 13 - Number of flashes to a line (per 100km/year) versus tower height - for N_g = 1 - based upon leader propagation model
(FLAT;SIDE;TOP)
(*) Eriksson equation

In summary, there is sufficient consistency between the results of the leader progression analyses and observations of practical transmission line performance, to justify their more general application to estimation of strike incidence to lines.

For this purpose therefore, the curves of Figure 13, or equations (2) and (3), may thus be applied directly, taking the regional ground flash density into account.

4.4 Generalised Shielding Analysis

4.4.1 The Simplified Electrogeometric Model (EGM)

To form a basis for further discussion, a simplified concept of the electrogeometric model, (EGM), will be presented first. Appendix 4A contains the background equations.
As the downward leader approaches the earth, a point of discrimination is reached at which point the leader, if a personality can be ascribed to it, decides the object it will strike. The EGM portrays this concept by the use of striking distances. If all striking distances, to the shield wire, to the phase conductor, and to earth are equal, the stroke would terminate on the closest object. However, these striking distances are, in general, not considered equal and therefore some alternative considerations are required. In general, the striking distance is of the form,

$$r = A\ I^b \qquad (4)$$

where A and b are constants dependent on the object, ie, the phase conductor, the shield wire, or earth and I is the stroke current.

The usual model is depicted in Fig 14 and is illustrated for one specific value of stroke current. Arcs of circles are drawn, centred at the phase conductor and the shield wire, having radii of r_c.

A horizontal line is drawn at a distance r_g from earth. If a downward leader, having a prospective current I for which the arcs were drawn, touches the arcs between A and B, the stroke is assumed to terminate on one of the phase conductors - and if between B and C, the stroke is assumed to terminate on one of the shield wires. Thus assuming that all leaders are vertical, the exposure distance for a shielding failure is D_c and the number of shield failures is $N_g.L_l.D_c$, given one specific value of current where L_l is the line length. Considering the probability of this current, which is f(I) dI, the number of shielding failures is $N_g.L_l.D_c$ multiplied by f(I) dI where f(I) is the probability density function of the current.

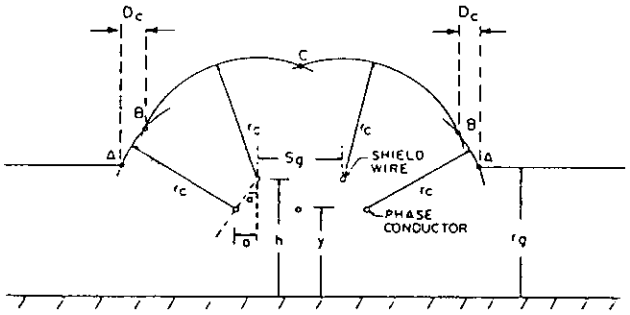

Fig 14 - Electrogeometric model representation of conductors and ground wires.

As the current increases, the radii of the arcs increase and the distance D_c decreases. Finally a point is reached at a current, I_m, where D_c is zero. Thus the number of shielding failures or the shielding failure rate, denoted as SFR, is:

$$SFR = 2N_g L_l \int_3^{I_m} D_c \, f(I) \, dI \qquad (5)$$

(The lower limit of 3kA recognizes that a lower limit to the stroke current exists.)

If voltages on the conductors, produced by these shielding failures, are less than the U_{50}, (negative polarity lightning impulse critical flashover voltage), no shielding failure flashover occurs. Thus to determine the shielding failure flashover rate, SFFOR, the lower integration limit of three is replaced by I_c where

$$I_c = 2 \, (U_{50})/Z \qquad (6)$$

where Z is the conductor surge impedance. Thus the SFFOR is

$$SFFOR = 2N_g L_l \int_{I_c}^{I_m} D_c \, f(I) \, dI \qquad (7)$$

As noted in Fig 14, the striking distances to the shield wire and to the phase conductor are assumed equal while the striking distance to earth is different. However, some authors assume all striking distances equal while others have alternate striking distances to the phase conductors and to the shield wire. In addition, one author does not use the striking distance to earth. A sample of the striking distance equations presently in use is shown in Table 6.

Table 6

Constants "A" and "b" of the Striking Distance Equation: $r = A\, I^b$

	Striking Distance to:			
	Earth r_g		Phase Cond and Shield Wire r_c	
Source	A	b	A	b
Young, et al	27.0	0.32	(1)	0.32
Armstrong, Whitehead	6.0	0.80	6.7	0.80
Brown, Whitehead	6.4	0.75	7.1	0.75
Love	10.0	0.65	10.0	0.65
IEEE Working Group	(2)	0.65	8.0	0.65
Eriksson	To phase conductor: $r_c=0.67\, y^{0.6} I^{0.74}$			
	To shield wires : $r_s=0.67\, H_T^{0.6} I^{0.74}$			
	To earth : $r_g=0$			

(1) A = 27.0 for $H_T < 18$ m
A = 27 (444)/(462-H_T) for $H_T > 18$ m
(2) A = 8.0 (y/22), must be greater than 4.8 but less than 7.2

As noted from the above equation, if I_m is equal to I_c, the SFFOR becomes zero and thus from a mathematical sense a "perfect" shielding angle exists (see Appendix 1 for equation). This concept of a perfect angle will be used in subsequent discussions; however it is realised that only if the phase conductor is completely surrounded by shield wires can perfect shielding be achieved. Perhaps a better definition for this condition should be used, such as critical angle or effective angle. However, the perfect angle is basically descriptive and is definitive in terms of the EGM. Therefore this notation will be retained.

With the above brief description of the EGM, in its generalised form, the following is a discussion of the background of alternate models, both the EGM, and several newer models based on leader progression concepts.

4.4.2 Background

Following the development of the simplified model of the last step of the lightning stroke by Wagner [34,33], Young [35] developed the electrogeometric model (EGM) with the primary purpose of showing that shielding angles should be decreased as tower height increases. Prior to this investigation, shielding angles of about 30 degrees were used with success on the great majority of lines for which tower heights were in the range of 24 meters [36,37]. The impetus for both Wagner's and Young's studies was the poor performance of the AG&E/OVEC 345 kV double circuit line in the USA, which had a tower height of 46 meters and employed a shielding angle of 33 degrees [38]. The result of Young's study is shown in Fig 15 where the recommended shielding angle is plotted

versus tower height. Note that Young's recommendation resulted in a shielding angle of about 15 degrees for the 345 kV tower and maintains the previous recommendation of 30 degrees for the then normal tower heights of 25 to 30 meters.

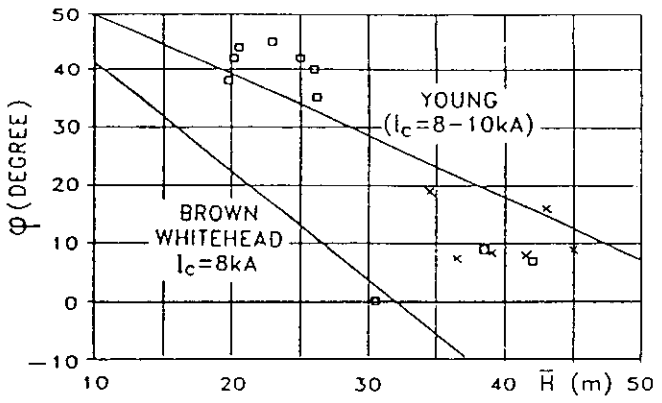

Fig 15 - Comparison between shielding angles calculated for zero SFFOR and observed data derived from pathfinder records.
□) 115-132 kV (I_c = 3.1 - 4.3 kA)
X) 345 kV (I_c = 8.5 kA)

Subsequently, Armstrong and Whitehead [39], and Brown and Whitehead [40] further developed the EGM. The breakdown gradient was modified, a stroke angle distribution was added (Young assumed vertical strokes), and their calculations were compared to the results of the Pathfinder experiment, which produced data showing shielding failures on instrumented lines [41, 42]. Their recommendation is also shown in Fig 15 where the average shielding angle is plotted against the average shield wire height. To be noted is that if Young's curve were plotted in the same manner, the two curves would compare favourably. The pathfinder data is also shown and is plotted as average height and average angle. Each data point represents one or more shielding failure flashovers. Comparing the points denoted by squares to the two curves indicates a good agreement between field data and theory.

To be emphasized further is that the primary purpose of this development of the EGM was to show the sensitivity of the shielding angle with tower or line height.

Following these initial studies, further investigations were undertaken to improve and extend the EGM [43-47]. A primary problem was that the EGM was calibrated using the AIEE stroke-current distribution, which had a median of 15 kA and a log standard deviation of 0.98. With the conclusion of Berger's data and the adoption of the CIGRE distribution (see Chapter 3), a new calibration was required. The search for an equivalent current distribution for strokes to level ground was initiated by Sargent [46] who found that a theoretical distribution having a median of 12.5 kA and a log standard deviation of 0.75 produced reasonable comparisons with distributions reported by AIEE, Berger, and Popolansky (see Chapter 3). More recently, Mousa and Srivastava [47] have suggested an equivalent ground level distribution having a median of 24 kA and a log standard deviation of 0.72.

The consensus in the contemporary literature is that the "reference" distribution of stroke amplitudes to "flat" ground has a median amplitude in the range of 24-30kA, and thus lies close to the distributions measured in structures [20]. This necessitates therefore further consideration of the EGM in its original form.

Recently, alternate approaches to shielding analysis, using leader progression model concepts, have been proposed. Eriksson's approach led to a modified EGM [31]. His formulation of the striking distance equations, presented in Table 6, provide a significant height sensitivity. Further, the stroke terminating to earth is treated as a default condition and thus a striking distance equation to earth is not required. The Dellera-Garbagnati [29] approach requires a significant calculation effort although curves are provided to obtain a quick estimate. The Rizk [48] approach results in two simple sets of curves describing the perfect shielding angle.

4.4.3 Comparison of Results

A comparison of the perfect shielding angles as calculated for the EGM, for three alternate striking distance equations, is presented in Fig 16. The IEEE Working Group equations are a modification of their earlier equations [25]. Because Young assumed only vertical strokes, these angles are limited to zero degrees. However, the other two curves are constructed assuming all stroke angles are possible, thus permitting even the horizontal stroke resulting in severe negative angles. However, in application, the IEEE Working Group method assumes only vertical strokes.

(Fig 16)

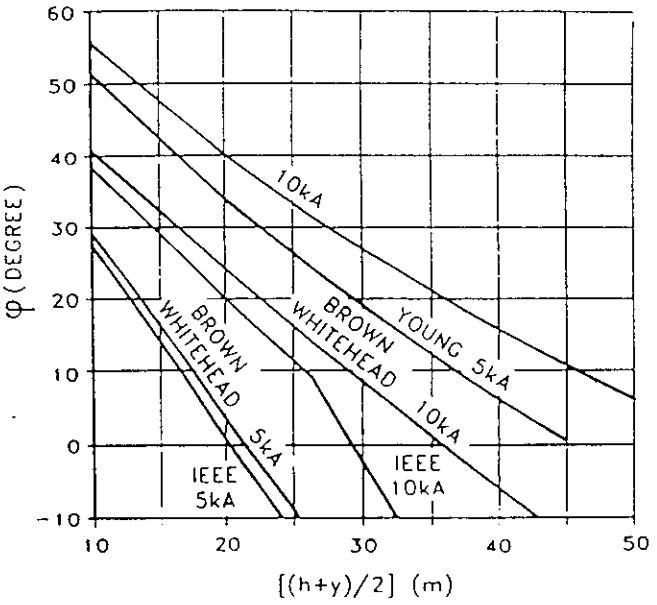

Fig 16 - Perfect shielding angle as determined by use of EGM for different formulations of striking distance.

The comparative results of Eriksson and Rizk, Fig 17, indicate a significant degree of agreement. Since the Dellera - Garbagnati approach does not permit the determination of the perfect angle, the results are shown for a SFFOR of 0.2 and 0.05, for an N_g of 4 in Fig 18. When compared to the results of Fig 17, significant deviations are apparent.

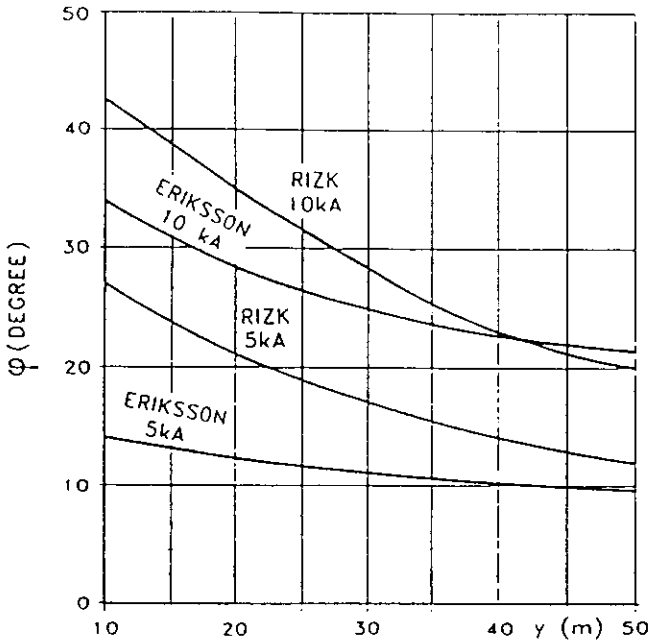

Fig 17 - Perfect shielding angle as determined by Eriksson's and Rizk's methods for (h-y)=5m.

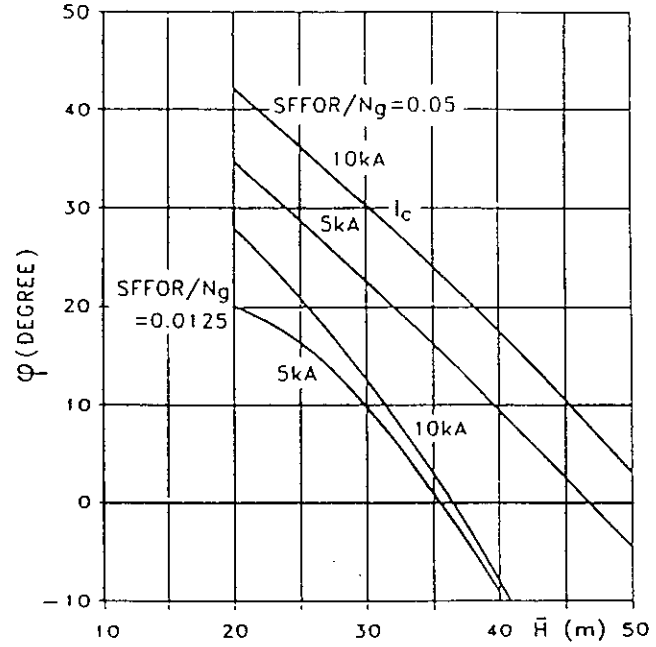

Fig 18 - Shielding angle as determined by Dellera/Garbagnati method.

Assuming vertical strokes, a further comparison of results for a SFFOR/N_g ratio of 0.01 is shown in Tables 7 and 8. The dispersion of results for the EGM is significantly reduced from those of Fig 15. However, the results shown in Table 8 for the leader progression model still indicate a degree of dispersion. In particular, the results from Dellera and Garbagnati produce negative angles, although all stroke angles were considered for these cases.

Table 7a

Comparison of Shielding Angles using the EGM for a SFFOR/N_g Ratio of 0.01 for Critical Currents of 5 and 10 kA. (h-y) = 4

	Brown-Whitehead		Young	
(h+y)/2 Meters	5 kA	10 kA	5 kA	10 kA
20	20	30	39	43
30	14	18	26	31
40	11	11	16	21
50	10	10	9	13

Table 7b

	IEEE		Eriksson	
(h+y)/2 Meters	5 kA	10 kA	5 kA	10 kA
20	18	27	37	45
30	10	10	33	41
40	5	5	31	38
50	4	4	29	36

Table 8

Comparison of Shielding Angles using Leader Progression Model Concepts for a SFFOR/N_g Ratio of 0.01 Critical Currents of 5 and 10 kA.

	Eriksson(1)		Dellera-Garbagnati(1)		Rizk(2)	
(h+y)/2 Meters	5 kA	10kA	5 kA	10 kA	5 kA	10kA
20	37	45	21	28	21	43
30	33	41	9	13	17	35
40	31	38	-9	-8	14	29
50	29	36	*(3)	*(3)	11	20

(1) for (h-y) = 4m

(2) for perfect shielding

(3) values could not be obtained

4.4.4 Selection of the Shielding Angle

The primary aim in selection of the number and location of shield wires is to provide a means of intercepting the lightning flash and to reduce the shielding failure rate to an acceptable level, fully realising that a SFFOR of zero is virtually impossible. The design value of the SFFOR, although frequently selected without regard to the backflash rate (see Chapter 6) should be treated with the latter together, or as a sum, to form the basis of the total lightning design. Similarly, in the past

the design shielding angle was frequently selected on the basis of perfect shielding. While this may be proper for areas of very high ground flash densities, in areas where N_g is 1 to 4, the restriction to a perfect angle may severely handicap an economical design. Thus one shield wire may be adequate for areas of low ground flash density, whereas two shield wires are required in areas of higher lightning intensity. Therefore, a design based on a target SFFOR is suggested. The actual design value of SFFOR must be the prerogative of the designer, so as to permit economical designs. For lines serving a critical load, a design value of 0.05 may be suitable. Design values as high as 2.0 have been reported.

An additional benefit of selecting a non-zero SFFOR is that the large deviations of shielding angles between alternative methods, as shown in Fig 15 are greatly reduced. Further reductions in these deviations result when vertical strokes only are considered.

To assist in selection of the shielding angle, the curves of Fig 19 have been prepared and are based on the Brown-Whitehead formulation of the striking distance equations, which represent a reasonably severe condition. In addition the curves are based on vertical strokes.

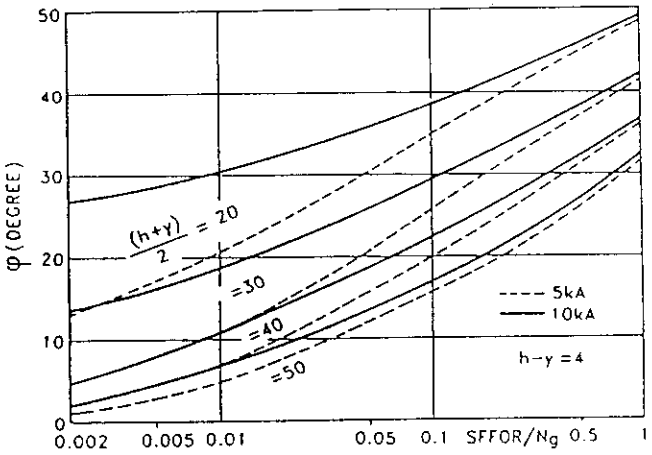

Fig 19 - A conservative approach to shielding angle as function of SFFOR/N_g. Brown/Whitehead equations with vertical strokes.

The shielding angles of Fig 19 are the average angle within the span, and thus the shielding angle at the tower may be larger. The angles also assume flat or rolling terrain. For towers located on hill sides, the average shielding angle is that obtained from Fig 19, minus the hill side angle. Trees, structures, etc along the right-of-way are beneficial in that they increase the effective height of the earth plane. That is, the striking distance to earth becomes that to the structure or tree-tops. Thus, for this case, larger angles may be used. Towers located on hilltops are especially vulnerable since more strokes are collected by such towers. Hilltop sites are even more vulnerable to the backflash however, since the tower footing resistance tends to be larger than normal (see Chapter 6). As has been noted in the literature, the performance of a few towers or line sections frequently determines the total performance of the line; thus the name "rogue" towers has come into the colloquial language. With all of the above factors, the final selection of the shielding angle at the tower must be highly judgmental, based on the experience of the designer and on the performance of other lines within the utility system.

This discussion has centred on shielding the outside phases of a line. While shielding failures to the centre phase may occur in extremely rare cases, they are predicted to be essentially zero. For all practical cases of tower design, shielding failures to the centre phase should be considered non-existent. This factor of greatly improved shielding to objects between shield wires or masts is employed in the design of station shielding, a subject beyond the scope of this present report.

As an illustration of use of Fig 19, assume a design value of SFFOR of 0.05/100 km yrs in an area having a ground flash density of 5, which produces a SFFOR/N_g of 0.01. For an average phase conductor and shield wire height of 30 meters and a critical current of 5 kA, a shielding angle of 11 degrees is obtained from Fig 19. For these same conditions but for a ground flash density of 1, or a SFFOR/N_g of 0.05, a shielding angle of 21 degrees results. Alternatively if the design SFFOR is increased to 1.0 for a ground flash density of 1, a shielding angle of over 40 degrees may be adequate.

4.4.5 Presently Used Shielding Angles

The suggestion of a design based on the SFFOR should not be considered as new. This design philosophy has been and is still used today. Furthermore, the decrease of shielding angle with tower height is presently employed in design. Some verification of the use of the angle/tower height sensitivity can be obtained from the results of the CIGRE survey [49] as presented in Fig 20. (One point at 34 meters with an angle of -19 degrees is not shown). As noted for lightning tripout rates of less than 0.8/100 km-yrs, shielding angles of 20 degrees are used for tower heights of 40 meters, whereas for lines having tower heights of less than 40 meters, larger angles are sometimes employed.

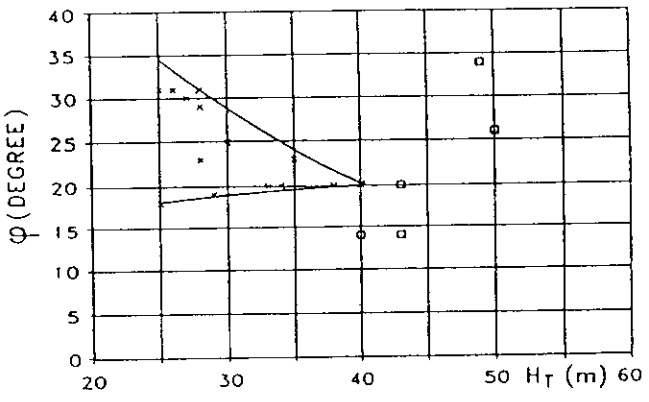

Fig 20 - Service experience of shielding angle versus tower height.
x ≤ 0.8 (tripout/100km year)
□ > 1 (tripout/100km year)

The line data contained in reference [50], although not giving the tower height may also be helpful. As shown in Table 9, higher towers generally have lower shielding angles, but higher angles are used in areas of lower lightning intensity.

Table 9

Shielding Angles Used for 345 and 500 kV Lines in the USA; Lightning Tripout Rate Less than 0.6/100km year.

Nominal System Voltage kV	Type	Thunder-Storm Days/Yr Range	Shielding Range (degrees)	Angle Average (degrees)
345	Single Circuit	22 to 50	0 to 33	22
345	Double Circuit	20 to 60	0 to 30	11
500	Single Circuit	30 to 110	-9 to 20	12
500	Single Circuit	2 to 25	15 to 30	23

4.4.6 The Present and Future

As is evident from the above discussion, the selection of a shielding angle is a combination of theory and experience, as perhaps occurs in all phases of engineering. It is the hope of the authors that the theory and practice are sufficiently clear so that a judgement can be made on the proper design shielding angle. The detailed study of shielding angles and of lightning incidence rates is currently hampered by the lack of sufficient reliable data. Although theoretical studies will continue, the lack of a quality database will tend to create more confusion than factual results.

As a final note, in a not too facetious manner, the lack of data and the lack of full agreement on the proper shielding angle has not hampered the industry. Lines have been and still are designed, constructed, and operating with acceptably low lightning tripout rates. This merely indicates that while overall agreement on shielding concepts and the proper shielding angle is important, practical application continues with success.

Appendix 4A: The Basic Electrogeometric Model

In transmission line design, the specification of the shield wire location is usually given by the shielding angle alpha, as defined in Figure 14. As indicated here, if the shield wires are horizontally disposed beyond the phase conductors, the shield angle is defined as negative.

The geometric model as generally used is depicted in Figure 14 for one specific value of stroke current. The striking distances, r_c, are drawn as arcs of circles from the phase conductors and shield wires, and a horizontal line is constructed parallel to the earth at a height of r_g. Downward leaders, or strokes, approaching the line with a prospective current as employed to construct the arcs, reaching the arc between B and C will terminate on the shield wire. Those reaching the arc between A and B will terminate on the phase conductor, and those beyond A will terminate on the earth.

For simplicity, assuming only vertical strokes, the number of strokes which terminate on the phase conductors or the shielding failure rate, SFR, is:

$$SFR = 2\, N_g\, L_1 \int_3^{I_{max}} D_c\, f(I)\, dI$$

Where, D_c is as shown in Figure 14 and
N_g = ground flash density
L_1 = line length
$f(I)$ = probability density function of crest current of the first stroke.

As noted, the integral is over the limits 3 kA, which is assumed as the minimum stroke current and I_{max} which is defined as the maximum current beyond which no stroke can terminate on the conductor. That is, as the current increases, r_c and r_g increase, and the distances A-B and D_c decrease. At I_{max}, D_c is zero. As an approximation, the maximum value of r_g, r_{gm} is:

$$r_{gm} = (h+y)/2\ (1 - \Gamma \sin \alpha) \qquad (8)$$

Where $\Gamma = r_c/r_g$

The value of I_{max} is then determined from Equation (4)

From geometry:

$$D_c = r_c\, [\cos \theta - \cos (\alpha + \beta)] \qquad (9)$$

Where α is the shielding angle shown in Figure 14 and:

$$\theta = \sin^{-1} [(r_g - y)/r_c] \qquad (10)$$

$$\beta = \sin^{-1} [(a^2 + (h-y)^2)^{0.5}/2r_c] \qquad (11)$$

To be noted is that the SFR is the number of strokes which terminate on the phase conductor, and these may or may not result in flashover. The critical current, I_c, below which flashover will not occur, is:

$$I_c = 2\, U^-_{50}/Z_c \qquad (12)$$

Where U^-_{50} = Lightning impulse critical flashover, negative polarity, (approximately 605 kV/m of insulator length or insulation strike distance, whichever is smaller)

Z_c = phase conductor surge impedance

Therefore, the number of strokes which terminate on the phase conductors and result in flashover, ie the shielding failure flashover rate, SSFOR, is:

$$SFFOR = 2\, N_g\, L_1 \int_{I_c}^{I_{max}} D_c\, f(I)\, dI \qquad (13)$$

And as noted from this equation, the SSFOR becomes zero if I_{max} is equal to or less than I_c. The resulting shielding angle when $I_c = I_{max}$, is denoted as α_p and termed the "perfect" shielding angle. Again, from geometry:

$$\alpha_p = 0.5[\sin^{-1}((r_g-h)/r_c) + \sin^{-1}((r_g-y)/r_c)] \qquad (14)$$

Where r_g and r_c are determined for the current, I_c.

5. REVIEW OF MODELLING CONCEPTS

5.1 Introduction

A lightning flash can only result in significant overvoltages on power-line insulation if substantial stroke current and charge are injected into the line's conductors. Both theoretical analyses and experimental data show that voltages induced by nearby lightning flashes to ground seldom exceed 200 kV and induced voltages are therefore principally of interest only on lightly insulated distribution lines.

Thus only those lightning flashes which terminate directly upon a line need to be modelled for most practical lightning performance calculations.

Once contact is made with the line, the injection of the lightning return stroke current is modelled as a transient current generator feeding into a system of transient surge impedances representing the line conductors and the tower (as discussed in sections 5.2 and 5.3, as well as in Chapter 6). The resulting overvoltages are then calculated using conventional travelling wave techniques (5.2), usually considering mainly the line spans close to the struck point.

The impedance of the return stroke channel is assumed to be substantially larger than the surge impedance of the line conductors (and/or tower), and is thus neglected. The return stroke can then be modelled as an ideal current generator having appropriate current magnitudes and waveshapes selected on the basis of the distributions given in Chapter 3. Experience indicates that in the majority of cases, it is sufficient to consider the single first stroke only.

Injection of return stroke current into the system initiates travelling waves which produce reflections and refractions at the various impedance discontinuities, and thus require appropriate modelling, as discussed in section 5.2 and in Chapter 6. Wave-modifying influences which have to be taken into account in most instances, include the effects of impulse corona at high voltages and the non-linear impulse current response of the tower footing resistances, as discussed in sections 5.4 and 5.6 respectively.

The resultant overvoltage stresses appearing across the line insulation (and the associated risk of failure) are only indirectly related to the conventional LI withstand strength (due to the non-standard waveform of the overvoltage stress), and this aspect thus also requires particular analysis, as in section 5.5.

Taken as a whole, this chapter does not set out to present a unique or exclusive calculation model. The aim is rather to emphasise the relative importance of the various aspects involved and to present appropriate simplified engineering approximations which are based upon up-to-date understanding of these processes.

Application of several of these aspects is then illustrated in the consolidated discussion of the backflash process in Chapter 6.

5.2 Transmission Line Representation

Apart from the lightning current parameters, the line characteristics determine the surge voltages that occur on a transmission line struck by lightning. In order to carry out calculations of lightning surge voltages with reasonable accuracy, it is therefore necessary to utilize a transmission line model in which the most important line parameters are represented in an appropriate way.

In this section guidelines for the inclusion of the basic line characteristics in computation models to study lightning performance of lines are presented. In such studies the earth wires should be included and, in detailed calculations, each span has usually to be handled separately. Furthermore, tower and line configuration, including tower impedance and tower footing impedance as well as insulation withstand and nonlinear corona effects must generally be considered. Accordingly, the necessary computation model may differ in comparison with models applied for switching overvoltages and other transients of system origin.

In general, the calculation model should be able to compute all line conductor voltages caused by a flash to earth-wire(s) or direct to a phase conductor (shielding failure). Accordingly, for instance, electromagnetic coupling between the conductors, as well as insulation withstand for different gap configurations must be included.

As already mentioned, earth wires as well as phase conductors should be included in the analysis. Accordingly, a mathematical model to handle multiconductor systems would be preferred, (as applied for example, in electromagnetic travelling wave analyses using discretised modelling). Such calculations are usually difficult and computationally intensive. In many practical engineering applications (which are mainly concerned with the voltages at specific locations) adequate accuracy is achieved using single conductor modelling and this is the approach principally followed in this document.

Travelling-wave calculation for multiconductor systems utilizing the different modes of propagation are well known [51, 52]. For switching surges and other internal system transients the earth wires can be eliminated from calculations assuming zero potential on these wires. The overhead lines may then be considered as a three conductor system and modal analysis with two line modes and one ground mode for the propagation can be applied.

For lightning surges, the earth wire potential cannot be neglected. Also, reflections at the towers must be considered. Accordingly, the line model needed is much more complex than that for the other transients mentioned.

Modal analysis is in principle possible for an arbitrary number of parallel conductors. Line impedance and admittance matrices are then mathematically transformed by transformation matrices so that diagonal matrices describing the separate modes are obtained. The transformation matrices necessary can be found by eigenvalue analysis. Generally, the line inductance (and resistance) are frequency dependent and, as a consequence, the transformation matrices and the wave velocities in the different modes also depend on frequency. However, bearing in mind parameter inaccuracies due to varying ground resistivity, non linear corona effects, conductor sag etc, it is sufficient to apply line constants for one frequency only [53, 54]. Accordingly, mode separation may be applied also for lightning surges on each line span. Such methods may be needed for studies on lightning surges travelling several spans as for instance, in relation to analyses of lightning overvoltages in substations.

The earth resistivity plays an important role for the damping and distortion of surges with ground return.

In accurate analyses of overvoltages for important installations (GIS, etc), therefore, mode separation is applied in more extensive calculation models [53, 54].

As mentioned in the introduction, however, consideration of only a few line spans is sufficient for line performance studies. Therefore, separation into different modes is not necessary in this case and it can be assumed that all surges travel with the velocity of light. Simple matrix analyses are then sufficient for all conductors involved.

If the line is considered lossless, the surge impedance and surge admittance matrices (Z,Y) can be calculated from the inductance or capacitance matrices (L,C):

$$Z = Y^{-1} = c_o L = (1/c_o)C^{-1} \qquad (5.1)$$

$$c_o = (\varepsilon_o \mu_o)^{-\frac{1}{2}} \qquad (5.2)$$

The conductor transient voltages and currents may then generally be represented by surges travelling with the velocity of light in both directions (V_1 and V_2). The power frequency voltage (U_p) can simply be added as a constant DC-voltage, since the time scale in lightning studies is in the microsecond range. Accordingly, conductor voltages (U) and currents (I) may be expressed by the matrix equations:

$$U = V_1 + V_2 + U_p \qquad (5.3)$$

$$I = Y(V_1 - V_2) \qquad (5.4)$$

For a system with n conductors U, V_1, V_2, U_p and I are vectors with n elements and Y is a n*n-matrix.

The surges V_1 and V_2 are determined by the conditions at each end of the span (tower surge impedance, footing resistance etc) with addition of a possible current source representing the lightning current. The impedance of the lightning channel is considered high compared to conductor and tower impedances (at least ten times higher than the conductor surge impedance). Therefore, an ideal current source can be applied.

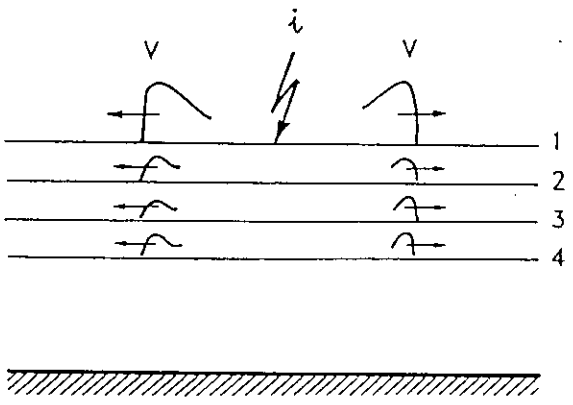

Fig 21 - Lightning flash to upper conductor on a line span.

For illustration purposes, the example shown in Fig. 21 is considered. Before reflections from neighbouring towers occur ($V_2 = 0$), eqs. 5.3 and 5.4 are modified to:

$$U = V + U_p$$

$$I = YV \text{ or } V = Y^{-1} I = ZI$$

The flash is assumed to hit conductor No 1, and the current will separate in two equal parts flowing in each direction. The conductor voltages are then:

$$\begin{bmatrix} U_1 \\ U_2 \\ U_3 \\ U_4 \end{bmatrix} = 1/2 \begin{bmatrix} Z_{11} i \\ Z_{21} i \\ Z_{31} i \\ Z_{41} i \end{bmatrix} + \begin{bmatrix} U_{p1} \\ U_{p2} \\ U_{p3} \\ U_{p4} \end{bmatrix}$$

In this equation, i is the lightning current, Z_{11} represents the surge impedance of conductor No 1, and Z_{ij} represents the mutual surge impedance between conductor No i and conductor No j. It is seen that the transient voltages on the neighbouring conductors are determined by the coupling factor:

$$K_{ij} = Z_{ij}/Z_{ii} \qquad (5.5)$$

The surge impedances and mutual impedances are found from the formulae:

$$Z_{ii} = 60 \ln (2h_i/r_i) \qquad (5.6)$$

$$Z_{ij} = 60 \ln (a_{ij}/b_{ij}) \qquad (5.7)$$

in which

h_i - height of conductor no i above earth

r_i - radius of conductor no i

a_{ij} - geometric distance between conductor no i and the image of conductor no j

b_{ij} - geometric distance between conductor no i and conductor no j

For practical purposes, the average height may be used, given by:

$$h_{av} = h_t - 2/3 s_{ag}$$

(h_t = height at the tower)

The self and mutual surge impedances shown are based on the physical line dimensions and conventional image theory ie, in principle lossless lines. This approximation is considered to be valid for line performance analyses for voltages below the corona on-set level. However, the overvoltages of interest are generally higher than this level, and therefore, account must be taken of the non-linear corona effects - as discussed further in section 5.6.

Line flashovers normally occur at the towers. Therefore, it is the voltage differences between the conductors at these points that are of interest. In order to calculate the voltages at the towers, of course, a computational model is needed for the tower as well as for the tower earth electrode - as discussed in the following sections.

5.3 Tower Surge Response Models for Lightning Calculations

5.3.1 Introduction

Under lightning surge conditions, currents with rates of change di/dt as high as 200 kA/μs can be applied to the transmission system. The fast rates of rise lead to transient overvoltages resulting from the surge response of the structures and wires. The front times of 1-4 μs are long with respect to typical line heights. Because of this, most models assume that tower response is dominated by the Transverse Electro-Magnetic (TEM) wave and that other types of radiation may be neglected. The TEM response is relatively easy to use because surge impedances of components such as conductors can be calculated, even under corona conditions. In simplified engineering calculations it is common practice to introduce the concept of a tower surge impedance - as an aid to determining the voltage across the line insulation. For simplicity, strokes to the tower line only are considered in this analysis.

5.3.2 Generalised Tower Surge Response

The tower could be represented variously as an inductance connecting shield wires to ground, as a constant-impedance transmission line, or as a variable-impedance transmission line. or as a radiating structure. As an adequate approximation, the travel time can be represented by t=h/c. Many experimental and theoretical studies of tower response have been initiated [55-62]. Wagner and Hileman [55] found the transient impedance of a cylinder to an impressed wave at tower top. Sargent and Darveniza [56] noted that a cone had a constant transient impedance, and also derived the average impedance of a cylinder. Chisholm, Chow and Srivastava [57] found that impedance depended on direction of injection, with vertical injection to cylinders and cones agreeing with [55], [56] and [63] and horizontal injection matching experiments [58-60] using this geometry. They continued the use of an average impedance Z_{av}, as defined below, for a constant-impedance model.

$$Z_{av} = 60 \ln (\cot \theta/2)$$

where $\theta = \tan^{-1} (r(h)/h)$

and h is the height along the tower.

As a practical simplification, Chisholm, Chow and Srivastava [57] proposed an equation for the impedance of a typical transmission tower. A weighted average of the tower radius, r_{avg}, is obtained as follows:

$$r_{avg} = \frac{r_1 h_2 + r_2(h_1+h_2) + r_3 h_1}{h_1 + h_2}$$

Where:

r_1 = Tower Top Radius, m
r_2 = Tower Midsection Radius, m
r_3 = Tower Base Radius, m
h_1 = Height from Base to Midsection, m
h_2 = Height from Midsection to Top, m
$H_t = h_1 + h_2$ = tower height

The weighted average radius is then used in the equation for a conical tower over a ground plane:

$$Z_T = 60 \ln \cot [0.5 \tan^{-1} (r_{avg}/H_T)]$$

This weighted average was found to agree with integrals of the tower impedance over height ("tower inductances") over a wide range of tower shapes. The initial transient rise of the tower in the skywire - ground plane waveguide may be modelled by this approach.

As an approximation, the equivalent inductance is given by

$$L = Z_T \cdot H_T/c$$

5.3.3 Square Cross-Section

In calculations of tower surge impedance or inductance, cross-sections that deviate from circular can be treated with a capacitance model [61], as originated by Chow and Yovanovich [64]. The self-capacitance of an object is computed:

$$C_{tower} = \varepsilon_o C_f (4\pi A_T)^{\frac{1}{2}}$$

$$C_f = (2\Gamma)^{\frac{1}{2}}/\ln(4\Gamma)$$

Where Γ = maximum height/maximum width, (the aspect ratio).
$\varepsilon_0 = 8.854 \times 10^{-12}$ F/m.
A_T = Area in m^2.

When the capacitance of the tower is known, its travel time and impedance are related by $t = Z_T C_{tower}$. For an example of a free-standing tower with 2.5 x 2.5 m square cross section and 50 m height, the following calculation gives the impedance and inductance:

$\Gamma = h_t/W = 20$ for a typical double circuit tower

where W = maximum width

$A_T = 4(50 \text{ m})\ (2.5 \text{ m}) = 500 \text{ m}^2$

$C_f = 1.443 \quad C_{tower} = 1.01$ nF

$t = \frac{h_t}{c} = 167$ ns; $Z_T = t/c = 165$ Ohms

$L = t^2/c = 27.5$ μH

In such a case, for a lightning current with dI/dt of 25 kA/μs, the additional tower-top voltage rise due to tower inductance would be 690 kV. Most lightning performance calculation models assume that this would fall linearly with tower height, to the footing voltage at the base of the tower.

5.3.4 Crossarms

The effect of crossarms on tower surge response have been studied by Chisholm, Chow and Srivastava [61]. They found that typical crossarms behave as electrically-short stub transmission lines with open-circuit ends. All effects of this model, including a short-lived doubling of voltage at the crossarm end, were verified experimentally. Observed travel times are longer than tower height divided by speed of light, but tower impedances are also reduced slightly. The net effect of the additional path length and consequent propagation delay can usually be ignored for practical purposes. Only the additional contribution of propagation in from skywire supports adds to the tower inductance.

5.3.5 Tower With Guy Wires

Many towers have metallic support ropes or guys that carry some lightning surge current. These guy wires reduce the total tower inductance and thus mitigate

some stress on the insulator strings. There are several calculation models that could be proposed to take mutual coupling into account. However, for typical guy-wire slopes less than 3(up):1(out), mutual coupling among the wires can be ignored. Mutual coupling can also be ignored for most H-frame towers. The surface-area model can be used with advantage, and Approaches 1 and 2 below illustrate the application to the above square tower, now with four guy wires at 45° angles to the tower.

Guy Length = $(2)^{\frac{1}{2}} H_T$ = 70.7 m

Guy Radius = r = .02 m

Approach 1: (simplification)

Z_{guy} = 60 ln (2h/r - 60) = 451 ohms

$t_{guy} = (2)^{\frac{1}{2}} H_T/c$ = 235.7 ns

$L_{guy} = Z_T . t_{guy}$ = 106.3 μH per guy

L_{tower} = 26.6 μH in parallel with 27.5 μH tower

= 13.5 μH

Approach 2: (Total Tower)

$A_T = 8 \ H_T^2$ = 10,000 m²

$C_f = \frac{(2\Gamma)^{\frac{1}{2}}}{\ln 4} = 1.44$

$C_{tower} = \varepsilon_o \ C_f \ (4\pi A_T)^{\frac{1}{2}}$ = 4.5 nF

t = 236 ns Z_T = 52 ohms L = 12.3 μH

5.3.6 Practical Values

Common experience with practical structures yields typical values for tower surge impedances in the range 150-250Ω.

5.3.7 Ground Plane Surge Response

Studies of reflections from the base of towers, using scale models [65], triggered lightning and theory, have shown that the initial reflection from the base is not that which would be predicted in the case of a lumped resistance. In the case when no shield wires are present, the lightning channel extending upwards forms a biconical radiator. When shield wires are present, a waveguide between the overhead shieldwires and the ground plane is excited. In both cases, expressions for a transient ground-plane impedance have been suggested [65]. For linear steep-fronted impulses estimated values for this effect lie in the range of about 2-10Ω for the first few μs.

In practice, however, due to the concave shape of the lightning current wavefront, the effect is much smaller and may be neglected in simplified calculations.

5.4 Earth Electrode Impulse Response

It is generally agreed that the resistance of an earth electrode decreases with the applied current due to ionization of the soil. Fig 22 and 23 show measured impulse current and voltage responses for two examples reconstructed from reference [66]. They refer to two very different electrode geometries, but buried in the same soil. From such measurements, voltage and current, a time-dependent resistance may readily be obtained by dividing the corresponding instantaneous values. Despite the different electrode geometries, the behaviour of the two earth impedances is similar.

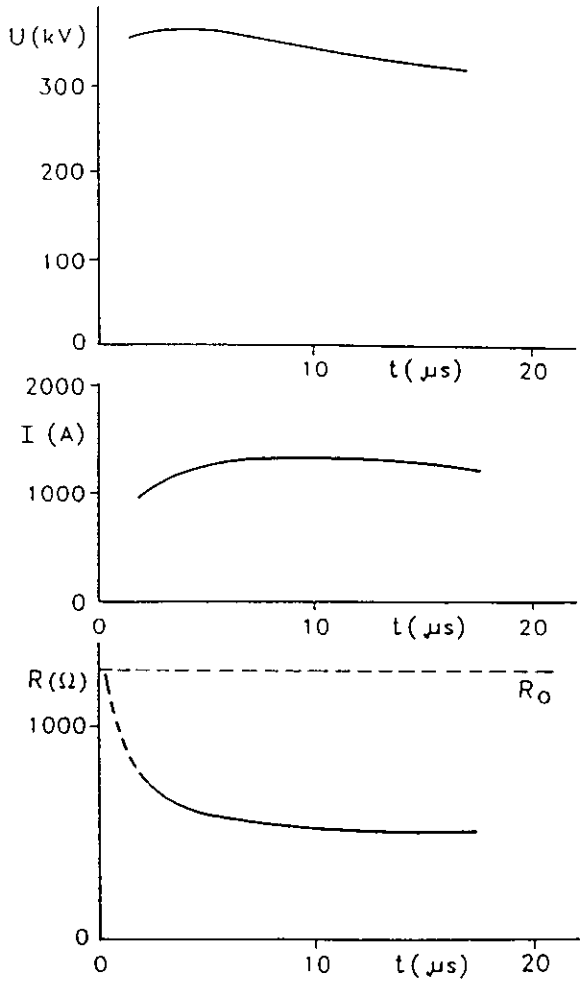

Fig 22 - Measured voltage, injected current and resistance of a 0.25m diameter hemisphere with 1000Ωm.

With the voltage developed, the earth impulse impedance rapidly drops from the original low current value R_o and reaches a minimum value after approximately 5 μs.

An explanation for the phenomena responsible for this resistance decrease with current has already been given in [69]. For a step voltage applied to the electrode an ionization process similar to the streamer discharge in air, occurs in those regions around the electrode in which a critical field gradient is exceeded. In this region, low ohmic discharge channels are formed, thus reducing the resistance of the ionized zone practically to zero.

It has previously been proposed that the current dependence of the tower footing impedance can be expressed by the normalised quantities [69].

$$\pi_1 = Rl_e/\rho \quad \text{and} \quad \pi_2 = \rho I/El_e^2$$

R = Resistance
ρ = soil resistivity
E = field gradient
I = impulse current
l_e = Electrode length

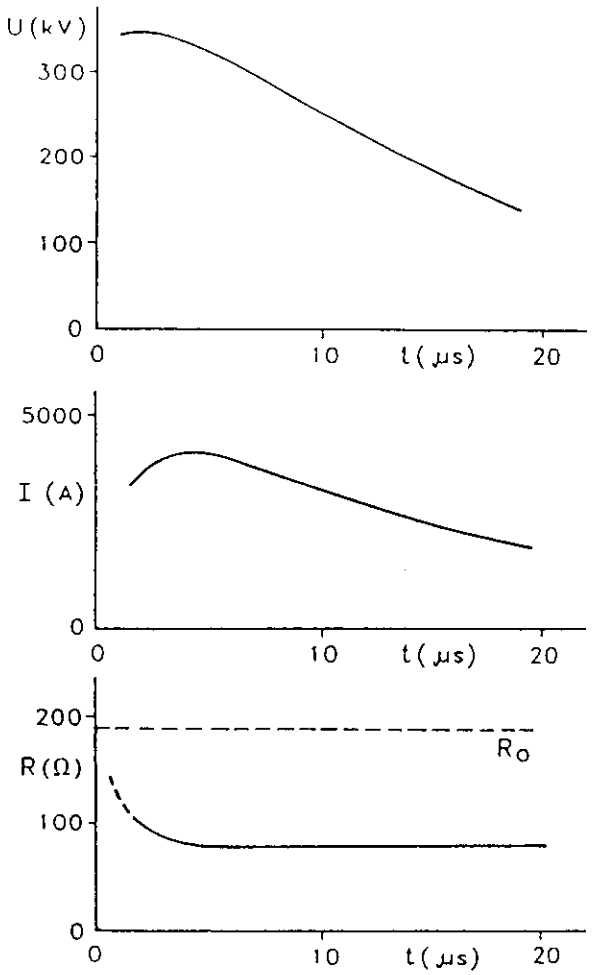

Fig 23 - Measured voltage, injected current and resistance of a horizontal rod of l = 18m and Φ = 6 mm with 1000 Ωm.

For hemispheres, the diameter is taken as length. These quantities have recently been redefined to include earth electrodes with a more complex shape [67]. Fig 24 has been redrawn from this reference but retaining the original normalisations.

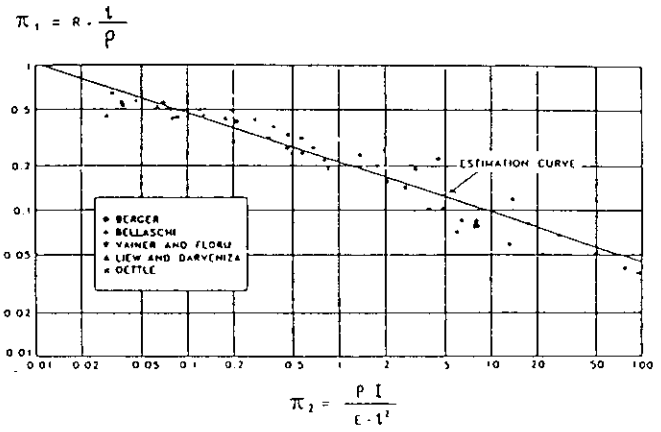

Figure 24 : Normalised Current Dependence of Earth Resistances [67].

When interpreting Fig 24, it should be noted that the full range of π_2 has not been obtained by varying the current amplitude for one earth electrode, but by varying the length of the diameter of the electrodes. Thus the data on the left corresponds to extended electrodes and that on the right to small electrodes, ie, spheres and short rods. A re-examination of the available data has led to the conclusion that results relating to such different earth electrodes should not be described by one single expression. It is preferable to apply the basic rules of the soil ionisation mechanism given below (as explained more fully in [71]):

- Sphere electrodes

1. The earth resistance remains at its geometrical value until the ionization onset is reached. This onset depends upon soil resistivity and on the instant considered.

2. After onset, the resistance decreases inversely proportional to the square root of the current.

- Rod electrodes

1. The earth resistance remains at the value determined by the electrode geometry and the soil resistivity until ionization onset is reached. As such electrodes usually have small material diameter, this onset occurs at rather small current values.

2. After onset, the resistance decreases with the logarithm of the current until the ionization zone is so large that an equivalent rod geometry is no longer maintained.

3. For higher currents the dependence of the resistance on the current is that of a sphere.

Taking into account the uncertainties in the present knowledge of the earth resistance, the use of a conservative simplification is deemed adequate. Such a simplification for rod electrodes could be an expression which approximates the above three ranges; ie, to have the low current resistance for currents close to zero, to approach the square root dependence for very high current values and to approximate the logarithmic dependence between these two extremes.

A possible expression is given by

$$R_i = R_o(1 + I/I_g)^{-\frac{1}{2}} \qquad (1)$$

The limit current I_g is given by equation 2, which states that the final decrease of the resistance is determined by the field E_g and the resistivity, together with the resistance R_o representing the physical dimensions:

$$I_g = E_g \rho / 2\pi R_o^2 \qquad (2)$$

Fig 25 shows the dependence of the ratio R/R_o dependent on I/I_g, and setting normalised field strength value equal to unity. The curve is calculated according to equations 1 and 2 with a field strength of 400 kV/m. In relation to the measured data, it is evident that the approximation is sufficiently conservative.

A change in the field strength shifts the curve in the horizontal direction. Owing to the flat characteristic in the high resistance range, an appreciable change in resistance is obtained only

when the resistance is already below 0.4 times its original value. The simplified relation, therefore, is not specifically sensitive to errors made in the assumption of the field strength, which is an advantage, taking into account the above mentioned uncertainties.

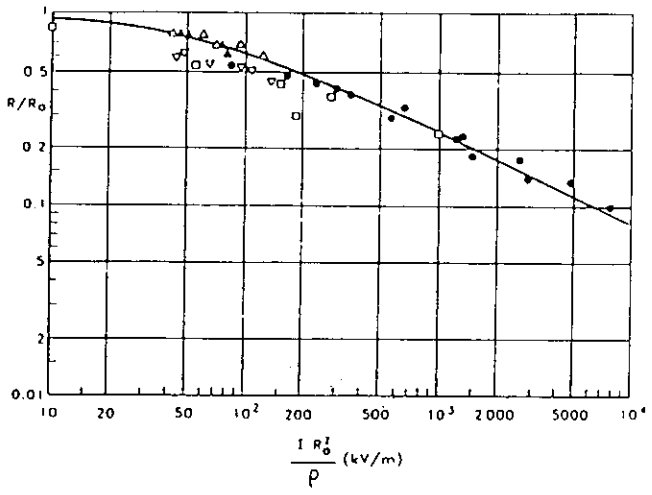

Fig 25 - Results and proposed simplification for rods.

The most important source of error lies in the determination of the resistance R_o, because the assumption of a constant soil resistivity may not be correct. The spread of results in Fig 25 corresponds to deviations in the assumption of soil resistivity of about 30% which could easily be obtained due to normal seasonal variations. In view of this, the proposed simplification is considered sufficiently accurate. It is, furthermore, in good agreement with the graphical simplification proposed in reference [70].

In those cases where it may be considered necessary to take the time dependence of the ionization into account the calculation has to be made numerically, taking an exponential decrease of each individual resistance fraction into consideration. This effort is justified only when all other parameters involved (eg, the upward bending lightning current front) are also carefully simulated. The time constant has been found to be in good agreement with reference [68] and to be about 2 μs.

The proposed simplification strictly applies to earth electrodes with small extensions. A maximum effective diameter of 30 m is estimated. In unfavourable soil conditions in which counterpoises with large extensions are required, the simplification will no longer be reliable. However, no measurements are available from which more adequate simulations could be deduced. Until such measurement results become available, for time-dependent calculations it is recommended to subdivide the earth electrode into suitable sections of 30 m extent, connected by leads, and to apply the simplified expression to each section, taking account of the appropriate time intervals and ionisation time delays where necessary. In many cases a propagation velocity of c/2 provides adequate accuracy.

5.5 Dielectric Strength of Air Insulation Under Non-Standard Lightning Impulses

5.5.1 Introduction

The wide variety of lightning stroke characteristics, together with the modification effects which the power system components have on the impinging current surges, stress the insulation structures in power systems with a diversity of impulse voltage wave shapes. While insulation co-ordination is usually based on impulse characteristics determined for standard impulse voltages (1.2/50 μs), it is important to be able to evaluate the performance of the insulation when stressed by non-standard lightning impulses.

Traditionally the withstand characteristics of air insulation under non-standard wave forms have been estimated with measured volt-time curves. In parallel with these, different type of analytical approaches have been developed. In the literature the following names have been used for these methods: "integration", "severity index" or "disruptive effect" method and "equal area" law. During the last 10 years, the increased knowledge of the physics of the breakdown process has been utilized to produce physical models (sometimes called leader propagation models).

This report summarises the main properties of the developed models and provides recommendations for the model to be used in the case of air insulation (including air gaps with insulators). Other gaseous insulations (such as SF_6) are not covered.

The report is based partly on a literature survey, and partly on the work done within the Working Groups 33.01 and 33.07.

5.5.2 Voltage/Time Curve

The voltage-time curve gives the dependency of the peak voltage of the specific impulse shape on the time-to-discharge. This curve is defined also in IEC-Publication 60-2, 1973. The voltage/time curves are readily determined experimentally for a specific gap or for an insulator string and may be represented with empirical equations - applicable only within the range of parameters covered experimentally [83].

However, empirical voltage/time curves bear little relation to the physical breakdown process. In practice, measurements can be affected by the following factors:

- impulse front shape (linearly rising versus double exponential),
- front times of the actually applied standard lightning impulse,
- gap distance and gap geometry,
- polarity and
- internal impedance of the impulse generator due to predischarge currents in the gap.

Amongst other disadvantages, the voltage/time curve generally connects together voltage and time values, which do not belong to the same instant. Also, for oscillating and other impulses, a suitable definition of the impulse shape to be used for voltage/time curves becomes difficult or even impossible. Therefore, the use of voltage/time curves to determine the dielectric strength of air gaps and insulator strings is restricted in general lightning modelling.

There are, however, special cases when the use of voltage-time curves can be advantageous. For example, in ref. [84] it is reported that the voltage/time curves for five wave-shapes on 3.36 m insulator string are within ± 4 % of the values computed for standard lightning impulse in the time-to-breakdown range from 1.5 μs to 3 μs. The "IEEE simplified backflash"-method, which is described eg. in ref. [25], takes advantage of this insensitivity to wave shapes by performing an overvoltage analysis at a fixed time of 2 μs.

At times-to-breakdown shorter than 3 μs, it is considered that non-standard impulse strength can be more than 10 % higher than the standard impulse strength. Therefore, more representative descriptions must be used for this type of application. The standard voltage/time curves do not apply to multiple flashover studies and their accuracy might be poor when low probability flashovers (ie, taking place on the tail of the surge), or long times to breakdown, are being studied.

5.5.3 Integration Methods

The basis of the integration (or severity index) methods is to develop an analytical withstand voltage prediction procedure, based on sparkover data obtained with standard impulse voltages, and then to predict the performance of the insulation as a function of one or more significant parameters of the non-standard voltage wave shape. The method was proposed in the fifties eg. by Witzke and Bliss, Jones, Akopian and Kind, [72-77]. Later, other workers have refined the method, eg. Darveniza and Huse, by determining the statistical dispersion of the empirical constants used in the integration method and by performing tests for typical line insulation configurations, [78, 81].

Kind had already developed his special case (the so called equal-area criterion) of the general integration method, on a partly physical basis by introducing the voltage dependence of the propagation velocity of leader in the air gap, [76]. Recently Darveniza and Vlastos have shown that even the general integration method is a model which can be explained on a physical basis, if the critical size of the electron avalanche necessary to produce any discharge at all is accepted as the criterion for the whole breakdown, [83].

The common basic assumptions for all the integration methods are that:

- there is a minimum voltage U_o which must be exceeded before any breakdown process can start or continue.
- the subsequent time to breakdown is a function of both the magnitude and the time duration of the applied voltage above the minimum voltage U_o.
- there exists a unique set of constants associated with breakdown for each insulator configuration.

In the most general formulation different weights can be given to the effects of voltage magnitude and time. The dielectric strength of the insulation is obtained then from the eq. (1)

$$D = \int_{t_o}^{t_c} (u(t)-U_o)^n \, dt \qquad (1)$$

in which t_o describes the time, after which the voltage u(t) is higher than the required minimum voltage U_o (also called reference voltage) and t_c describes the time to breakdown. The constant D is often called the disruptive effect constant.

Different proposals exist for the values of U_o, n and D, but each proposal refers to a particular set of results. Originally Witzke, Bliss and Jones encountered difficulties in selection of the constants and they found it more convenient to work with the simplification where $U_o = t_o = 0$, and n = 4.4. Kind also proposed a simplification by setting n = 1 and obtained the equal-area law. He could also experimentally show that the discharge voltage of the linearly rising voltage increases linearly with the square root of the steepness, a result which supports the equal-area law.

Later, the equal area law has been applied in several gap configurations typical for overhead lines and substations and usually describes the test results better than the simplification of Witzke et al. In [83] Darveniza reported that the best model for the result obtained with a eight unit insulator string was found when the following constants D/U_o were applied: 369 kV μs/643 kV for positive polarity and 525 kVμs/639 kV for negative polarity. The U_o-values were approximately 90 % of the corresponding 50% sparkover voltage. For horizontal rod-rod gaps, however, the U_o-values varied in the range 82...92 % of the corresponding 50 % sparkover voltage and D-values calculated per gap length in the range 3.8...5.6 kVμs/cm depending on the polarity and the gap length.

One of the problems of the equal-area law has been that for the non-uniform gaps, the value of the reference voltage U_o which gives the best conformity between the test results and the equal-area criterion, does not coincide with any of the usually measured 50% breakdown voltages.

Therefore a model based on the complete integration method has been proposed in [81] for suspension insulator strings. In the study 6, 9 and 12 unit strings were stressed with different impulses of double-exponential type, as well as with highly damped oscillatory impulses. The results showed that the best conformity between the test results and the model was obtained with values n = 2.25 and U_o = 58 kV per insulator unit. The model, although contradictory with some aspects of the equal-area method, has worked well also when applied to the results of other workers.

Although easy to use, a disadvantage of the integration methods is that they relate to specific geometries and voltage shapes, which can restrict their application. In an effort to eliminate this disadvantage, methods have been developed which attempt to take more exactly into account the various physical phenomena observed in the breakdown of air gaps under non-standard impulses.

5.5.4 Physical Model

The comprehensive analyses of the discharge development have confirmed that, from the qualitative point of view, despite the variety of impulse shapes and gap geometries the discharge development always consists of three different phases: corona inception, streamer propagation and leader propagation, [80, 82, 84-86]. The different phases are shown in Fig 26 for a double-exponential lightning impulse and a rod/rod gap.

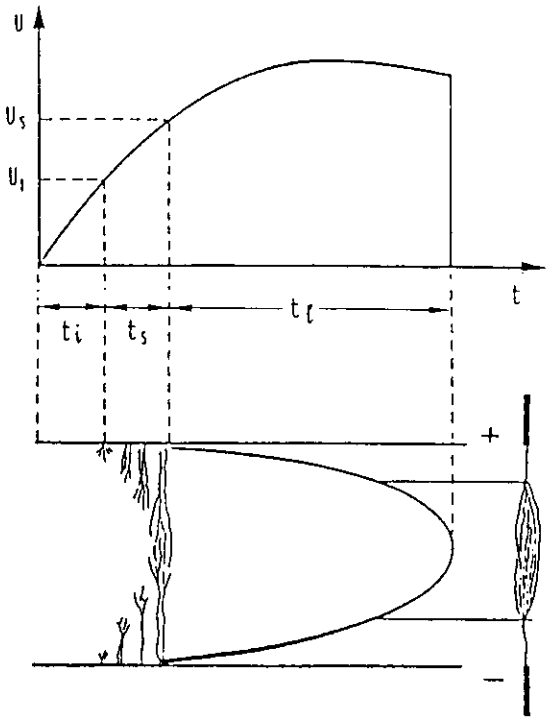

Fig 26 – Phases of discharge process.

t_i : corona inception time
t_s : streamer propagation time
t_l : leader propagation time.

When the applied voltage exceeds the corona inception voltage, streamers propagate and cross the gap after a certain time if the voltage remains high enough. The streamer propagation is accompanied by current impulses of appreciable amplitude. Only when the streamers have crossed the gap can the leaders develop to a significant extent. Usually the leader velocity increases in this phase exponentially. During the leader propagation, an exponentially increasing current can also be observed. Both the streamer and leader phase can develop from only one, or from either electrode. When the leader has crossed the gap or when the two leaders meet, the breakdown occurs.

Consequently the time-to-breakdown t_c can be expressed as a sum of three components:

$$t_c = t_i + t_s + t_l \qquad (2)$$

where t_i describes the corona inception time, t_s the time the streamers need to cross the gap or to meet the streamers from the opposite electrode, and t_l the leader propagation time.

Most studies on the gap breakdown have been performed with double-exponential type impulses (including linearly rising fronts). In Refs [82,85,86] it has been shown that the presence of oscillations or other abrupt changes in the applied voltage does not change the overall behaviour of the breakdown process. They can, however, disturb the leader propagation, causing breakdown development to be discontinuous, as the voltage can fall below that necessary for leader propagation. The result is a discharge where the leader propagates and stops at each cycle, as modulated by the presence of the oscillations.

5.5.4.1

Corona phase

Most of the practical air insulations involve relatively high non-uniform field distributions and their corona inception voltage is far below the breakdown voltage. Therefore, and taking into account also the high rate of rise of the applied voltage, the corona inception time can be neglected without introducing large errors.

5.5.4.2

Streamer propagation phase

The time t_s is usually computed as the time that the voltage takes to reach a fixed average field strength in the gap. The best streamer models have been developed for the positive polarity rod/plane gaps. Difficulties have been met when models have tried to take into account simultaneously the influence of the impulse shape and the gap geometry. Difficulties are also experienced when negative streamers are concerned, as in negative polarity rod-plane gaps or in rod-rod gaps, due to the composite structure of the negative streamer filaments or to the interaction of the different streamers. However, in Ref [85] it has been shown that independent of the polarity and gap configuration the time for the streamer propagation can be obtained indirectly through consideration of the gap factor and the gradient for positive and negative streamers. In addition, because t_s is only about 30% of the total breakdown time, a 20–30% error in its determination causes only about a 10% error in the calculation of the breakdown time t_c.

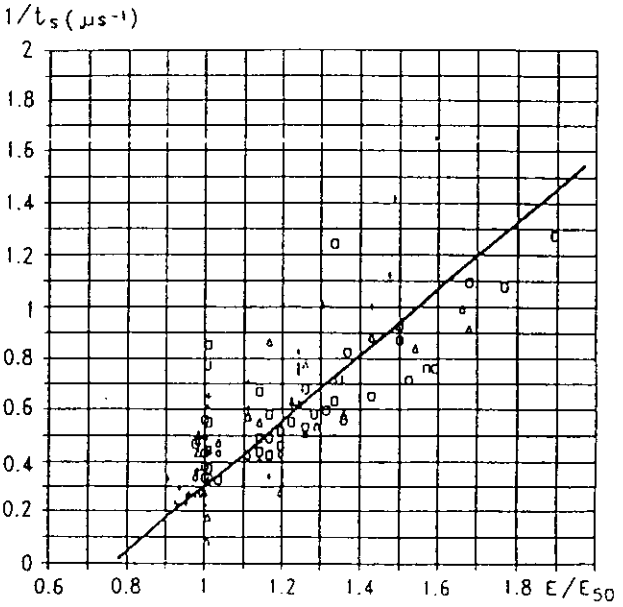

Fig 27 – Inverse streamer propagation time as function of the average stress in the gap.

The average stress is given in pu of U_{50} for a 1.2/50 μs impulse.

It is shown in Ref [85], that the most significant parameter influencing the streamer-phase duration t_s is the overstress in the gap, which can be expressed as the ratio between the maximum value of the average gradient reached in the gap before the breakdown (E), and the average gradient (E_{50}) at 50% flashover voltage U_{50}. With a good approximation, t_s may be assumed independent of the voltage polarity, the configuration characteristics and the gap clearance. Fig 27 illustrates the dependence of $1/t_s$ on the ratio E/E_{50}. On the basis of this figure the duration of the streamer phase in μs can be estimated with the equation.

$$1/t_s = 1.25\ (E/E_{50}) - 0.95 \qquad (3)$$

The E_{50} values for different gap configurations and polarities can be obtained with the help of Figs. 28a and 28b.

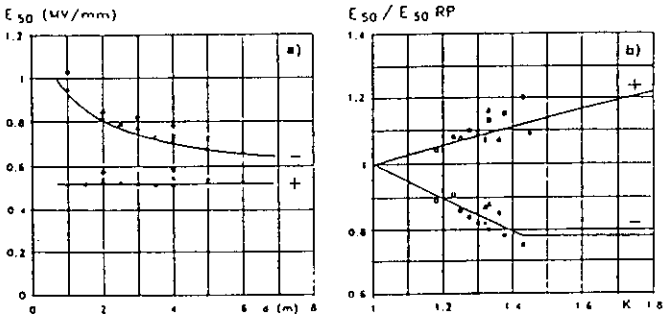

Fig 28 - Average gradient at 50% flashover voltage U_{50} in the gap.

a) Average gradient in the rod/plane gap as a function of the gap clearance (d).

b) Average gradient in the gap as a function of the gap factor. (Average gradient is given in pu of the values relevant to a rod/plane gap with the same gap length).

For geometries different from the rod/plane configuration, where two streamers are present, the resulting velocity of the streamer has to be interpreted as the average velocity of an equivalent streamer, which would cross over the same gap in the same time but starting from one electrode only.

5.5.4.3

Leader phase

The time for leader propagation is generally calculated on the basis of the knowledge of the velocity of the leader advance which depends on the applied voltage and leader length.

Various formulae have been proposed for the leader velocity. The experimental evidence shows that the leader velocity V_l increases inversely proportionally to the length of the gap which is not yet covered by the leader. Therefore the leader velocity can be described with formulae of the type:

$$V_l(t) = g[u(t),d_g]\ [u(t)-U_o(d_g-l_l)]/(d_g-l_l) \qquad (4)$$

Where g and U_o are some functions , d_g describes the gap length and l_l the leader length. u(t) is the actual voltage (absolute value) in the gap, which does not generally correspond to the theoretical value, due to the current flowing into the circuit.

The model described (as in the case of that for the streamer) considers an equivalent leader, which, for all geometries, propagates from one electrode only, across the gap with a propagation time equal to that of the actual leaders. The use of eq. (5) or (6) for the calculation of the leader velocity, implies that the leader progression stops if the average gradient in the unbridged part of the gap falls below the value E_o.

Ref. [85] gives a summary of the different models proposed. There it is also shown that for all the configurations examined the most satisfactory results are obtained with the help of eq. (5), (dimensions kV, m, m/s).

$$dl/dt = V_l \qquad (5)$$
$$= 170 d_g (u(t)/(d_g-l_l)-E_o)\exp(0.0015u(t)/d_g)$$

The values of E_o are obtained from Fig. 28 for the relevant polarity and geometry.

The constants for equation (5) relate to rod/rod air gaps however, and are thus not optimally applicable to other geometries.

As a practical simplification in reference [104] the formula

$$dl/dt = ku(t)[u(t)/(d_g-l_l) - E_o] \qquad (6)$$

was introduced as a "best-fit" to the voltage/time curves for standard lightning impulses. Contrary to the assumptions made in reference [86] however, the constants k and E_o have been found to be dependent on the gap configuration and insulator type. As guidance the following values apply to practical configurations:

Configuration	Pol	k $m^2V^{-2}s^{-1}$	E_o KVm^{-1}
air gaps, post and longrod insulators	+	$0.8 \cdot 10^{-6}$	600
	−	$1 \cdot 10^{-6}$	670
cap and pin insulators	+	$1.2 \cdot 10^{-6}$	520
	−	$1.3 \cdot 10^{-6}$	600

When the voltage/time curve for standard 1.2/50 lightning impulses is known, the best fitting constants may also be determined by numerical calculations for selected combinations of flashover voltage and time to breakdown, as in Chapter 6 (app 4), for example.

5.5.4.4

Leader current

The methods based on the physical approach allow the interaction between the breakdown process and the generating circuit to be taken into account. During the discharge development a current flows in the circuit so that the voltage applied at the gap is not the voltage from the unloaded generating circuit. The voltage drop is more pronounced the higher the overvoltages considered.

Reference [85] proposes the use of a simplified

linear expression of the type (7) for the estimation of the leader current.

$$i = qV_l \qquad (7)$$

q = charge per unit leader length (400 μC/m for practical gap configurations)

The estimate obtained of the leader current is inaccurate due to measurement problems. Inaccuracies are also caused due to the assumption on the basis of which the streamer propagation is assumed to be completed. Any possible further streamer delay after the instant the average gradient has reached the critical value, is included in the leader propagation time and may lead to inaccurate current calculations.

The error made, however, is not very significant, because errors in calculating t_c with high overvoltages are already much reduced when the voltage drop is estimated with any of the proposed models.

5.5.5

Conclusions and recommendations

The evaluation of discharge parameters should preferrably include a procedure for taking into account the circuit behaviour. This is essential when voltage/time curves have to be calculated, especially at high overvoltages. In the physical model the streamer phase can be considered with sufficient accuracy, through knowledge of the gap factor and the gradient for positive and negative streamers. In the case of negative polarity, the gradient depends also on the gap length.

Correspondingly, the leader velocity and leader current can be evaluated from the equations given above.

Despite the simplifications made, the physical model given by the equations (2)-(6) is valid for a large variety of impulse shapes and allows an accuracy generally better than 10 % for most configurations. The integration methods have comparable accuracies but more restricted application in relation to waveshapes. Based on the above, it can be concluded that no single approach alone can exclusively be recommended for all applications. The empirical methods can give a good accuracy when they are used within their validity limits; i.e. when specific data are used for a specific insulator or gap, together with a careful application of the empirical model. The use of voltage/time curves as recommended by IEEE, works well in the short time-to-breakdown domain (2-6 μs).

The physical model presented in section 4 has the greatest general validity and can be used in the evaluation of dielectric strength of a variety of geometries, provided the appropriate constants are correctly derived for the corresponding V/t curves.

As a general guide therefore, the leader-progression based simplification of equation (6) has proved to have adequate accuracy for most normal engineering calculations, and is recommended for such purposes.

In its given form, this yields an estimate of the 50% breakdown value. Statistical calculations may be addressed using the corresponding dispersion observed in E_o.

5.6 Impulse Corona Representation

5.6.1 Introduction

The effect of corona on overvoltage surges on lines has been known for many years and many of the fundamental assumptions still valid today have been known since 1937. The first important investigations on the subject were carried out by Skilling and Dykes [87], who stated that the effect of corona is due to the loss of energy necessary to form the corona space charge around the conductor and can be expressed by a time delay.

This time delay applies to the front of the impulse and the tail is assumed to be unaffected by corona. The applicability of the concept has been checked with measurements on a 250 m long artificial line and with measurements on real lines, by Brune and Eaton [88].

The second important series of investigations on the effect of corona was carried out in the 1950's, [89,90], from which, in particular, the line measurements by Wagner, Cross and Lloyd [90] still represent the most suitable source to check assumptions on corona effects. From analysis of these various results the following conclusions can be drawn:

- For positive surges and for sufficiently high voltages the corona effect is independent of the conductor size and geometry. Except for one conductor (24 mm diameter), the same applies for the negative polarity.
- For low voltages the curves differ due to the different corona-inception voltages.
- Weather conditions have no significant influence on the corona distortion.
- The coupling factor increases with increasing voltage values.
- The tail of the surges is not influenced by corona.

In addition, Wagner, Cross and Lloyd proposed to represent the time delay ΔT_c in the front of an overvoltage by

$$\Delta T_c/d=[(1+\Delta C/C)^{\frac{1}{3}}-1]/V \qquad (1)$$

Where $\Delta C/C$ is the slope of the Q/U curve at a given voltage, a quantity which has been called the "dynamic capacitance" by Gary and co-authors [92, 93]. They point out that ΔC is purely voltage dependent and the addition of this voltage-dependent capacitance to the geometrical capacitance can be used in analog or digital computer calculations.

The concept of the dynamic capacitance was also used by Gary, Dragan, and Cristescu [92, 93], giving in addition, quantitative dependencies [93]. With their definition Weck and Köster [94, 95] propose to describe the Q/U curves by

$$Q = [C_o + C_I + K(U-U_i)]U \qquad (2)$$

where

C_I = initial capacitance jump at U_i
C_o = geometrical capacitance
K = constant

Further investigations that should be mentioned are the line measurements by Inoue [96], because they report the only measurements on conductor bundles, the Q/U curve measurements by Garbagnati [97], because they cover a wide range of conductor geometries, and the coupling measurements by Gary e.a. [98], which represent useful additions to the line measurements of [90].

In the presented summary the following items are discussed:

- Determination of the corona inception voltage.
- Description of Q/U curves.
- Methods of determining the distortion of travelling waves on lines.
- Coupling due to corona; multiple-phase representation.

5.6.2 Corona Inception Voltage

The corona inception voltage U_i is determined by calculating the corona inception field strength on the conductor surface and from this the corresponding inception voltage. The corona inception field strength depends on the electrode curvature which can be described by [99-101]:

$$r_{eq} = E/-(dE/ds) \approx 2r_1 \cdot r_2/(r_1+r_2)$$

Where r_1 and r_2 are the two radii of curvature at the point of interest. For conductors the equivalent r_{eq} is equal to the conductor diameter d_c.

For the determination of the inception field strength the streamer approach has been considered most applicable [98]:

$$E_o = 2300\ (1 + 1.22/r_{eq}^{0.37})\ \text{kV m}^{-1}$$

with r_{eq} in cm

5.6.3 Charge Versus Voltage Curves (Q/U curves)

The three groups of investigators Wagner e. a. [90 91], Gary e. a. [92, 93] and Weck e. a. [94, 95] agree in the principal division of the Q/U curves into three parts

- Below corona inception the Q/U curve is a straight line determined by the geometrical capacitance.
- Above corona inception the Q/U curve shows an increased charge due to corona as long as the voltage increases.
- For decreasing voltages the Q/U curve again is practically determined by the geometrical capacitance.

For the description of the corona affected second part, three proposals exist:

- description by the energy loss [92, 93]
- description by the dynamic capacitance [90, 91]
- description by the corona capacitance [94, 95]

As the proposals are based on the same or similar measurements, they are equivalent. The proposal of references [94, 95], however, lends itself to easy application. The corona capacitance is obtained from formula (5):

$$C = Q/U = C_o + C_I + K\ (U-U_i) = C_o + C_k \qquad (5)$$

Figs 29 and 30 show two examples obtained from the results of references [92, 103, 105], which demonstrate sufficient accuracy of the linear approximation. Note that in this approximation the current obtained by

$$i = \frac{dQ}{dt} = \frac{dQ}{dU} \cdot \frac{dU}{dt}$$

(ie, the dynamic capacitance) is equal to

$$C_{dyn} = C_o + C_I - K_i + 2\ KU$$

The initial capacitance C_I is caused by the streamer onset mechanism and causes a jump in the capacitance, which is less than 1pF/m. Its determination is difficult, because it requires an accurate determination of the corona inception voltage.

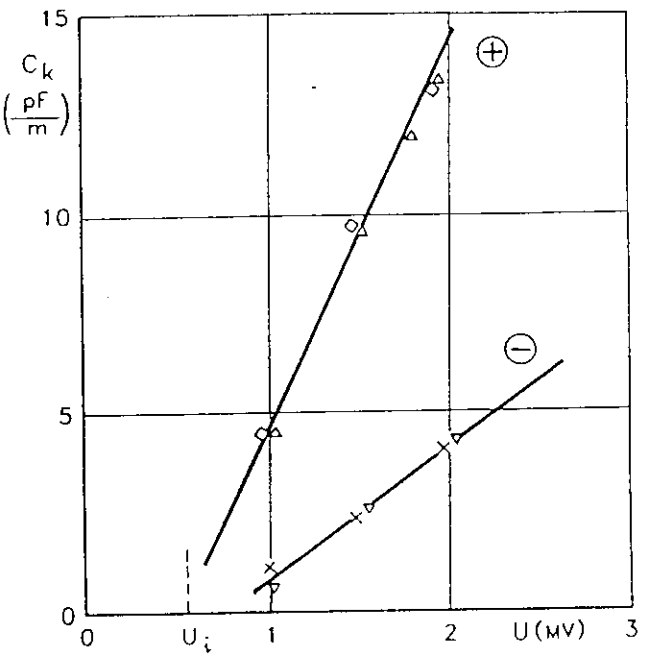

Fig 29 - Corona capacitance versus voltage amplitude; 65mm conductor diameter.

◇X) 1.2/50 impulse

△) 16/80 impulse

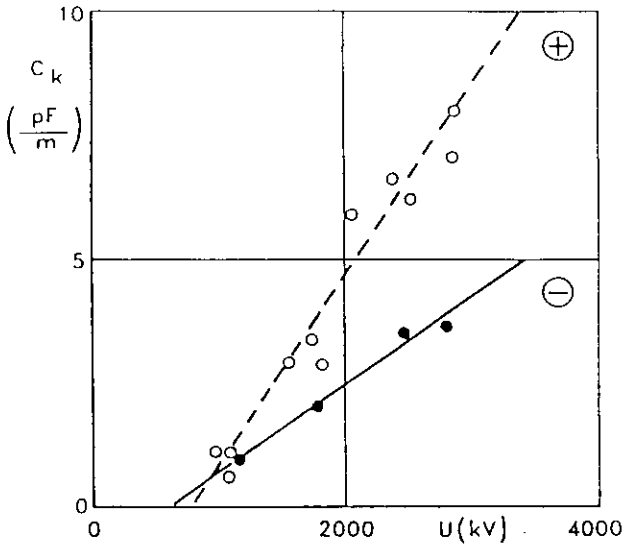

Fig 30 - Corona capacitance versus voltage amplitude: 3 x 31 mm bundle conductor.

o) 1.2/50; 10/100 and 250/2500
•) 1.2/50

The constants K for single conductors are given in Fig 31 dependent on the conductor diameter. Fig 32 shows the approximate dependence of the constant on the number of subconductors.

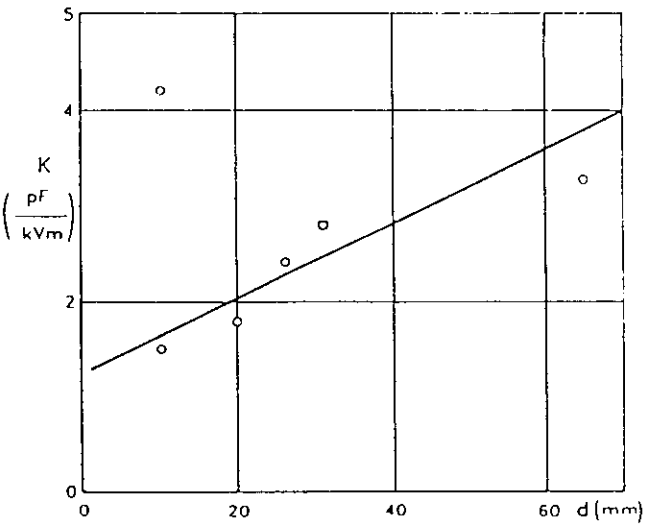

Fig 31 - Corona constant versus conductor diameter, positive polarity.

In reference [97] it is proposed to simplify formula (5) to

$$C_k = KU$$

above corona inception. For practical applications such a formula is useful; it is, however, too inaccurate for the description of Q/U curves and the constants derived from this approximation may differ considerably from those derived from formula 5.

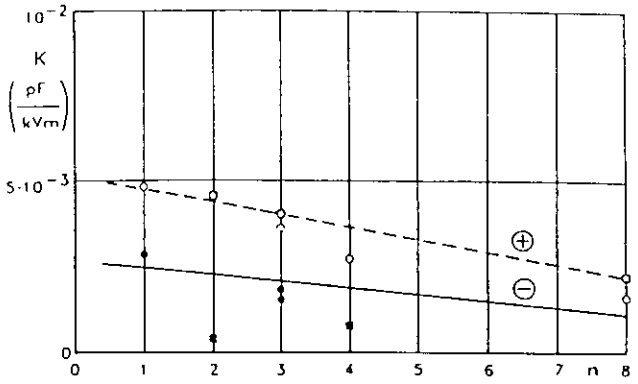

Fig 32 - Corona constant K versus number of subconductors; 31mm conductor diameter.

As impulse corona may make very large extensions, measurements from cages show higher corona than those made at high potential on lines. Therefore, such results from cages should not be used. As shown in reference [97] the height above ground has only little influence and an accurate simulation of the actual height in the laboratory is not necessary. In relating laboratory measurements to practical line situations, the basis should be in terms of corona-onset gradients. The applied voltage should, however, be sufficiently smaller than the breakdown voltage to avoid an accelerated streamer charge. This means that the applied voltage should not be higher than half the height above ground (or distance to earthed objects) multiplied by 500 kV/m, when the actual line dimensions are not maintained in the laboratory. The corona charge of a given conductor can then be determined by the following principles.

1. Below the corona inception voltage the charge is determined by the geometrical capacitance C_o.

2. When the voltage rises above the corona inception voltage, the charge is determined according to equation (5).

3. When the voltage drops, the charge is determined by the geometrical capacitance as in step 1. This situation persists as long as the voltage stays below the maximum value reached in step 2. If it further increases equation (5) is again valid.

5.6.4 Coupling Between Conductors

The increase of the coupling between the conductors due to corona has been reported by Wagner e. a. [90] for line measurements and by Gary e. a. [98] for short conductors in the laboratory. The coupling factor for the unsurged conductors is given by

$$K_c = U_2/U_1 = \{\ln[((H_1+H_2)^2+D_d^2)/((H_1-H_2)^2+D_d^2)]\}^{\frac{1}{2}} / \ln(2H_1/r_1) \qquad (6)$$

H_1 : height of the surged conductor

H_2 : height of the unsurged conductor

D_d : horizontal distance between conductors

r_1 : radius of surged conductor including corona

In equation (6) the denominator can be replaced by

$$\ln(2H_1/r_1) = 2\pi\varepsilon_o/C = 2\pi\varepsilon_o/(C_o+C_k) \qquad (7)$$

which leads to

$$K_c = (1/2\pi\varepsilon_o)\ln[(C_o+C_k)((H_1+H_2)^2+D_d^2)/((H_1-H_2)^2+D_d^2)] \qquad (8)$$

Since according to equation (5)

$$C_K = C_I + K\,(U-U_i)$$

the coupling factor increases linearly after corona inception.

Measurements on such short sections were carried out by Gary e. a. [98] at 16 mm ϕ, 31 mm ϕ and a 2 x 31 mm ϕ conductor. The results are reported as the ratio of the coupling factor to the geometrical coupling factor without corona. From formula 8 it follows immediately that this ratio is given by

$$K_c/K_g = 1 + C_K/C_o$$

above corona inception. Where K_g = geometric coupling factor (ie, eqn 6 with r_1 = conductor radius). A systematic difference between the various voltage shapes investigated is not present.

Owing to the large dispersion in available data, the initial capacitance C_I could not be evaluated. Therefore, the following summary of results relates only to the corona constant K.

Conductor Diameter mm	Corona Constants	
	K+ pF/kVm	K− pF/kVm
16	$5.4.10^{-3}$	$1.6.10^{-3}$
31	$4.8.10^{-3}$	$1.8.10^{-3}$
2 x 31	$4.4.10^{-3}$	$1.6.10^{-3}$

A comparison with the K-values determined from the Q/U curves shows good agreement with the exception of the negative 2-conductor bundle. Here as in the line measurements the corona behaviour is the same as for the single conductors.

As a conclusion it can be stated that the coupling between conductors can be determined from the geometry and from the corona behaviour of the conductor to earth. It could thus also be included in a travelling-wave calculation.

5.6.5 The Deformation of Travelling-Waves on Lines

Only a few measurements on lines exist:

- Single conductor lines
  Wagner, Cross, Lloyd [90]: 23.6, 41.9 and 50.8 mm ϕ conductor, height 15 m, distance between phases 9.8 m.
  Gary, Dragan, Cristescu [92]: 26.4 mm ϕ conductor, height 7.5 m (?), distance between phases 7 m.

  Inoue [96]: 25.3 mm ϕ conductor, height 22.2 m, distance between phases 11 m to conductor below, 14.8 m to conductor aside.

- Bundled conductors
  Inoue [96]: 2 x 25.3 mm ϕ bundle and 4 x 22.4 mm ϕ conductor, height 14 m, distance between phases 8 m to conductor above, 16.4 m to conductor aside.

The results were evaluated by Wagner e. a. using $\Delta T/d$ depending on the instantaneous voltage value. The curves are given in Fig 33. A comparison with the other measurements for single conductors shows that this adopted approximation holds true within the measuring accuracy. It can be seen that the curve approaches a linearly rising characteristic at high voltages, ie, the steepness of the overvoltage in this part is independent of the voltage value. This observation has been used by Weck [104] to determine the steepness of an incoming lightning surge by

$$S = \frac{1}{1/S_o + A \cdot d} \qquad (9)$$

where A is a function of the line geometry only.

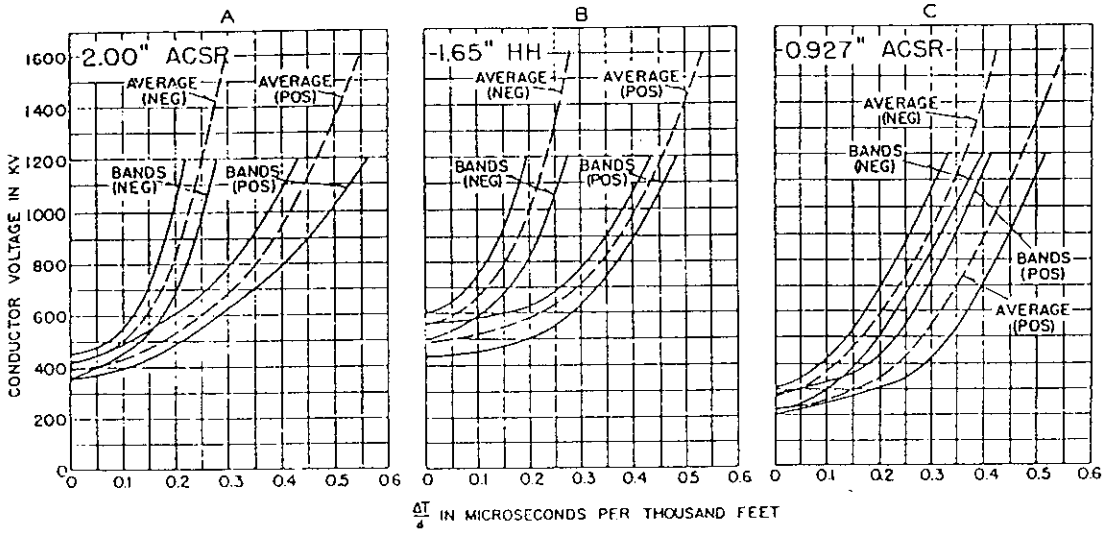

Fig 33 - Average $\Delta T/d$ curves for surges on single conductors for the three conductors tested. The bands show the variation in the construction curves (Reference [91]).

From the available data, as above, the following values for A have been derived:

Conductor	A_+ $\mu s/kVm$	A_- $\mu s/kVm$
23.6-26.4	8.10^{-7}	$8.6.10^{-7}$
41.9	$1.1.10^{-6}$	$4.6.10^{-7}$
50.8	$1.4.10^{-6}$	$4.1.10^{-7}$
2-bundle	$1.4.10^{-6}$	$6.5.10^{-7}$
4-bundle	$1.1.10^{-6}$	$6.5.10^{-7}$

Although these approaches may be advantageous for application, they must be carefully considered.

Firstly, the evaluation of steepness in some cases is very difficult. This results in a large dispersion of the results, as already shown in Figure 33 for the $\Delta T/d$ approach. Fig 34 shows an example of the evaluated steepness emphasizing the important negative polarity.

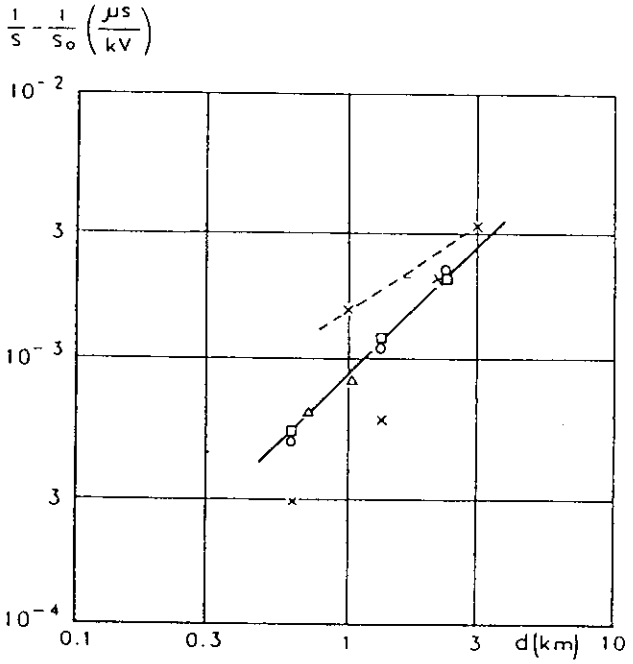

Fig 34 - Inverse steepness versus distance. 22-26 mm conductor diameter, negative polarity.

+ Wagner 800 kV X Gary 850 kV
o Wagner 1300 kV Δ Inoue 1650 kV
□ Wagner 1700 kV

It is interesting to note in the table above that the constant A_+ increases with increasing conductor radius. This has been already recognized for the corona constant K_+ in chapter 5.6.3. Fig 35 compares the constants dependent on the conductor diameter. They approximately follow the same trend.

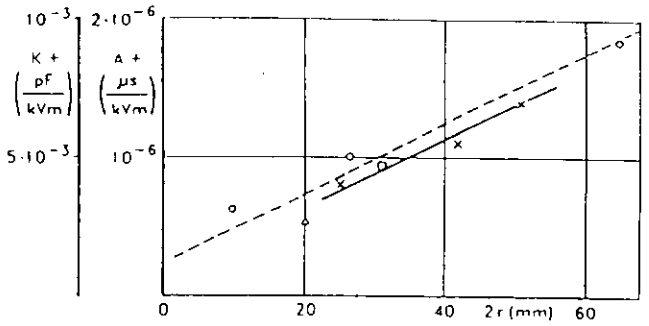

Fig 35 - Constants A_+ and K_+ versus conductor diameter, positive polarity.

x A_+ Wagner o K_+ Gary
□ K_+ Garbagnati Δ K_+ Weck

The ratio

$$\frac{A_+}{K_+} = 180\Omega$$

which is about half the surge impedance of the line. This is an important factor in establishing an equivalent corona model. It has to be observed, however, that the constant A_- does not follow the same law. It decreases with increasing conductor diameter, although the corona constant shows the opposite trend.

It is interesting to note that the ratio of the constants A_- for the conductor bundles to the small conductors is practically equal to the ratio of the surge impedances. For these small conductors the ratio

$$A_-/K_- \approx 400\Omega$$

which would correspond to the surge impedance of the line, approaching values less than half the surge impedance for the higher conductor diameters as for positive polarity. These uncertainties have to be kept in mind, when judging the applicability of models.

Concerning the time delay at the corona inception voltage, an obvious assumption is that at the instant of corona inception, the dynamic capacitance, provided by corona at U_i is added to the line capacitance. The evaluation of Wagners data gives the values:

Conductor mm ϕ		corona. cap at U_i $= C_i + K U_i$
23.6	+	3.9 pF/m
	-	2.2 pF/m
41.9	+	4.8 pF/m
	-	2.0 pF/m
50.8	+	4.9 pF/m
	-	2.3 pF/m

With the corona constant K evaluated as described above, one derives initial capacitances of 2 pF/m - 3 pF/m for positive polarity and of 0.6 - 1.7 pF/m

for negative polarity, the highest value belonging to the 23.6 mm ϕ conductor.

It must be specifically mentioned that bundled conductors differ from single conductors mainly in the time delay at the corona inception voltage. Starting from the single conductors this time delay decreases for the 2-conductor bundle and is practically 0 for the four conductor bundle. As far as further increase of the voltage is concerned, no additional systematic differences appear to exist between the single conductor and bundled conductor situations.

5.6.6 Modelling of Corona in Travelling-Wave Calculations

As shown by Gary [105] corona favours a quasi-cylindrical discharge around the conductor, which consists of distinct streamers with leader stems. This observation suggests the assumption that corona increases the capacitance of the conductor by increasing the current to earth without decreasing the inductance.

The realisation of this approach is to add a voltage-dependent capacitance to the line

$$C_{dyn} = C_I - KU_i + 2KU \qquad (10)$$

according to formula (6) neglecting the geometrical capacitance C_o, because it is already included in the travelling-wave concept.

As an example, Fig 36 shows calculated voltage shapes for the measurements of Wagner [90], 23.6 mm ϕ conductor, positive polarity. The line was matched with the geometrical surge impedance of 450Ω. Good agreement was reached for C_I = 3pF/m and K = 3.10^{-3} pF/kVm, both values being in agreement with those found in chapter 5.6.3. Evaluating the variation of the steepness with the travel length, a ratio of A+/K+ = 270 ohms is obtained, again in a reasonable agreement with the values found in chapter 5.6.5.

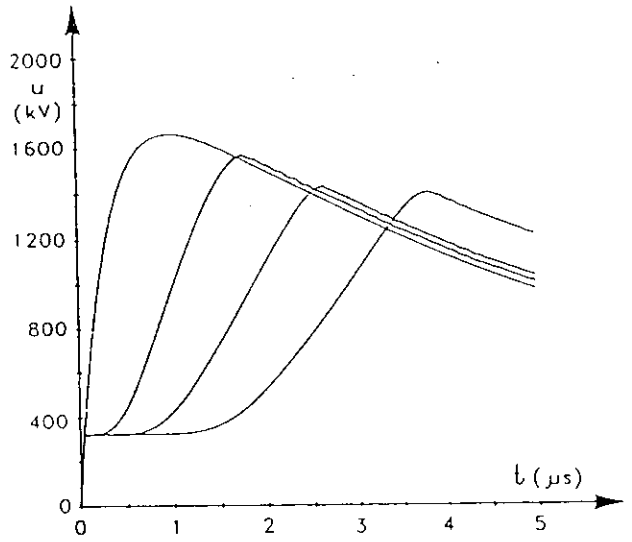

Fig 36 – Calculated voltage shapes after 620, 1300 and 2200m travel. Conductor diameter 23.6 mm, positive polarity.

When corona is modelled in a multi-phase calculation, the voltage dependence of the corona has to be transformed into a charge dependence, because corona depends on the dielectric field around the conductor. However, measurement on lines with voltages on several conductors are not available and, therefore, definite recommendations cannot be given.

5.6.7 Estimation of the Corona Deformation

The basic assumption for an estimation of the corona deformation of overvoltages on lines has already been given in reference [90]. It may be assumed that the travelling-wave velocity is decreased by the action of the dynamic capacitance owing to corona.

$$v = v_o(1 + C_K/C_o)^{-\frac{1}{2}} \qquad (11)$$

where

$$C_K = (C_I - KU_i) + 2KU \qquad (12)$$

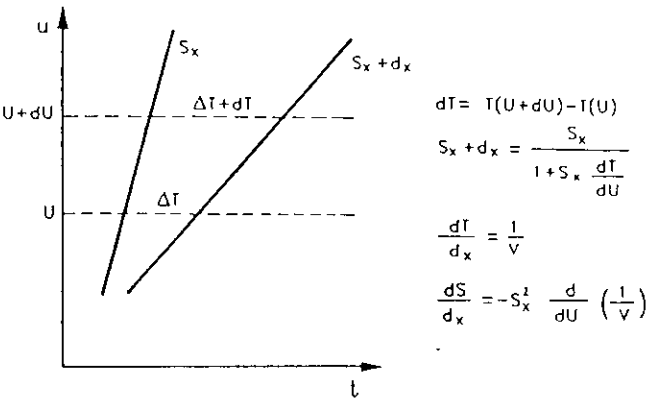

Fig 37 – Schematic steepness retardation.

The application of this concept to the steepness retardation (as illustrated in Fig 37) results in the dependence

$$\frac{dS}{dX} = -S^2 \; KZ_o(1+C_k/C_o)^{-\frac{1}{2}} \qquad (13)$$

With the approximation that $C_I - Ku_i$ is approximately equal to zero this formula changes into

$$\frac{dS}{dX} = -S^2 \; KZ_o(1+2KU/C_o)^{-\frac{1}{2}} = AS^2 \qquad (14)$$

The steepness change with the travel distance X depends on the voltage considered. For the example in chapter 5.6.6 with K = 3.10^{-3} pF/kVm, Z_o = 450 ohm, C_o = 7.4 pF/m and voltage values 400 kV and 1600 kV, the ratio

$$A/K = Z_o(1+2KU/C_0)^{-\frac{1}{2}} \qquad (15)$$

varies between 390 and 300 Ohm with an average of 330 Ohm.

When A is considered to be approximately constant, equation (14) can be integrated and results in the distance dependence of the steepness given in formula 9. Furthermore, the effect of the voltage increases, the higher the corona constant K. This supports the observation made in chapter 5.6.5 that the ratio A/K decreases with increasing conductor radius in negative polarity and that it is smaller for positive polarity than for negative. The approximations proposed by Wagner [90] and by Weck [95] are, therefore, consistent with each other.

As a conclusion it can be stated that for a known conductor geometry the corona constant K can be estimated from Fig 31 and Fig 32. With the voltage level known, the constant A can be determined from formula 15 and the steepness retardation with the travel distance on the line is given by formula 9.

6. THE BACKFLASH

6.1. Introduction

A lightning stroke, terminating on the shield wires, creates waves of current and charge which produce potential differences across the line insulation. If the potentials exceed the line insulation strength, flashover occurs. This event is called a backflash (or backflashover) and the number of flashovers per 100 km per year is defined as the backflash rate or BFR.

The purpose of this chapter is to present the essential background and the general concept of the backflash event and to provide guidance not only to the practising engineer but also to the investigator. Equations and curves are provided to permit an estimination of the required insulation strength and footing resistance for a new design, or alternatively, to permit an assessment of an existing design. Consistent with the rest of this report, this chapter concentrates upon the more important negative downward flash.

6.2. Background

1. In 1950, measurements of currents on transmission line towers were assembled into a "AIEE statistical distribution", having a median of 15 kA and a log standard deviation of 0.98. Using this distribution and assuming a 2μs linear front of the stroke current, Harder and Clayton [106] produced curves to estimate the BFR. This was followed by an AIEE Committee Report [107] in which the authors changed the front assumption to 4 μs since the 2μs front resulted in more midspan flashovers than was justified by field data.

2. Field theory was invoked to provide a detailed analysis of the shield-wire/tower/phase-conductor system [108-112]. Lundholm, Finn, and Price [109] developed the "loop-voltage" method to determine potential differences across the line insulation. Wagner [110-111] applied this method to show that travelling wave theory could be used to approximate the results of field theory provided that the artifice of a surge impedance be employed to represent the tower. He further calculated the voltage produced across the insulation caused by the charge in the channel above the tower and suggested that this component may exceed that produced by the current and charge injected into the tower.

3. Wagner [113-114] also investigated predischarge currents (those which are a precursor of the breakdown process), and noted that the current shape is similar to that of the lightning stroke current and that these currents could inhibit flashovers. He noted further that these predischarge currents may be responsible for the apparent lack of midspan flashovers.

4. Fisher, Anderson, and Hagenguth used reduced-scale models of the system (called nanosecond models) to obtain the response of the tower-shield wire system [115]. Monte Carlo methods were then used by Anderson to determine the BFR [116]. In this study Anderson employed new distributions for both the current and the time-to-crest. The stroke current distribution was piece-wise log-normal, having a median of 46.5 kA and log standard deviations of 0.71 for currents below the median and 0.41 for currents above the median. The distribution of time-to-crest had a median of 1.57 μs and a log standard deviation of 0.60.

5. During the following years, new methods of estimating the BFR's were devised by several investigators taking into account the results of the above investigations but with the overriding practical principle to produce methods which would agree with field experience. In 1964, Clayton and Young [117] reformed the previous estimating method [106] using the AIEE current distribution but employing a relationship between the crest current and wave fronts of 2, 4, and 6 μs. Anderson, Fisher, and Magnusson [118] and Anderson [24] furthered their earlier work producing a comparative method which employed the results of reduced-scale model tests and the current and time-to-crest distributions as mentioned in the preceding paragraph. Sargent and Darveniza [119] developed a method to estimate both the single and double-circuit BFR's and applied these to evaluate alternative designs [120]. For this method they also used the AIEE current distribution and the crest-current/time-to-crest relationship of Clayton and Young.

6. During this period, the results of more extensive measurements of lightning parameters were becoming available. Spzor [121] showed that Polish records indicated median currents of 30 kA, Popolansky's [122] records showed median currents of 25 kA, and Berger's [23,20] results gave a median of 31 kA and a log standard deviation of 0.46. The use of these results, as shown by Ah Choy and Darvenzia [123] produced BFR's which exceeded those previously calculated by over 200 percent.

7. Ah Choy and Darvenzia [123] analyzed the effect of the charge in the stroke channel as first discussed by Wagner. Assuming a finite length of an upward streamer, as opposed to zero length, decreased the voltage across the insulator by up to 100 percent. However, the voltage still represented 17 to 28 percent of the insulator strength. A discussion of this paper by Giudice and Piparo showed results of their investigation which indicated further reductions in voltage. Therefore, this component of voltage has been neglected in all estimating methods.

8. In 1982, with the recognition of the revised stroke current distribution, Anderson [24] produced a new estimating method using a constant 2 μs front. This method with minor modifications was adopted by the IEEE working group and published as the IEEE method [25].

As noted in this brief background, significant advances have been made in both the theory of calculation of the BFR and in the practical application of this theory to produce estimating methods. To a significant degree these developments were a result of attempts to explain the high flashover rate of the AG&E/OVEC 345-kV double circuit line (see Chapter 4). However, of equal importance, the maelstrom of activity was a result of the new lightning crest-current distributions which required alterations and reformation of estimating methods.

6.3 The General Concept

A lightning stroke terminating on the shield wire, Figure 38, creates waves of current and voltage which travel along the shield wire. At the tower, or at any point of impedance discontinuity, these waves are

reflected back toward the stroke terminating point and are transmitted down the tower and outward on the shield wire to an adjacent tower. Travelling with these voltages and currents are coupled voltages on the phase conductor. This process of reflection and transmission continues and voltages are produced (1) across the air insulation within the span and (2) across the air insulation or the insulators at the tower.

The highest potential differences occur at the stroke terminating point and decrease as a function of the distance from this location. In contrast, the maximum insulation strength occurs at the midspan; the minimum at the tower. Thus, the flashover location, either within the span or at the tower, is dependent on the comparison of the potential differences caused by the stroke to the insulation strength. As shown in Appendix 3, flashovers within the span are possible but are insignificant compared to flashovers at the tower. Thus, for the usual situation, in which the shield wire to conductor clearance is much greater than the tower insulation length, span flashovers may be neglected and only flashovers at the tower need be considered.

The maximum voltage produced across the tower insulation occurs for a stroke terminating at the tower. Thus, only considering this event would produce a BFR which exceeds the BFR if all stroke terminating points are evaluated. An analysis of this is presented in Appendix 3 where it is shown that if all stroke terminating points are considered, the BFR of the line is approximately 60% of the BFR if only a stroke to the tower is assumed. Thus the problem of calculating the BFR is considerably simplified.

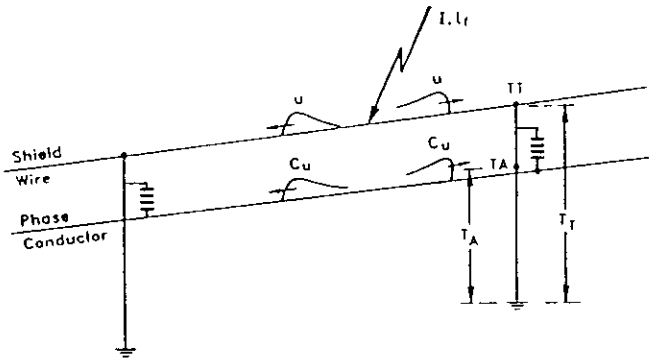

Fig 38 - General concept of backflash.

6.4 Stroke to Tower

As shown in Appendix 1, for a stroke terminating at the tower, the surge voltages produced at location TA Fig 38 on the tower directly opposite the phase conductor may be characterized as shown in Fig 39. The initial voltage, U_A, and the voltage decrease from the crest, U_{TA}, to the voltage, U_R, are caused by the tower. The time-to-crest of the voltage, U_{TA}, occurs at the time-to-crest of the stroke current. The voltage decrease on the tail of the surge, caused by reflections from adjacent towers, may be defined by the time constant, τ, as derived in Appendix 2. The voltage, U_R, is primarily caused by the tower footing resistance.

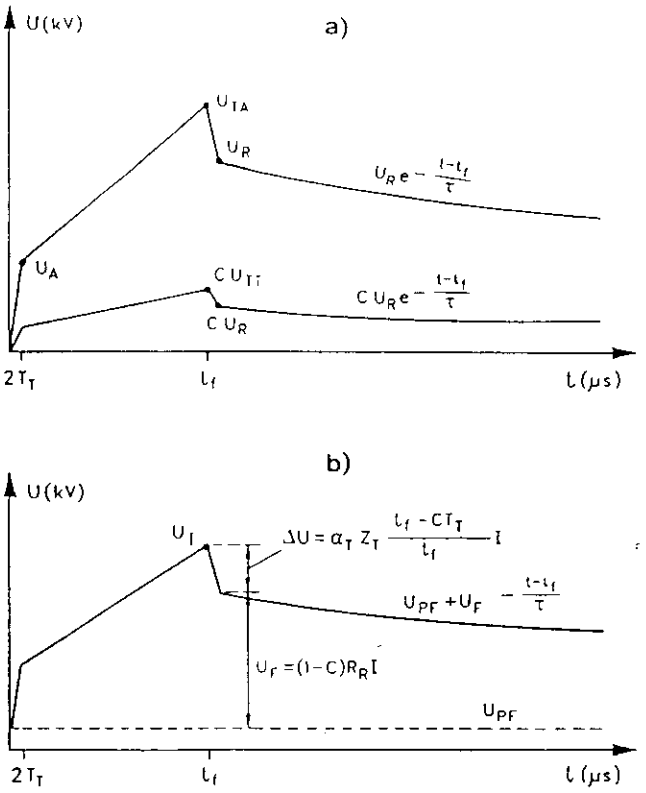

Fig 39 - Voltage for linearly rising front of stroke current.

a) Surge voltages on tower opposite phase conductor.

b) Voltage across the tower insulation.

Reflection from adjacent towers may also decrease the crest voltage provided the time-to-crest of the voltage, t_f, is greater than twice the travel time along the span to the adjacent towers. This effect of the possible decrease in crest magnitude is also considered in Appendix 2 and a multipling factor, K_{SP}, is derived so that the resulting crest voltage becomes K_{SP} times the original voltage.

The surge voltage on the phase conductor, also shown in Fig 39, is simply the coupling factor, C, times the voltage on the shield wire at the tower-top.

The voltage across the air clearance or across the insulator string, Fig 39, is composed of the difference in the surge voltages of Fig 39 plus the power frequency voltage, U_{PF}, which exists on the phase conductor at the time of the stroke. Usually the value of this voltage is assumed to be the average value of 0.83 times the crest value of the line-to-neutral phase voltage. (See Section 6.9 for a further discussion.)

Crest voltage, U_I, is:

$$U_I = IK_{sp}\left[R_i(1-C)+\alpha_T Z_T(T_A-CT_T)/t_f \right] + U_{pf} \qquad (1)$$

where T_T and T_A are the travel times to points TT and TA on the tower (Fig 38), Z_T is the tower surge impedance, and α_T and R_e are defined as:

$$\alpha_T = (Z_T - R_i)/(Z_T + R_i) \qquad (2)$$

$$R_e = Z_g R_i/(Z_g + 2R_i)$$

where R_i is the impulse- or current-reduced tower footing resistance and Z_g is the surge impedance of the shield wires. From Chapter 5,

$$R_i = R_o(1 + I_R/I_g)^{-\frac{1}{2}} \qquad (3)$$

$$I_g = E_g \rho/2\pi R_o^2$$

where R_o is the measured or low current tower footing resistance, ρ is the soil resisitivity, I_R is the current through the footing resistance, and E_g is the soil breakdown gradient of 400 kV/m.

To obtain the critical current, I_c, defined as the current at and above which flashover occurs, the critical flashover voltage for the waveshape of the voltage of Fig 39 must be known. Using the leader progression model, a regression equation is presented in Appendix 4 which permits the estimation of the critical flashover voltage, U_{50NS} (or the permissible crest of the voltage, U_I), in terms of the standard lightning impulse critical flashover voltage, U_{50}. Therefore, from equation 1, the critical current becomes:

$$I_c = (U_{50NS} - U_{PF})/K_{SP}[R_e(1-c) + \alpha_T Z_T(T_A - CT_T)/t_f] \qquad (4)$$

The BFR is the probability of exceeding this current multiplied by the number of flashes to the line, N_L, times 0.6 to take account of the span effect (Appendix 3). However, since the voltage, U_I, and the non-standard critical flashover voltage, U_{50NS}, are both functions of the time-to-crest of the stroke current, the critical current of equation (4) is a variable. Therefore, the BFR considering all times-to-crest is:

$$BFR = 0.6N_L \int_0^\infty \int_{I_c}^\infty f(I/t_f) f(t_f)\, dI\, dt_f \qquad (5)$$

where $f(I/t_f)$ is the conditional probability density function of the stroke current given the time-to-crest and $f(t_f)$ is the probability function of the time-to-crest.

As noted in Fig 38, only one phase of the line is considered. However, in principle, all phases should be considered. That is the critical current should be determined for each of the phases and the lowest critical current should be used in equation 5. See Section 9 for a further discussion.

Before dealing further with the above equation, the actual stroke current waveshape is examined in the following section.

6.5 Stroke Current Waveshape

The preceeding equations and the voltages as shown in Fig 39 are developed for a linearly rising front of the stroke current. However, the front of the first stroke current is concave upward which may be approximated by the equations developed in Chapter 5. This formulation of the wavefront produces the tower-top voltage as shown by the solid line curve of Fig 40 for a 100kA stroke having a median value of the minimum equivalent front (t_m) of 2.7μs and a median front defined by the 30%/90% points of 6.0 μs. The dotted line curves show the voltage as produced by linearly rising fronts for time-to-crest equal to these wave fronts. As noted, the actual crest voltage lies approximately between the crest voltage for the two linear fronts. Therefore, the use of the minmum equivalent front represents a conservative approximation and is used for further study.

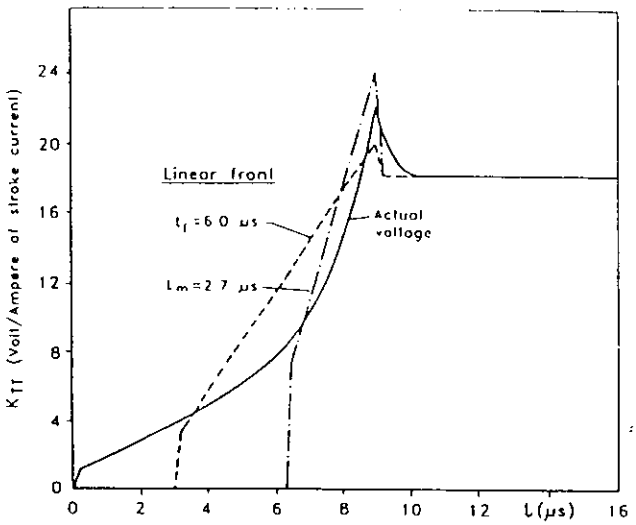

Fig 40 - Comparison of tower-top voltage for a concave upward front having a median value of time-to-crest for 100 kA first stroke with tower-top voltages for a linearly rising front. Minimum equivalent front of 2.7 μs. Median 30/90% front of 6.0 μs.

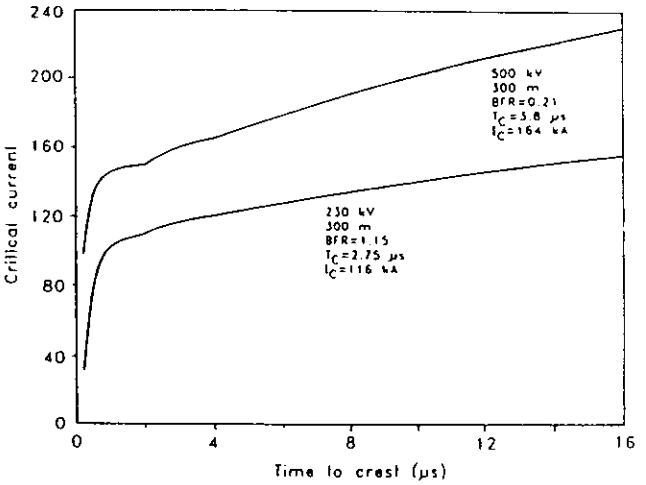

Fig 41 - Critical currents for 230 kV and 500 kV lines of Fig 42.

6.6 Effect of Wave Front on the BFR

Returning to an examination of equation 5, the critical current as a function of time-to-crest is presented in Fig 41 for a double-circuit 230kV line and a single-circuit 500kV line whose parameters are given in Fig 42. The resultant BFR from equation 5, is also shown on the curve. This same value of BFR can be obtained by use of a single front, T_e, also shown on the curves which results in the critical current as indicated. As may be expected from statistical considerations, these fronts, T_e, are approximately the median fronts for the critical currents, which, as obtained from Chapter 3, are presented in graphical form in Fig 43.

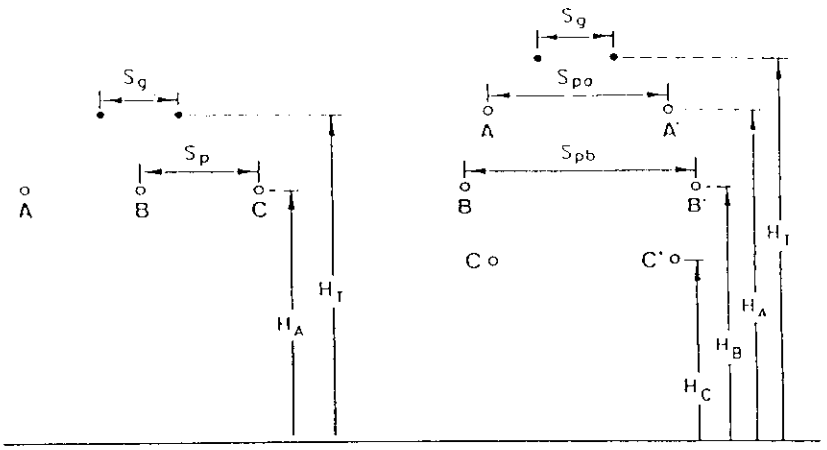

Characteristics of Typical Lines
(Distances in meters)

A Double-Circuit Lines

System Voltage kV	H_T	H_A	H_B	H_C	S_g	S_{po}	S_{pb}	Z_g	C_A	C_B	C_C
115/138	25	21.3	17.7	14.1	3.5	6.7	8.5	370	.360	.262	.199
230	35	29.5	24.1	18.7	5.0	8.5	11.0	379	.350	.248	.183
345	40	32.4	25.1	17.8	6.8	11.0	15.0	378	.321	.215	.147
*230	35	29.5	24.1	18.7	0	8.5	11.0	600	.223	.158	.116
**230	70	64.5	59.1	53.7	5.0	8.5	11.0	421	.420	.335	.283

* Single Shield Wire
** Used for sensitivity study

B Single-Circuit Lines

System Voltage kV	H_T	H_A	S_g	S_p	Z_g	C_A	C_B
115/138	17	13.5	4.5	4.2	339	.278	.313
230	20	15.6	6.0	5.5	340	.264	.301
345	20	14.0	7.6	7.2	334	.238	.283
500	25	17.0	14.0	9.0	329	.232	.253
765	30	18.0	18.0	13.0	333	.188	.213

Fig 42 - Parameters of typical lines. All shield wire diameters are 6.35 mm.

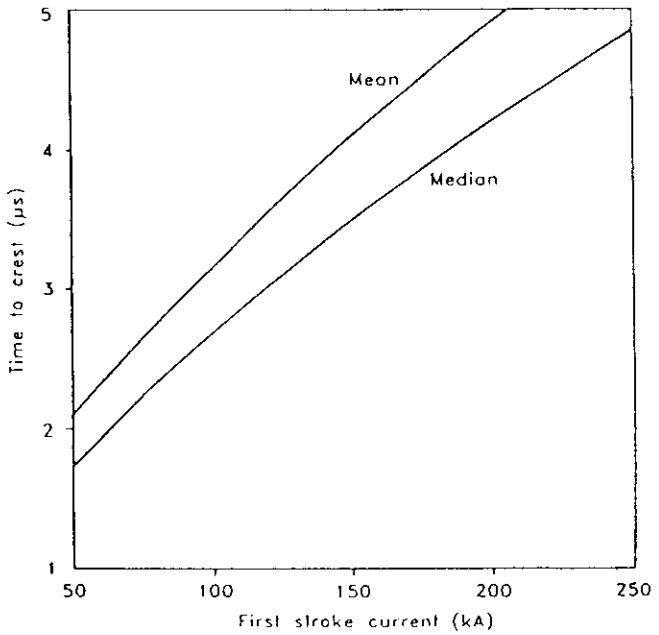

Fig 43 - Median and mean values of time-to-crest (minimum equivalent front) given the stroke current.

Since a single equivalent front may be used to obtain the BFR, equation 5 is reduced to:

$$BFR = 0.6N_L \int_{I_C}^{\infty} f(I)\, dI = 0.6N_L P(I_C) \qquad (6)$$

where $P(I_C)$ is a convenient notation for the integral.

The front to be employed for equation 6 is the median front as per Fig 43. This requires an iterative solution since the current and front are dependent variables. From Fig 43, it is to be expected that for lower voltage lines having lower critical currents, fronts of 2 to 2.5 μs are appropriate whereas for higher voltage lines, fronts of 3 to 5μs are indicated.

In calculation of the critical current of Fig 41, all phases with their attendent coupling factors and heights were considered. For example, for the 230-kV line, for fronts less than 0.5 μs, flashover occured on the top phase. As the front increased, flashovers occurred on the middle phase and for fronts greater than 0.8 μs, flashovers ocurred on the bottom phase, the phase with the lowest coupling factor.

Therefore, since the equivalent front greatly exceeds 0.8 μs, the coupling factor to be employed in use of equation (6) is the lowest one; that for the bottom phase for a line having a vertical phase configuration or the outermost phase for a line having a horizontal phase configuration.

Note, for the purposes of this analysis, the leader progression model of Appendix 4 was maintained using a positive polarity critical flashover gradient of 560kV/m, together with a constant soil breakdown gradient E_g = 400 kV/m.

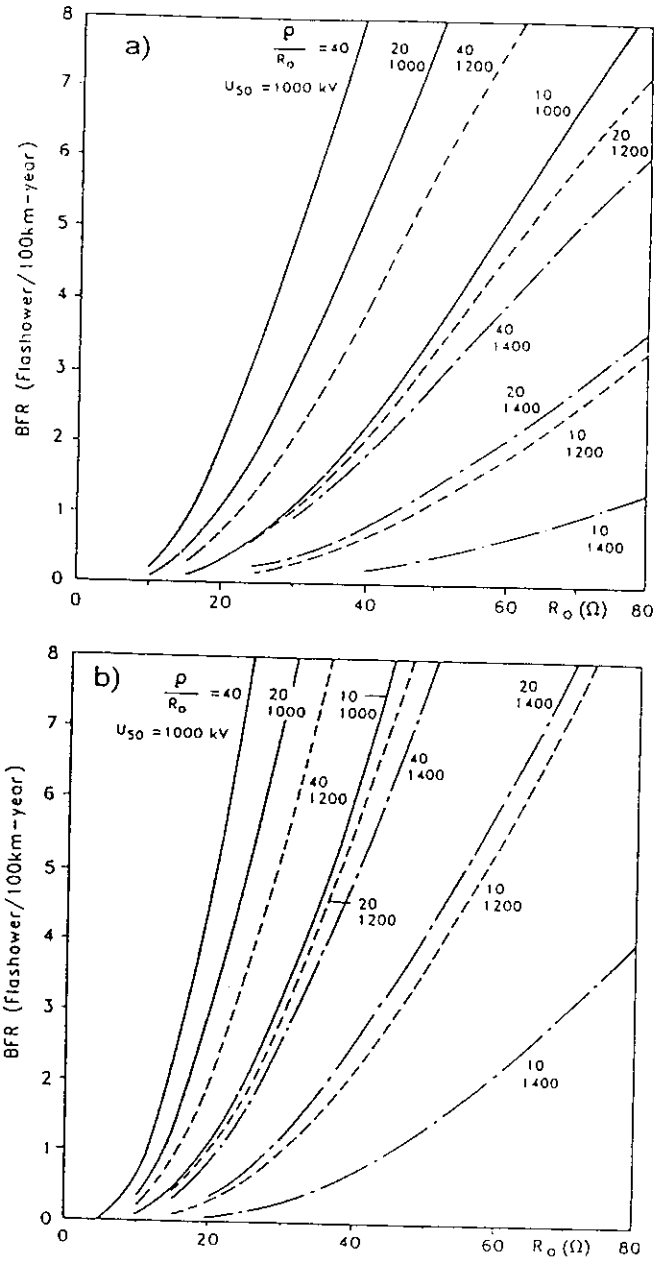

Fig 44 - Estimation of the BFR.
Span length of 300 m, N_g = 4.

a) 230 kV single-circuit line of Fig 42.

b) 230 kV double-circuit line of Fig 42.

6.7 Sensitivities

The BFR of a double-circuit 230-kV line and a single-circuit 230-kV line whose parameters are given in Fig 41 are presented in Fig 44 as a function of the normally measured low current resistance, R_o, with the ratio ρ/R_o and U_{50} as the parameters. As shown in Fig 45 for one case, the time-to-crest varies between 2 and 5 μs, the impulse resistance is about 50% of the low-current value, and $\Delta U/U_F$ (as defined in Fig 39) is limited to a value of 0.3. This portrayal of results indicates that for this case, the tower component of voltage may be minor.

The curves of Fig 44 use the surge impedances and coupling factors unmodified by corona. Also, no additional effect of grounding inductance as discussed in Chapter 5 is included. This latter effect could imply on an apparent increase in tower height of up to about 100 percent.

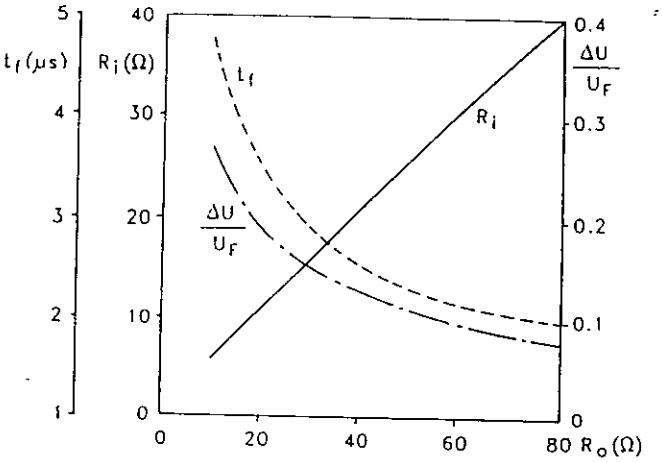

Fig 45 - Variation of parameters for 230 kV single-circuit line of Fig 42(a).
U_{50} = 1200 kV; ρ/R_o=20; N_g=4.

To assess these effects, (1) the coupling factor was increased by 10 % and the shield-wire surge impedance was decreased by 10% and (2) the tower height was increased by 50 %. The results are portrayed in Fig 46 where the base curve is that taken from Fig 44. As noted, these two effects are somewhat cancelling. The increase in tower height increases the BFR while the increase in coupling factor and the decrease in shield wire surge impedance decreases the BFR. For the single-circuit line, the increase in coupling factor is dominant. However for the double-circuit line, since a tower height increase of 50% represents a larger absolute value of tower-height increase, the two effects are about equal.

To assess the sensitivity to the tower component of voltage, the tower was neglected. The resultant curve is shown by the dot-dash line in Fig 46 illustrating that the principle voltage component is that caused by the footing resistance. To provide a further assessment of the tower component, the tower height was increased to 70m for the double-circuit 230-kV tower. The results are presented in Fig 47 where again the base curve is that taken from Fig 44. The other solid line curve includes the tower component of voltage while the dotted line curve neglects this component. In explanation, as the tower height increases, the surge impedance of the shield wire increases and the coupling factor

increases so as to lower the BFR. However, the tower component of voltage increases and the number of strokes to the line increases tending to increase the BFR. The result, as shown, is an increase in the BFR. For this case, neglecting the tower shows that the tower component is the dominant effect for this incremental change in performance.

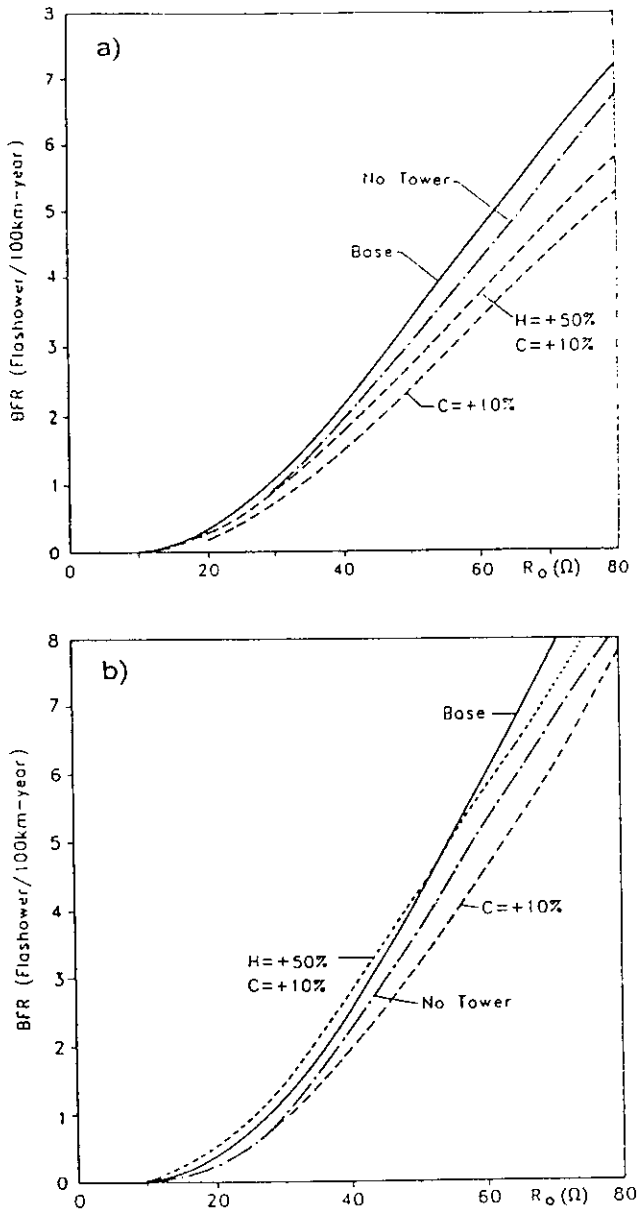

Fig 46 - Effect of increase in coupling factor, C, caused by corona and increase in apparent tower height, H, to represent inductive grounding effects. Also effect of the tower component of voltage. 300 m span; ρ/R_0=20; N_g=4.

a) 230 kV single-circuit line, U_{50} = 1200 kV.

b) 230 kV double-circuit line.

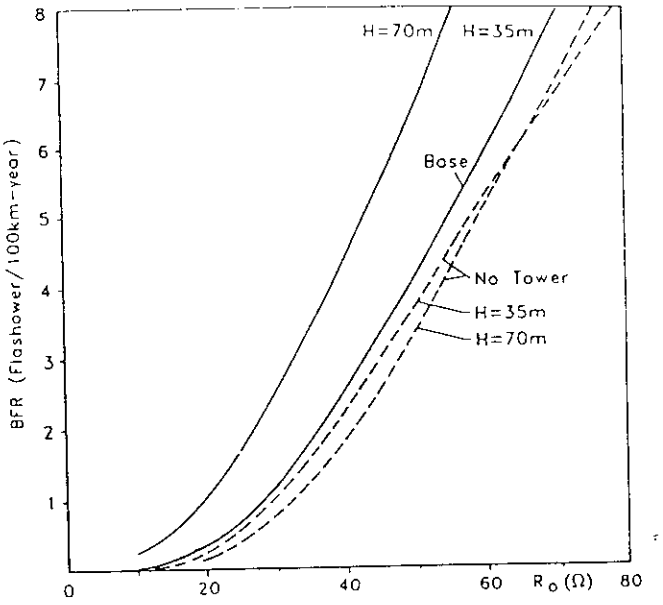

Fig 47 - Effect of tower height. 230 kV double-circuit line. ρ/R_o = 20, 300 metre span, U_{50} = 1400 kV, N_g = 4.

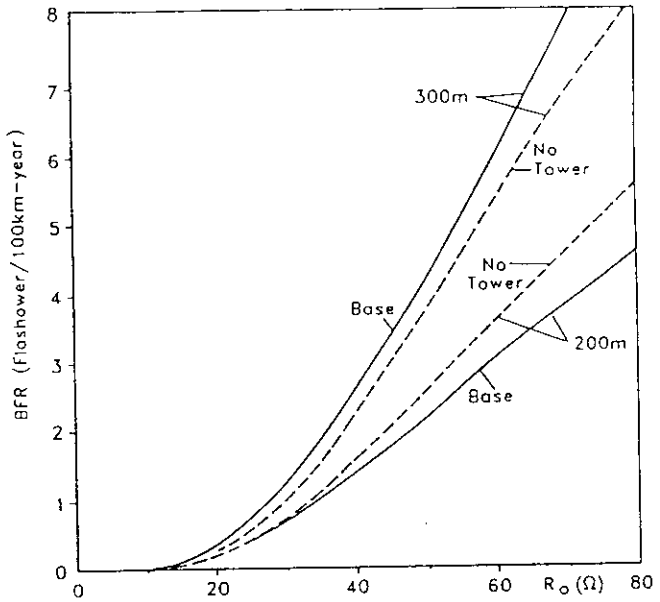

Fig 48 - Effect of span length. 230 kV double-circuit line. ρ/R_o = 20; U_{50} = 1400 kV; N_g = 4.

The effect of span length is shown in Fig 48. The "no tower" curves are those for which not only is the tower neglected but the effect of the decrease in crest voltage caused by adjacent spans, the factor K_{SP}, is also neglected. As noted, the dotted line curves provide an acceptable approximation.

6.8 A Further Simplification

From the observations of sensitivities, a further simplification can be made in the equations to estimate the BFR. For tower heights less than about 50 m , both the tower component of voltage and the factor, K_{SP}, can be neglected, thus simplifying the equation for the non-standard critical flashover voltage to:

$$U_{50NS} = (0.977 + 2.82/\tau)U_{50} \quad (7)$$

where τ = time constant of the surge voltage tail in which the small correction for U_{PF} has also been neglected. As displayed by this equation, the voltage is not significantly effected by the time-to-crest. Also the critical current becomes:

$$I_c = (U_{50NS} - U_{PF})/(R_e\ (1-C)) \quad (8)$$

Equations 7 and 8 correspond essentially to the simplified approach presented in reference [124].

6.9 Discussion

6.9.1 BFR Design Value

No universal agreement exists as to the recommended design value of the BFR since this is not only a function of economics but also of the total utility system design. However, customer reliability requirements are becoming more stringent and in some locations, the lightning-tripout design values have decreased. As discussed in Chapters 1 and 4, the total lighting tripout rate, the sum of the shielding failure flashover rate and the BFR, combined with the probability of a successful reclose operation should be the design goals.

6.9.2 Calculating the BFR

Calculating the BFR is an iterative process. For calculations for which the tower component is to be included, a suggested method is to first select the time-to-crest of the stroke current as per Fig 43. Approximately, for 115- to 230-kV lines, a front of 2.5 μs is appropriate. For 345-kV or above, a 4.0 μs front is more appropriate. Next, assume a value of R_i equal to 0.5 of R_o and solve for I_c using equation (4) and the equations in the appendix for U_{50NS} and for K_{SP}. Then solve for R_i and again for I_c. If the two values of I_c are not wihin about 1 kA, continue the iteration. After I_c is obtained within the desired degree of accuracy, a check may be made to determine if the time-to-crest reasonably coordinates with the value of time-to-crest selected. Either Fig 43 may be used or the equation:

$$M_{tm}/I = 0.154\ I^{0.624} \quad (9)$$

where $M_{tm/I}$ is the median value of the time-to-crest for a specific value of current.

If the tower component is to be neglected, again estimate R_i as 0.5 of R_o and solve equation 8 for I_c. Next, find R_i and again find I_c. Compare the two values of the critical current and if not within the accuracy desired, continue the iteration process. No iteration or check concerning the time-to-crest is necessary.

For estimate of U_{PF} and Z_T, see below.

6.9.3 Tower Surge Impedance

The tower surge impedance may be determined by use of equations from Chapter 5. However, because the tower component of voltage is not of major importance and considering that it is a time-varying quantity which acts as a type of transfer function to obtain the voltage across the insulation, an approximation appears valid. For two-shield-wire lines, a value equal to 0.5 times the shield-wire surge impedance is suggested: in general a value between 150 and 200 ohms may be used.

6.9.4 Power-Frequency Voltage

The power-frequency voltage can add or subtract from the surge voltage on the phase conductor. To more accurately estimate the BFR and to estimate the relative probability of the flashover of each phase, all instantaneous values of power-frequency voltages should be considered equally likely. However, this would require numerous solutions of the equations. To circumvent this an average value of power frequency may be used which is sufficiently accurate to estimate the BFR. This average or mean value is dependent on the surge voltages across each of the phases. For example, if the surge voltage can be considered approximately equal across all phase insulations, as is approximately correct for a single-circuit horizontally-configured line, the mean value is 0.827 times the crest line to neutral voltage. If the surge voltage is approximately equal on only two of three phases, which is approximately correct for double-circuit vertically-configured line, then this factor reduces to 0.551. A conservative factor 0.83 is suggested for practical use.

For DC lines, the value of U_{PF} is the crest pole to ground voltage.

6.9.5 Critical Flashover Voltage

The standard lightning impulse critical flashover voltage, denoted as U_{50}, is the lowest value considering all possible flashover paths. In most cases, except for wood pole designs, only two flashover paths need be considered: to the tower side and across the insulator strings (in the majority of cases, the insulator string is limiting). In the absence of directly measured data, the value of this insulation strength, in terms of the gradient, may be considered constant at about 560 kV/m (positive polarity) for either air strike distances or insulator length [125].

The insulation of wood-pole lines usually consists of wood and porcelain in series. The wood increases the insulation strength and also provides arc deionization. These effects have been investigated by several authors [126-128] with varying results. A summary including results of new investigations is contained in a book by Darveniza [128]. In general to obtain both effects, the length of wood should be double the insulator length, at which point wood adds approximately 130 kV/m. The benefits of the arc deionization may be stated in terms of the ratio of tripouts to flashovers, which has been estimated at typically between 0.35 and 0.50 [107-117] subject to the influence of many variables such as wood type, age, fault current magnitude, and power-frequency voltage. Thus, the BFR for wood-pole lines should be multiplied by this ratio.

A ratio of tripouts to flashovers also applies for steel and has been taken to be 0.85 [107]. However, this ratio for steel towers is normally not considered.

Insulators not constrained from movement, i.e. vertical insulator strings, may be moved closer to the tower by the action of wind, thus decreasing the strike distance to the tower and possibly decreasing the critical flashover voltage. This effect has been studied [129] and while the effect does increase the BFR, the increase is minor and may be neglected.

6.9.6 The BFR and Double-Circuit Lines

The BFR as calculated by the preceeding equations is in terms of flashovers per 100 km of line route or per 100 km of towers. For a single-circuit line, flashovers may involve one or more phases. For a double-circuit line, flashovers may involve one or more phases and one or more circuits.

For a double-circuit line having a vertical phase disposition, flashover to one of the lower phases is usually most probable. Assuming this phase flashes over, the most probable phase to flashover next is usually the lower phase of the other circuit - being determined principally by the coupling factor effect. Estimates of the double-circuit flashover rate may be made by use of the previous equations, modified to include the decreased value of Z_g and the increased value of the coupling factor. For the 230-kV, double-circuit line of Fig 42, having a critical flashover voltage of 1200 kV, a R_o of 30 ohms, and a earth resistivity of 600 ohm-meters, the total or tower flashover rate is estimated as 3.0 flashovers/100 km-yrs of which 0.6 are double-circuit backflashes. Thus 2.4 backflashes only involve one circuit and 20 % of the total backflashes involve both circuits.

To decrease the double-circuit BFR, differential insulation has been used with varying degrees of success. For example, for the same parameters as before, except assuming that one circuit has a critical flashover of 1400 kV with the other remaining at 1200 kV, the total BFR remains at 3.0 while the double-circuit BFR is reduced to 0.18. However, since for this vertical configuration, space within the tower must be capable of employing a sufficient number of insulators to obtain a critical flashover voltage of 1400 kV, this improvement should be compared to a tower having 1400 kV on both circuits. For this case, the total BFR becomes 1.19 and the double-circuit BFR remains at 0.18. Thus, while it appears true that differential insulation decreases percentage of double-circuit flashovers, the use of increased insulation on both circuits results in improved performance for both the double-circuit BFR and total BFR.

The calculation method as used above has been substantially improved by Sargent and Darveniza [119-120]. These authors show the same tendency as illustrated above and in addition suggest designs which may substantially improve the double-circuit BFR. For a horizontal phase configuration with one circuit below the other, the most probable flashovers will be only to the lower circuit. That is, flashover to the lower circuit, essentially provides shield wires which completely encase the upper circuit, thus improving coupling factors to all phases of the upper circuit.

6.9.7 Tower Grounding

In the previous sections, "concentrated" grounding -- that achieved by tower footing and supplemental driven ground rods was considered. From references listed in Chapter 5, the low-current resistance is not significantly affected by the diameter of the rod or for driven depths greater than 6 meters in uniform resistivity soil. Also, in general, to achieve the effectiveness of parallel rods, spacings need not exceed about 3 meters. However, these "rules of thumb" must be altered when considering lightning impulse currents which essentially cause an apparent increase in rod diameter and rod length as shown in Chapter 5. Weck shows that the final ionized diameter, D_r, for the rod may be approximated from the equations for sphere electrodes, i.e.

$$D_r = (2pI_R/\pi E_g)^{\frac{1}{2}} \qquad (10)$$

Thus, ionized diameters may range from 5 to 10 meters and to obtain the maximum effectiveness of parallel rods, spacings should be increased to approximately 5 meters.

In areas of high soil resistivity, where rod electrodes do not provide sufficiently low ground resistance, counterpoises are frequently used. Tests performed in the 1930's were analyzed by Bewley [130] and recently Devgan and Whitehead [131] re-examined counterpoise characteristics and emphasized the need to consider the frequency-dependent nature of soil dielectric parameters. Whereas the effect of impulse currents in decreasing the resistance of concentrated grounds has been investigated, (see Chapter 5), the impulse-current effects on the distributed grounds, (ie, counterpoise), has not yet been determined.

It is of importance to recognize that the BFR of the line is not that obtained by the use of an average footing resistance. Higher values of resistance produce larger than a proportional increase in the BFR. Therefore, the BFR should be obtained with a distribution of footing resistances as predicted or as measured along the line.

6.9.8 Single vs Double Shield Wires

For some applications where either the cost of two shield wires is not economically and technically justified or in areas of low ground-flash density, a single shield wire may be used. This single wire increases the value of R_e, decreases the coupling factors, and thus increases the BFR. To illustrate, Fig 49 has been constructed for the parameters as listed in Fig 42 for a single shield wire, 230-kV line. Note that the ground flash density is altered to 1 which is equivalent to about 13 thunderstorm days. Comparison to the values given in Fig 44 shows a substantial increase in BFR.

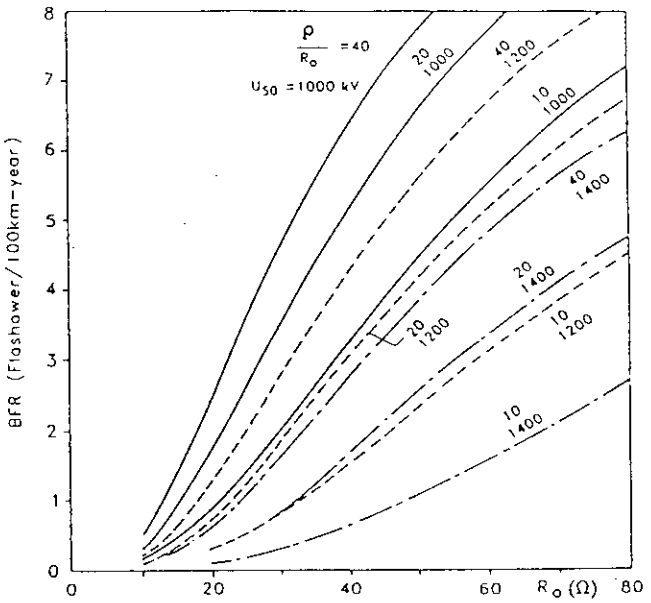

Fig 49 - BFR for 230 kV double circuit line of Fig 42 with one shield wire. Span = 300 m; N_g = 1.

6.9.9 Arresters

For cases where acceptable BFR's are not attainable and for cases of unshielded lines, surge arresters have been placed across the line insulation [132-134]. Presently, arresters are used or planned for use on towers having nominal system voltages up to 230 kV although their principle application has been on lower voltage circuits. Also, arresters are being employed on one circuit of double-circuit lines essentially to eliminate double-circuit backflashes. Sufficient field data is not yet available to form a complete judgement of their effect.

6.10 Conclusions

1. The analysis of the backflash event shows that:

(A) Although flashovers within the span are possible, they appear to be insignificant compared to flashovers at the tower. Therefore, flashovers within the span may be neglected.

(B) To account for flashovers at the tower caused by strokes terminating within the span, the BFR as calculated for a stroke to the tower should be multiplied by 0.6.

(C) The use of the statistical distribution of time-to-crest of the stroke current may be replaced by a single equivalent front whose value is approximately equal to the median value of time-to-crest for the specific critical current.

2. Simplified equations were developed to estimate the BFR which included the tower component of voltage. However, a sensitivity anaylsis indicated that the calculation of the BFR may be further simplified by neglecting this component of voltage for tower heights of less than about 50 m. Considering the inaccuracies inherent in estimation techniques, this further simplification may be used to quickly obtain an estimate of the BFR for higher towers.

APPENDIX

Appendix 1

Voltages on Tower - Neglecting Adjacent Towers

Assume that the first stroke of a lightning flash, having a current i(t), terminates on the top of a tower as illustrated in Fig 1.1. The initial surge voltage, U(t), which travels outward on the shield wires and down the tower, is equal to the current multiplied by the parallel combination of the tower surge impedance and half of the shield-wire surge impedance, Z_t and Z_g respectively or

$$u(t) = \frac{Z_g Z_T}{Z_g + 2 Z_t} i(t) \qquad (1)$$

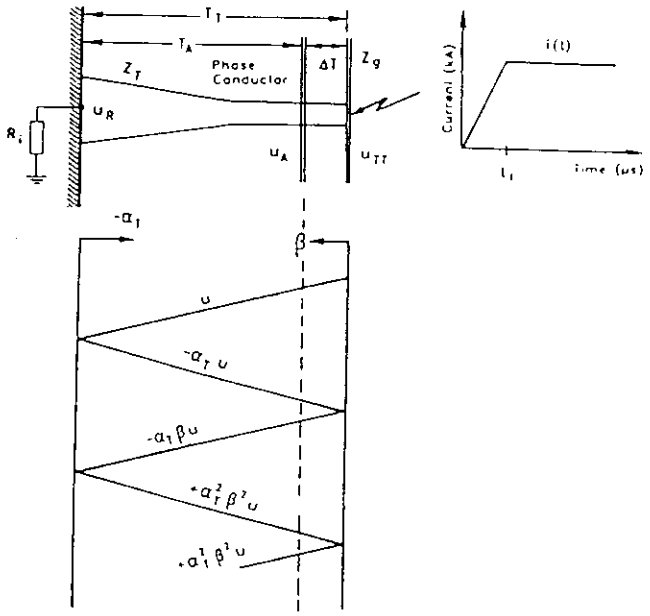

Fig 1.1 - Lattice diagram for calculating the tower voltage.

Using the lattice diagram Fig 1.1 with α_T and ß as defined below, the voltages at the tower top, U_{TT}, at the position of the phase conductor, U_{TA}, and at the footing resistance, U_R, are:

$$u_{TT}(t) = u(t) - \alpha_T(1+\beta)\left[u(t-2T_T) - \alpha_T \beta u(t-4T_T) + (\alpha_T\beta)^2 u(t-6T_T) - \ldots \right] \qquad (2)$$

$$u_{TA}(t) = u(t-\Delta T) - \alpha_T u\left[t-(2T_T-\Delta T)\right] - \alpha_T \beta u\left[t-(2T_T+\Delta T)\right] + \alpha_T^2 \beta u\left[t-(4T_T-\Delta T)\right] + (\alpha_T\beta)^2 u\left[t-(4T_T+\Delta T)\right] \qquad (3)$$

$$u_R(t) = (1-\alpha_T)\left[u(t-T_T) - \alpha_T \beta u(t-3T_T) + (\alpha_T\beta)^2 u(t-5T_T) - \ldots \right] \qquad (4)$$

where:

$$\alpha_T = \frac{Z_T - R_i}{Z_T + R_i} \qquad \beta = \frac{Z_g - 2Z_T}{Z_g + 2Z_T} \qquad (5)$$

and the travel times, T_T, T_A, and ΔT are defined in Fig 1-1 using the velocity of light. R_i is the tower footing resistance which is a function of the current through the resistance, I_R, and the normally measured low-current resistance, R_o, i.e.

$$R_i = R_o(1 + i_R(t)/I_g)^{-\frac{1}{2}} \qquad (6)$$

$$I_g = E_g \rho / 2\pi R_o^2 \qquad (7)$$

$$i_R(t) = u_R(t)/R_i \qquad (8)$$

where E_g is the soil breakdown or ionization gradient, assumed at 400 kV/m and ρ is the soil resistivity in ohm-m. Although i_R is a function of time, and therefore R_i is also a function of time, in determining the value of R_i, the crest value, I_R, is normally used.

Assuming that i(t) has a linearly rising front achieving crest at t_f and an infinite tail, then as an approximation:

(1) The voltage u_{TT} at t = 2 T_T, defined as U_T, and the voltage u_{TA} at t = 2 T_A, defined as U_A, are:

$$U_T = Z_T (T_T/t_f) \qquad (9)$$

$$U_A = Z_T(T_A/t_f)$$

(2) The crest voltages of u_{TT} and u_{TA}, U_{TT} and U_{TA} respectively, at t = t_f are:

$$U_{TT} = (R_e + \alpha_T Z_T T_T/t_f) I = K_{TT} I$$

$$U_{TA} = (R_e + \alpha_T Z_T T_A/t_f) I = K_{TA} I \qquad (10)$$

Where:

$$R_e = R_i Z_g/(Z_g + 2R_i) \qquad (11)$$

(3) The crest value of the current through the footing resistance, I_R is:

$$I_R = I\ Z_T/(Z_T + R_i) \tag{12}$$

(4) At $t = t_f + 2\ T_T$, the tower voltages, defined as U_R, are equal and given by:

$$U_R = I\ R_e \tag{13}$$

Also at this time the current, I_R becomes:

$$I_R = I\ Z_g/(Z_g+2R_i) = I\ R_e/R_i \tag{14}$$

For practical values of surge impedances and for t_f greater than 1 μs, the error in using the approximate equations 9 to 14 is less than 1 percent. For t_f of 1 μs, the error is about 5 percent and for smaller values of wavefront, the error increases. Considering that Z_T is a time varying quantity and also the inaccuracy in establishing an equivalent constant value of Z_T, the use of equations 9 to 14 appears justified. To be noted is that the approximate equations could be simply derived by assuming that $Z_g = 2\ Z_T$.

Also note that if the tower is neglected, the crest values of the tower voltages and the final voltages are identical. These voltages and the current through the footing resistance are:

$$U_{TT} = U_{TA} - U_R = R_e I \tag{15}$$

$$I_R = I\ Z_g/(Z_g+2R_i) = IR_e/R_i \tag{16}$$

The tower top voltages, both with and without the tower, are illustrated in Fig. 1.2.

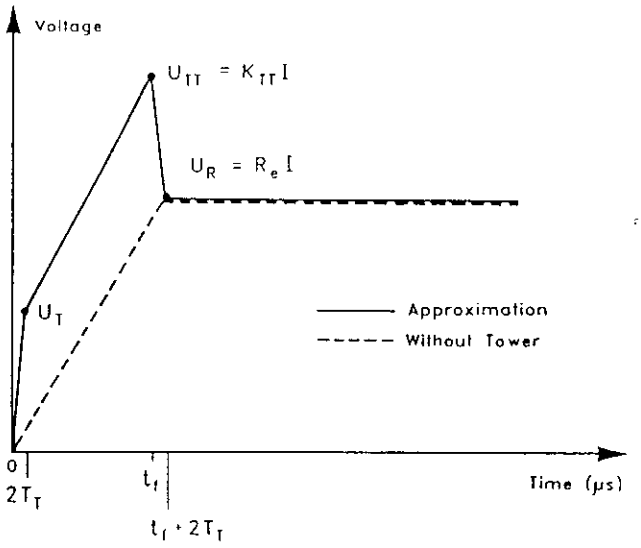

Fig 1.2 - Tower-top voltage for current waveshape of Fig 1.1.

Appendix 2

Effect of Reflections from Adjacent Towers

In Appendix 1 simplified equations are developed to determine the voltages along the tower neglecting reflections from adjacent towers. These reflections have two effects. First, the crest voltages, U_{TT} and U_{TA}, are decreased provided twice the span travel time, T_S, is less than the time to crest, t_f. Secondly, the wave tail is decreased.

Decrease in Crest Voltage

First consider only the effect of the first adjacent tower on each side of the struck tower. As shown in the lattice diagram of Fig 2.1, the reflection and transmission coefficients are greatly simplified if Z_g is assumed equal to 2 Z_T, as was the result in developing the simplified equation of Appendix 1. The initial voltage, u(t), and the reflection coefficient, α_T, are given by equations 1 and 5 of Appendix 1. As noted in Fig. 2.1, the tower travel time and the surge impedance of the adjacent towers are neglected. Also since the current through the footing resistance of the adjacent towers is much smaller than that through the footing resistance of the struck tower, the footing resistance of the adjacent towers is conservatively maintained at its low-current measured value of R_o. The reflection coefficient α_R is:

$$\alpha_R = Z_g/(Z_g+2R_o) \tag{1}$$

From the lattice diagram, the voltage at the tower top is

$$u_{TT}(t) = \Big[\, u(t)-\alpha_T u(t-2T_T)\Big]\Big[\, 1-\alpha_R(t-2T_s) + \alpha_T\alpha_R[t-(2T_s+2T_T)]-\alpha_R^2\ \alpha_T[t-(4T_s+2T_T)] + (\alpha_R\alpha_T)^2[t-(4T_s+4T_T)] + \ldots\Big] \tag{2}$$

Neglecting the travel time of the struck tower for the reflections, equation (2) becomes:

$$u_{TT}(t)=\left[u(t)-\alpha_T u(t-2T_T)\right]\left[1-\alpha_R(1-\beta_R)(t-2T_S)\right.$$
$$\left.+\alpha_R\beta_R(t-4T_S)+(\alpha_R\beta_R)^2(t-6T_S)+\ldots\right] \quad (3)$$

Where:

$$\beta_R = (Z_g-2R_i)/(Z_g+2R_i) \quad (4)$$

The crest value of the quantity $[u(t) - \alpha_T u(t-2T_T)]$ is U_{TT} given by equation (10) of Appendix 1 and is the voltage when reflections from adjacent towers are neglected. For purposes of simplification and approximation, assume that this voltage has a linearly rising front. Then new crest voltage, U_{TT}', becomes:

$$U_{TT}' = K_{TT}\, K_{SP} I \quad (5)$$

Where:

$$K_{SP} = 1-\alpha_R(1-\beta_R)\left[(1-2T_s/t_f)+\alpha_R\beta_R(1-4T_s/t_f)+\right.$$
$$\left.(\alpha_R\beta_R)^2(1-6T_s/t_f)+\ldots\right] \quad (6)$$

If the struck tower is neglected, then

$$U_{TT}' = R_e K_{SP} I \quad (7)$$

The terms of the equation for K_{SP} are only valid where the term $(1 - n\, T_S/t_f)$ is positive. That is, if $T_S = 0.5\ \mu s$ and $t_f = 4\ \mu s$, then only 4 reflections are considered, i.e. n = 8.

Reflections from other towers may further reduce the crest voltage, provided they arrive before crest voltage is attained at the struck tower. For example, the first reflection from the second tower, arriving at 4 T_S is equal to:

$$\Delta u_{TT}(t) = -\alpha_R(1-\beta_R)(1-\alpha_R)^2 \quad (8)$$

which is $(1-\alpha_R)^2$ times the first reflection from the first tower. For practical values, this reflection decreases the tower-top voltage by less than 1 percent. Therefore to approximate the voltage at the struck tower, only the first adjacent towers need be considered.

The factor K_{SP} also applies to the voltage U_{TA} and to U_F. Thus:

$$U_{TA} = K_{TA} K_{SP} I$$
$$U_R = K_{SP} R_e I \quad (9)$$

Considering only the first traveling wave that arrives at the adjacent tower, the ratio of the current through the footing resistance of the adjacent tower, I_{RA}, to the current through the footing resistance of the struck tower, I_R, is:

$$I_{RA}/I_R = 2R_i/(Z_g+2R_o)$$

Initially, the current through the footing resistance of the adjacent towers is 10 to 30 percent of the current through the footing resistance of the struck tower. However, as the resistance R_i decreases, the current increases and the current through the adjacent towers decreases. Thus the current through the adjacent towers will decrease to only about 5 percent of that of the struck tower and therefore the initial assumption appears valid.

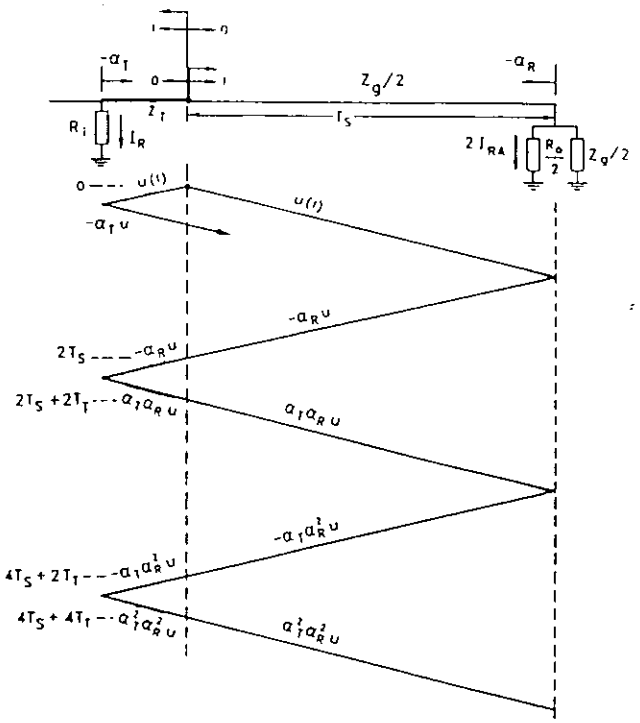

Fig 2.1 - Lattice diagram to determine effect of adjacent towers.

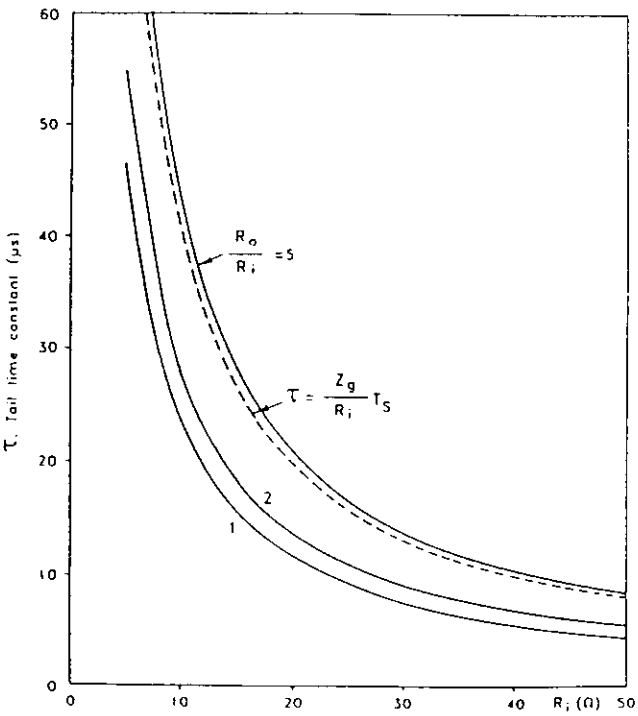

Fig 2.2 - Variation of the apparent tail time constant evaluated at a voltage obtained at τ/2.

$Z_g = 400\ \Omega$; $T_S = 1\ \mu s$.

Decrease of Tail

In Appendix I, the tail of the stroke current was assumed infinite and the resultant tail of the tower voltage was infinite. To assess the decrease of the tail, the surge impedance of the shield wire is replaced by its equivalent inductance, the tower is neglected, and additional inductive/resistive pi-sections are added. Therefore, for an infinite line, the final voltage approaches zero and as may be noted from this network the method of achieving zero voltage is through time constants consisting of the inductance and various combination of R_o and R_i. However, the tail or voltage, u_R, for t equal to or greater than t_f, may be approximated by a single time constant, τ, such that

$$U_R(t) = U_R e^{-(t-2t_f)/\tau} \qquad (11)$$

To evaluate the value of apparent or approximate value τ, a step function of current having a magnitude of 1.0 pu was injected into the struck tower, i.e. into the inductance/resistance network. The time to decrease to 0.607 per unit was obtained and multiplied by 2 to obtain the apparent time constant. Fig. 2.2 shows the variation of τ as a function of R_i using the ratio R_o/R_i as a parameter. Expected ratios of R_o/R_i vary between about 4 to 8 and as shown in the figure, for ratios of 5 or greater, the equation given in the figure is valid, that is:

$$\tau = (Z_g/R_i)T_S \qquad (12)$$

Appendix 3

Effect of Strokes Within The Span

A stroke terminating on the shield wire within the span produces voltages across the air insulation between the shield wire and the phase conductor and also across the air-porcelain insulation at the tower. Although the voltage across the span insulation exceeds that across the tower insulation, the span insulation strength exceeds the that of the tower. Thus, dependent on the relative voltages and insulation strengths, flashover may occur either across the span or across tower insulations.

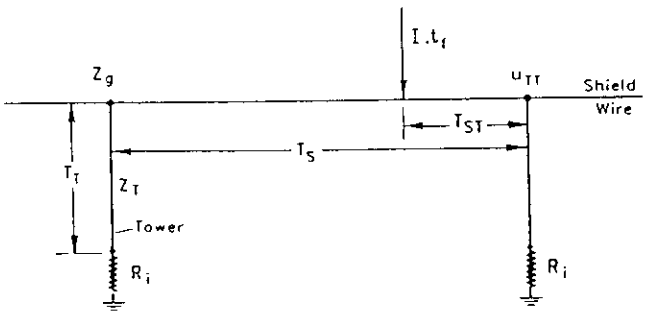

Fig 3.1 - Definition of variables for stroke to shield wire.

Flashovers Within the Span

Considering a stroke to the shield wire, as defined in Fig 3.1, the voltage at the stroke terminating point attempts to reach a crest voltage of $Z_g I/2$. However, reflections from adjacent towers reduce this voltage provided t_f is greater than $2(T_S - T_{ST})$. The maximum voltage occurs at the stroke terminating point and voltages decrease as the distance from the stroke terminating point increases, reaching a minimum at the tower. To illustrate, Fig 3.2 shows the voltage at the midspan and at a location defined as $T_S/5$ from the tower for a stroke terminating at midspan. This decrease in voltage is better illustrated by the curves of Fig 3.3 where the parameter is the stroke terminating point defined by T_{ST}.

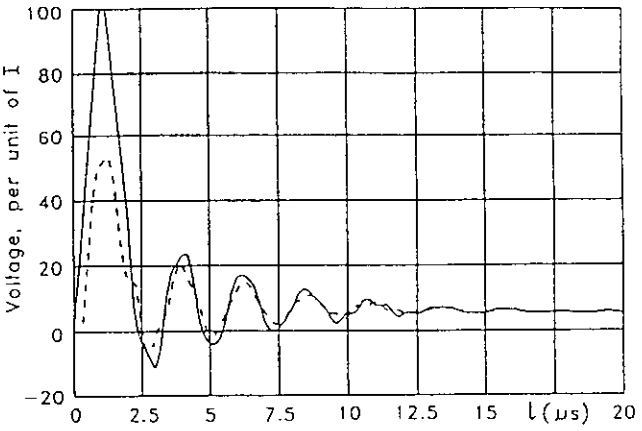

Fig 3.2 - Comparison of surge voltages for a stroke terminating at midspan.

t_f = 2.0 μs; R_i = 20 Ω

_____ voltage at midspan
- - - - - - - - - - - voltage at $T_{ST} = T_S/5$

To obtain an approximation of the expected number of span flashovers as opposed to tower flashovers, assume that the waveshapes of all the voltages are identical so that non-standard critical flashover voltage, U_{50NS}, is a linear function of the gap spacing. For a typical 500-kV line, the minimum strike distance at the tower is 3.35 m while the shield wire to phase conductor spacing varies from 9.2 m at the tower to 11.6 m at midspan. Thus the ratio of insulation strength is 3.5. For a stroke terminating at T_{ST}/T_S = 0.20, and for t_f = 2.0 μs, and R_i = 20 ohms, the ratio of the voltages at

midspan to the voltage at the tower is 2.4. Thus , for this case, flashover would occur at the tower. If all stroke terminating points are considered, for t_f = 2.0 μs, approximately 16 % of the strokes result in span flashover. For t_f = 4.0 μs, span flashover is reduced to about 2 %.

Another phenomenon further reduces the probability of span flashover. At high overvoltages, predischarge currents flow from the shield wire to the phase conductor producing a voltage on the phase conductor which decreases the voltage across the span insulation [113,114]. Although no quantitative calculation will be made, suffice it to note that this phenomenon inhibits flashover.

Thus, considering both the example calculations and the predischarge current phenomena, although flashover within the span are possible, they appear to be insignificant compared to flashovers at the tower.

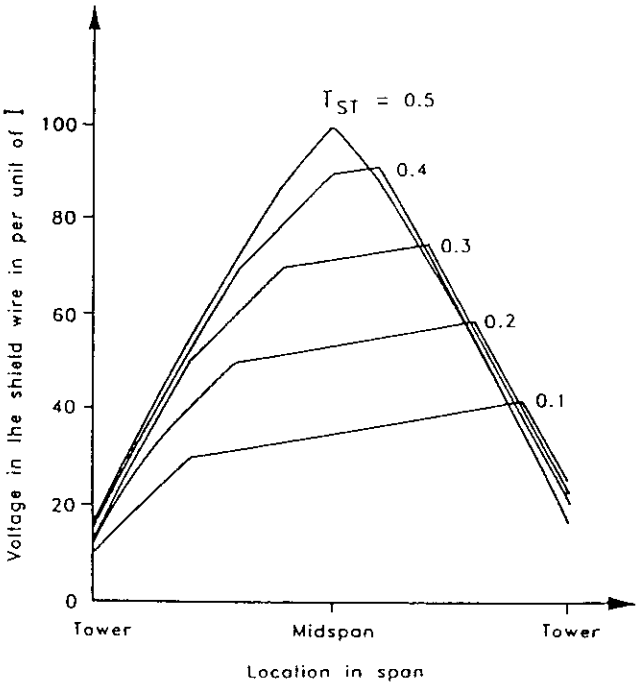

Fig 3.3 - Voltages on the shield wire for stroke terminating points defined by T_{ST}

t_f = 2.0 μs; R_i = 20 Ω; T_S = 1 μs

Flashovers at the Tower Caused by Strokes to the Shield Wire

For a stroke terminating within the span, the crest voltage at the tower in terms of K_{TT} (see Appendix 1) is:

$$U_{TT} = I\ K_{TT} \qquad (1)$$

where:

$$K_{TT} = R_e + \alpha_T Z_T (T_T/t_f) \quad \text{for } 2T_T \le t_f \le 2(T_T - T_{ST}) \qquad (2)$$

If

$$2(T_s - T_{TS}) \le t_f \le 2T_S \qquad (3)$$

the crest voltage occurs either at t_f or at $2(T_S - T_{ST})$, dependent on the value of the tower footing resistance, ie, if the crest voltage occurs at t_f, then:

$$K_{TT} = 2R_e(T_S - T_{ST})/t_f + \alpha_T Z_T (T_T/t_f) \qquad (4)$$

or if the crest voltage occurs at $2(T_S - T_{ST})$, then:

$$K_{TT} = \left[R_e/(Z_g + 2R_i) \right] \left[2R_i + 2Z_g(T_T - T_{ST})/t_f + 4\alpha_T (R_i/R_e) Z_T (T_T/t_f) \right] \qquad (5)$$

As noted by comparing these equations to those of Appendix I, the voltage resulting from a stroke within the span equals that produced by a stroke to the tower only when $t_f < 2(T_S - T_{ST})$. Therefore, the voltage produced at the tower by a stroke within the span is equal to or less than that produced by a stroke to the tower. Fig 3.4 shows a comparison of these voltages and as noted, for these cases, the voltage produced by a stroke to midspan is approximately 60% of the voltage produced by a stroke to the tower.

The crest voltage at the tower in terms of K_{TT} for R = 20 ohms, for various stroke terminating points, and for various wave fronts, is presented in Fig 3.5. Values on the curves are ratios of the K_{TT} for strokes to the midspan to the K_{TT} for strokes to the tower. This ratio initially decreases as the front, t_f, increases but then gradually increases as the front increases further. This ratio, denoted as the K_{TT} Ratio, is plotted as a function of t_f/T_S in Fig 3.6 for $t_f > 2T_S$. The range of this ratio is relatively narrow, from about 0.58 to 0.77.

Assuming a K_{TT} Ratio of 0.7, the effect of strokes to the span on the backflash rate, BFR, can be estimated. Knowing the K_{TT} Ratio and the critical current for strokes to the tower, I_c, the critical current for strokes along the span can be obtained if the U_{50NS} for all voltages is considered equal since I_c is approximately:

$$I_C = U_{50NS}/[K_{TT}(1-C)] \qquad (6)$$

Using this approach, the ratio, K_{SF}, of the total BFR considering all possible stroke terminating points to the BFR when only considering the strokes to the tower can be obtained and is shown by the solid line curve of Fig 3.7 as a function of I_c. This assumes that the number of strokes to each incremental length of the shield wire is constant. If the number of strokes is assumed to vary with the height of the shield wire, the curve decreases; an estimate being provided by the dotted line in Fig 3.7. The resultant ratio K_{SF} or Span Factor ranges from 0.63 for 50 kA to 0.42 for 200 kA and thus is a function of the system operating voltage. However, for purposes of estimating the BFR, a single value of 0.6 is suggested, in order to remain conservative.

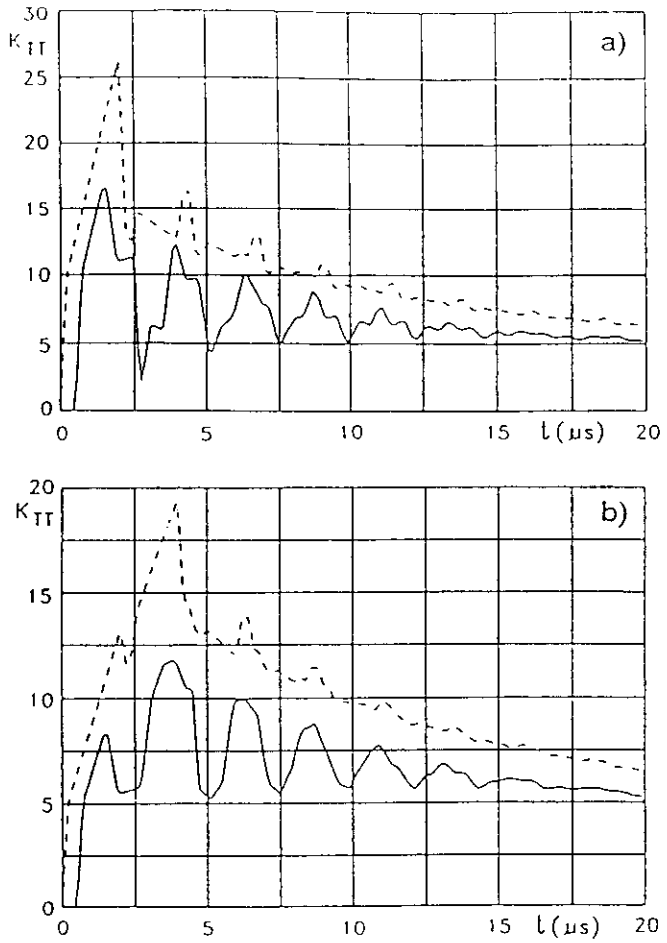

Fig 3.4 - Comparison of surge voltages at the tower produced by:

_____ stroke to midspan
---------- stroke to tower

a) t_f=2 μs R_i=20 Ω T_S=1 μs

b) t_f=4 μs R_i=20 Ω T_S=1 μs

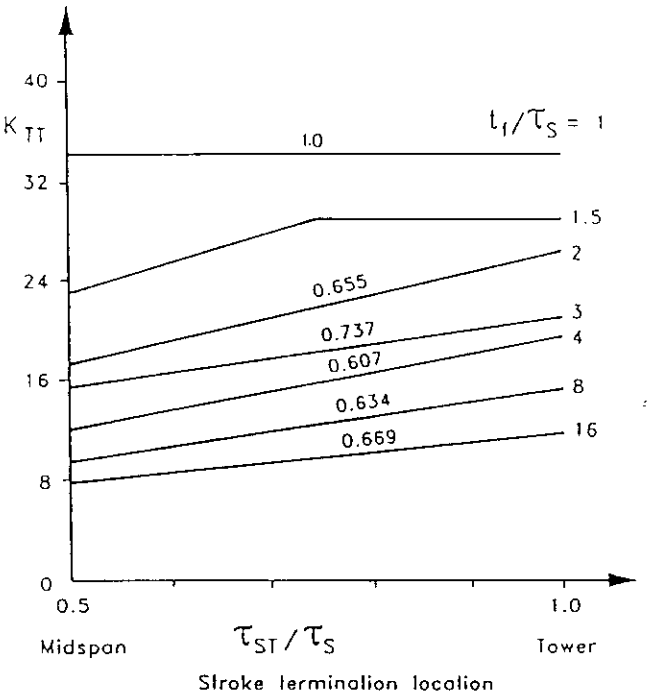

Fig 3.5 - Voltages at the tower as a function of the stroke termination location for various wave fronts.

R_i = 20 Ω. Values on the curve are the K_{TT} ratios of the K_{TT} at midspan to the K_{TT} at the tower.

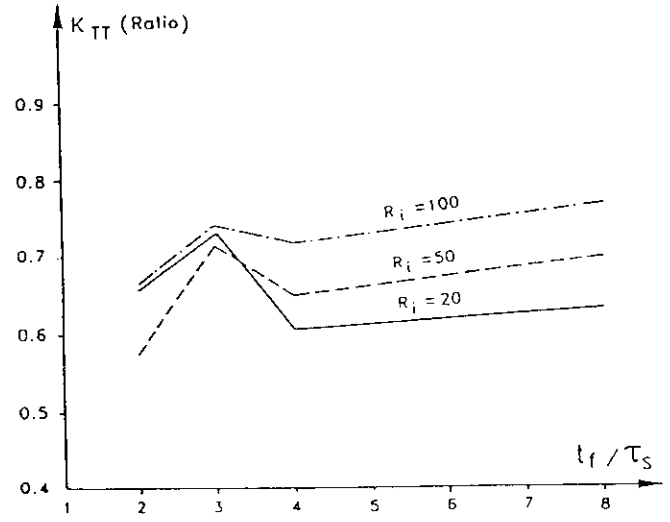

Fig 3.6 - K_{TT} ratio as a function of wave front for the three values of R_i.

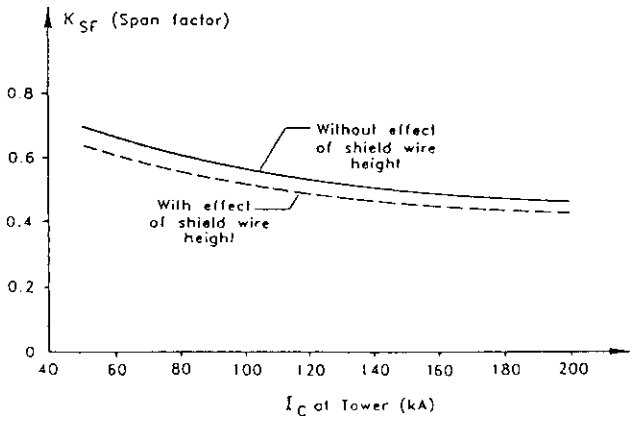

Fig 3.7 - Span factor, K_{SF} as a function of the critical current at the tower, I_C.

Appendix 4

Critical Flashover Voltage of the Voltage Across the Tower Insulation, U_{50ns}

The waveshape of the voltage across the tower insulation, shown by the solid line of Fig 4.1, is composed of a power-frequency voltage, U_{PF}, a voltage produced by the tower footing resistance, U_F, and a voltage produced by the tower, ΔU. The decreasing voltage on the tail of the surge voltage may be described by a time constant, τ. A further simplified approximation of this voltage is shown by the dotted line.

The critical flashover voltage for this non-standard voltage waveshape, defined in terms of the crest voltage, U_I, may be estimated by use of the leader progression model of gap breakdown as discussed in Chapter 5. The leader velocity equation selected from Chapter 5 is:

$$v(t) = k_L u(t)\left[u(t)/x - E_o \right] \qquad (1)$$

where $v(t)$ is the leader velocity, $u(t)$ is the voltage as discribed by Fig 4.1, E_o is the critical leader starting gradient, x is the distance of the unbridged gap, and k_L is a constant. The value of E_o is primarily depended on the gap configuration or, in more practical terms, on the critical flashover voltage gradient for the standard lightning impulse whereas the value of k_L is primarily depended on the upward curvature of the time-lag curve for the standard lightning impulse.

Considering a sample time lag curve (in this case, for V-strings) and using a value of 560 kV/m for the positive polarity critical flashover voltage gradient, a 3-μs chopped wave voltage of 1.38 times the critical flashover voltage, U_{50}, and assuming a double expotential waveshape for the standard lightning impulse, the values of these constants are:

$$E_o = 535.0 \text{ kV/m} \qquad (2)$$

$$k_L = 7.875 \times 10^{-7}$$

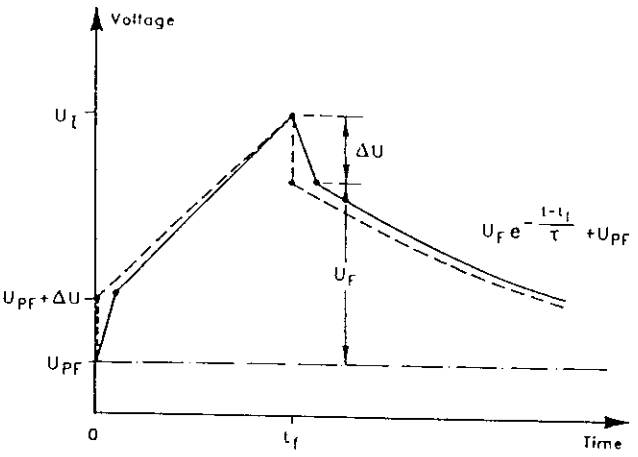

Fig 4.1 - Voltage across tower insulation.

———— actual shape
- - - - - - - - - - approximation

for x in meters and u(t) in kV. The resultant time-lag curve displays a 2-μs chopped wave voltage of 1.66 times the critical flashover voltage.

Using equations 1 and 2, and employing regression analysis, the critical flashover voltage of the non-standard surge voltage of Fig 4.1, U_{50NS}, was found to be best approximated by the following equation:

$$U_{50NS}/U_{50} = \left[0.977 + (2.82/\tau) \right] \left[1+(\Delta U/U_F) \right]$$

$$\left[1-0.2(1+\Delta U/U_F)(U_{PF}/U_{50}) \right] \left[1-0.09\ (1+10/\tau)(\Delta U/U_F) \right]$$

$$\exp-[(\Delta U/U_F)(t_f/13)] \qquad (3)$$

This equation was developed for values of τ between 10 and 100 μs, for values of $\Delta U/U_F$ between 0 and 1.0, and for values of t_f between 0.5 and 5 μs.

REFERENCES

[1] Popolansky F. "Measurements of lightning currents in Czechoslovakia and the application of obtained parameters in the prediction of lightning outages of EHV transmission lines" CIGRE Paper 33-03, Paris 1970.

[2] Popolansky F. "Correlation between the number of lightning outages of 220 kV and 400 kV overhead transmission lines and the number of registered flashes in CSSR and Finland" CIGRE 33-73 (WG-01) IWD 04.

[3] Turman B.N. and Edgar B.C. "Global lightning distributions at dawn and dusk" J. Geophys. Res. 87, 1191-1206, 1982.

[4] Orville R.E. "Lightning phenomenology" - Chapter 1 in The Earth's Electrical Environment (National Academy Press, Washington, 1986).

[5] Prentice S.A. and Mackerras D. "The ratio of cloud to cloud- ground lightning flashes in thunderstorms" J. Appl. Meteorol. 16, 545-549, 1977.

[6] World Meteorological Organisation "World distribution of thunderstorm days" WMO, Geneva, No. 21, 1956.

[7] Cortina, R., Dellera, L., Garbagnati, E., Pigini, A., Serravalli, W. and Thione, L., "Some aspects of the evaluation of the lightning performance of electrical systems." CIGRE paper 33-13, 1980.

[8] Popolansky F. and Laitinen L., "Thunderstorm days, thunderstorm duration and the number of lightning flashes in Czechoslovakia and in Finland" Studia Geophysica and Geodetica, 16, Prague 1972

[9] Kolokolov V.P. and Pavlova G.P. "Relations between some thunderstorm parameters" Trudy No 277, A.I. Voeikov Main Geophysical Observatory, Leningrad 1977.

[10] MacGorman D.R., Maier M.W. and Rust W.D. "Lightning strike density for the contiguous United States from thunderstorm duration reports" U.S. Nuclear Regulatory Commission Report NUREG/CR-3759, May 1984.

[11] Anderson R. B., Van Niekerk H., Prentice S. and Mackerras D. "Improved lightning flash counters". Electra No.66, 85-98, 1979.

[12] Anderson R.B., Eriksson A.J., Kroninger H., Meal D.V. and Smith M.A. "Lightning and thunderstorm parameters" IEE Conference Publication No. 236, "Lightning and Power Systems", London, June 1984.

[13] Australian Bureau of Meteorology, "Lightning flash counter registrations" Melbourne, June 1988.

[14] Anderson R.B., Van Niekerk H.R., Kroninger H. and Meal D.V. "Development and field evaluation of a lightning earth flash counter" Proc. IEE, Vol. 131, Pt A, No. 2, 118-124, March 1984.

[15] Weck K.H. "Statistical elements in lightning performance" CIGRE 33-86 (WG 01) IWD 04, 1986.

[16] Orville R.E., Weisman R.A., Pule R.B., Henderson R.W. and Orville R.E.(Jr) "Cloud-to-ground lightning flash characteristics from June 1984 through May 1985". J. Geophys. Res. Vol. 92, No. D5 5640-5644, May 1987.

[17] Hojo J. et al, "Seasonal variation of cloud-to-ground lightning flash characteristics" Proceedings of Intl. Conf. on Atmospheric Electricity, Graz, 1988

[18] Huse J. "Preliminary notes on comparative lightning field change analysis and stroke multiplicity CIGRE 33-86 (WG 01) IWD 02, 1986.

[19] Eriksson A.J., Kroninger H. and Hefer S.M. "Comparative analysis of lightning electromagnetic field change data" CIGRE 33-85 (WG01) IWD 04

[20] Anderson R.B. and Eriksson A.J. "Lightning parameters for engineering application" Electra No. 69, 65-102, March 1980.

[21] Eriksson A.J., Kroninger H. and Hefer S.M. "Comments on lightning flashing rates and storm durations" CIGRE 33-85 (WG01) IWD 06.

[22] Lundquist S., Scuka V. and Vedda D. "Some statistical features of discharging processes in thunderstorms" Report UURIE 67-74, Uppsala University, 1974.

[23] Berger, K., Anderson, R. B. and Kroninger, H., "Parameters of lightning flashes". Electra No 41, pp 23-37, July, 1975.

[24] Anderson, J. G., "lightning Performance of Transmission Lines", Chapter 12, Transmission Line Reference Book, Electric Power Research Institute, Palo Alto, CA.

[25] IEEE Working Group on lightning performance of transmission lines, 1985, "A simplified method for estimating lightning performance of transmission lines". IEEE Trans. PAS-104, pp 919-932, April 1985.

[26] Eriksson, A. J., Goldenburgs, H. J., Kroninger H. and Heyers, M., "A study of lightning stresses on metal oxide surge aresters". CIGRE paper 33-08, Paris, 1986.

[27] Dellera, L., Garbagnati, E., Lo Piparo, G., Pomponi, R., Ronchetti, P. and Solbiati, G., "Lightning protection of structures. Part IV: Lightning current parameters". L'ENERGIA ELETTRICA_N.11. 1985.

[28] Golde, R. H., "Lightning" (book), Academic Press, London, 1977.

[29] Dellera, L. and Garbagnati, E., "Lightning Stroke Simulation by Means of the Leader Progression Model, Parts I and II", IEEE Trans on Power Delivery, Presented at the IEEE/PES Summer Meeting, July 1989.

[30] Eriksson, A. J., "The Incidence of Lightning Strikes to Transmission Lines", IEEE Trans on Power Delivery, July 1987, pp 859-70.

[31] Eriksson, A. J., "An Improved Electrogeometric Model for Transmission Line Shielding Analysis", IEEE Trans on Power Delivery, July 1987, pp 871-86.

[32] Eriksson, A. J., "Lightning and Tall Structures", Trans SAIEE, vol 69, pt 8, Aug 1978.

[33] Wagner, C. F. and Hileman, A. R., "The Lightning Stroke - II", IEEE Trans on PA&S, Oct 1961, pp 622-42.

[34] Wagner, C. F., "The Relation Between Stroke Current and the Velocity of the Return Stroke", IEEE Trans on PA&S, Oct 1963, pp 609-17.

[35] Young, S. F., Clayton J. M. and Hileman, A. R., "Shielding of Transmission Lines", IEEE Trans on PA&S, vol 60, 1941 pp 132-54.

[36] Wagner, C. F., McCann, G. D. and MacLane, G. L. "Shielding of Transmission Lines", AIEE Trans, vol 60, 1941, pp 313-28.

[37] Wagner, C. F., McCann, G. D. and Lear, C. M. "Shielding of Substations", AIEE Trans, Vol 61, 1942, pp 96-100.

[38] Price, W. S., Bartlett S. C. and Zobel, E. S., "Lightning and Corona Performance of 330 kV Lines of the American Gas and Electric and the Ohio Valley Electric Corporation Systems", AIEE Trans, Vol 75 pt III, Aug 1956, pp 270-81.

[39] Armstrong, H. R. and Whitehead, E. R., "Field and Analytical Studies of Transmission Line Shielding - II", IEEE Trans on PA&S, 1969, pp 617-26.

[40] Brown, G. W. and Whitehead, E. R., "Field and Analytical Studies of Transmission Line Shielding - II", IEEE Trans on PA&S, 1969, pp 617-26.

[41] Armstrong, H. R. and Whitehead, E. R., "Field and Analytical Studies of Transmission Line Shielding - II", IEEE Trans on PA&S, 1969, pp 617-26.

[42] Whitehead, E. R., "Mechanism of Lightning Flashover Research Project", Final Report of the Edison Electric Institute, Publication No 72-900, Edison Electric Institute, New York, NY.

[43] Brown, G. W., "Lightning Performance - I, Shielding Failures Simplified", IEEE Trans on PA&S, Jan/Feb 1978, pp 33-38.

[44] Currie, J. R., Ah Choy, L. and Darrenzia, M., "Monte Carlo Determination of the Frequency of Lightning Strokes and Shielding Failures", IEEE Trans on PA&S, Sept/Oct 1971, pp 2305-12.

[45] Love, E. R., "Improvements on the Lightning Stroke Modelling and Application to Design of EHV and UHV Transmission Lines", MSc Thesis, University of Colorado, Denver, CO, 1973.

[46] Sargent, M. A., "The Frequency Distribution of Current Magnitudes of Lightning Strokes to Tall Structures", IEEE Trans on PA&S, 1972 pp 2224-29.

[47] Mousa, A. M. and Strivastava, K. D., "The Implications of the Electrogeometric Model Regarding Effect of Height of Structure on the Median Amplitude of Collected Strokes", IEEE trans on Power Delivery, April 1989, pp 1450-60.

[48] Rizk, F. A. M., "Modelling of Transmission Line Exposure to Direct Strokes", IEEE Trans on Power Delivery, 1990, Presented at the IEEE/PES Winter Meeting.

[49] Whitehead, E. R., "CIGRE Survey of the Lightning Performance of Extra High-Voltage Transmission Lines", ELECTRA, March 1974, pp 63-89.

[50] Ellert, F. J., Miske, S. A. and Truax, C. J., "EHV and UHV Transmission Systems", Chapter 2 of the Transmission Line Reference Book, Electric Power Research Institute, Palo Alto, CA.

[51] WG 13.05: "The calculation of switching surges. II. Network representation for energization and re-energization studies on lines fed by an inductive source". ELECTRA 32, pp. 17-44 (1974).

[52] WG 13.05: "The calculation of switching surges III. Transmission line representation for energization and re-energization studies with complex feeding networks". ELECTRA 62, pp. 45-78 (1979).

[53] Huse, J., Larsen, V. and Olsen, K.,: A complete simulation/calculation model for lightning overvoltages in power system. "Lightning and Power Systems", IEE, London, 1984, pp. 21-25

[54] Marti, J. R., Dommel, H. W., Marti, L., Brandwajn, V.,: "Approximate transformation matrices for unbalances transmission lines". 9th Power System Conference, Lisbon 1987.

[55] Wagner, C. F. and Hileman, A. R., "A New Approach to the Calculation of the Lightning Performance of Transmission Lines - Part III", AIEE Trans. PAS Vol 79, 1960, pp 589-603.

[56] Sargent, M. A. and Darveniza, M., "Tower Surge Impedance", IEEE Trans, PAS Vol. 88 No 5, May 1969, pp 680-687.

[57] Chisholm, W. A., Chow, Y. L. and Srivastava, K. D., "Lightning Surge Response of Transmission Towers", IEEE Trans. PAS. Vol 102 No 9, September 1983, pp 3232-3242.

[58] Breuer, Shultz, Schlam and Price, "Field Studies of the Surge Response of a 345 kV Transmission Tower and Ground Wire", AIEE Trans, PAS Vol 76, February 1958, pp 1392-1396.

[59] Caswell, Johnson, Koncel and Schultz, "Lightning Performance of 138 kV Twin-Circuit Transmission Lines of Con Ed Co-Operating Experience and Field Studies", AIEE Trans Vol 76 February 1958 pp 1480-1491.

[60] Bouquegneau, C., "Contribution a L'Etude due Comportement des Pylones Foudroyes", DScA Thesis, Faculte Polytechnique de Mons, Belgium.

[61] Chisholm, W. A., Chow, Y. L. and Srivastava, K. D. "Tower Travel Time", IEEE Trans PAS Vol 104 No 10, October 1985, pp 2922-2928.

[62] Kawamura, T., Suzuki, T., Kojima, S. and Osaki, E., "New Models for Analyses of Lightning Surges in Transmission Lines and Substations." CIGRE SC33 Conference, IWD 02-03, Tokyo, 1987.

[63] Kawai, M., "Studies of Surge Response on a Transmission Tower", IEEE Trans Pas Vol 83, January 1964, pp 30-34.

[64] Chow, Y. L. and Yovanovich, M. M., "The Shape Factor of the Capacitance of a Conductor", Journal of Applied Physics, Vol 52, December 1982.

[65] Chisholm, W. A. and Janischewskyj, W., "Lightning Surge Responsible for Ground Electrodes", IEEE Trans PWRD Vol 4, No 2, April 1989.

[66] Berger, K., "Das Verhalton von erdungen unter hohen stossstromen". Bull Assoc. Suisse Elek. SEV 37, 197, 1946.

[67] Oettle, E. E., " A new general estimation curbe for predicting the impulse impedance of concentrated earth electrodes", IEEE 87 SM 567-1.

[68] Liew, A. C. and Darveniza, M., "Dynamic model of impulse characteristics of concentrated earths". IEE Proc. pp 123-135, 1974.

[69] Korsuntcev, A. V., "Application of the theory of similitude to the calculation of concentrated earth electrodes". Electrichestvo 5, 31, 1958.

[70] Ryabkowva and Miskin, "Impulse characteristics of earthings for transmission line towers". Electrichestvo, No 8, 1976, pp 62-70

[71] Weck, K. H., ea, to be published.

[72] Witzke R.L., Bliss T.J., "Surge protection of cable connected equipment", AIEE Trans. vol. 69, pp. 527-542. 1950.

[73] Witzke R.L., Bliss T.J., "Co-ordination of lightning arrester location with transformer insulation level", AIEE Trans. vol. 69, pp.964-975. 1950.

[74] Akopian A.A. et al.," On impulse discharge voltages across high voltage insulation as related to the shape of the voltage wave", CIGRE Paper 411 15 p, 1954.

[75] Jones A.R., "Evaluation of the integration method for analysis of non-standard surge voltages", AIEE Trans. vol. 73, pp. 984-990. 1954.

[76] Kind D., "Die Aufbauflache bei Stossspannungs-beanspruchung technischer Elektrodenanordnungen in Luft", ETZ-A vol. 79, pp. 65-69. 1958.

[77] Rusck, S., "Effect of non-standard surge voltages on insulation". CIGRE paper 403, Paris, 1958.

[78] Caldwell R.O., Darveniza M., Experimental and analytical studies of the effect of non-standard waveshapes on the impulse strength of external insulation, IEEE Trans. on PAS, vol. 92, pp. 1420-1428, 1973.

[79] Darveniza, M., Popolansky F., Whitehead E.R., "Lightning protection of UHV transmission lines". ELECTRA 41, pp. 39-69. 1975.

[80] Suzuki, T., Miyake, K., "Experimental study of the breakdown voltage time characteristics of large air-gaps with lightning impulses", IEEE Trans. on PAS, vol. 96, pp. 227-233. 1977.

[81] Alstad, K., Huse, J., Schei, A. et al., "Lightning impulse flashover criterion for overhead line insulation", paper 42.19, 4 p ISH Milan. 1979.

[82] Weck, K. H., "Lightning protection of substations. Comments to previous documents and results of decided calculations", Document CIGRE 33-86 (TF01.02) 03 IWD, 10 + 11 p. Private communication.

[83] Darveniza, M., Vlastos A.E., "The generalized integration method for predicting impulse volt-time characteristics for non-standard wave shapes - a theoretical basis", IEEE Trans. on Electrical Insulation, vol. 23 (1988) no. 3, pp. 373-381.

[84] Baldo, G., Pigini, A., Weck, K. H., "Non-standard lightning impulse strength", Part IV of the document CIGRE 33-81 (SC) 03 IWD, 29 p. Private communication. 1981

[85] Pigini, A. et al., "Performance of large air gaps under lightning overvoltages: Experimental study and analysis of accuracy of predetermination methods", IEEE Paper 88 SM 592-8, 9 p, 1988.

[86] Baldo, G., Pigini, A., "Representation for non standard LI strength of air insulation", CIGRE 33-86 (WG01) 08 IWD. 12 p. Private communication. 1986.

[87] Skilling, H. H. and Dykes, P. de K., "Distortion of travelling waves by corona". Trans. AIEE 56 850-857, 1937.

[88] Brune, O. and Eaton, J. R., "Experimental studies in the propagation of lightning surges on transmission lines". Trans. AIEE 50, 1132-1138, 1931.

[89] Bockmann, M., Hylten-Cavallius, N. and Rusck, S., "Propagation of surge generator waves up to 850 kV on a 132 kV line". CIGRE report 314, 1950.

[90] Wagner, C. F., Cross, I. W. and Lloyd, B. L., "High voltage impulse tests on transmission lines. Trans". AIEE PAS 73, 196-209, 1954.

[91] Wagner, C. F. and Lloyd, B. L., "Effects of corona on travelling waves". Trans. AIEE PAS 74, 858-872, 1955.

[92] Gary, C., Dragan, G. and Cristescu, D., "Attenuation of travelling waves caused by corona". CIGRE report 22-13, 1978.

[93] Gary, C., Timotin, A. and Cristescu, D., "Prediction of surge propagation influenced by corona and skin effect". IEE Proc. 130 A, 264-272, 1983.

[94] Weck, K. H. and Köster, H. J., "Dämpfung von Blitzüberspannungen durch Stobkorona". ATZ-A 3 (1981) 419-426.

[95] Weck, K. H. and Köster, H. J., "Attenuation of travelling waves by impulse corona". CIGRE 33-81 (WG01) 4 IWD. Private communication, 1981.

[96] Inoue, A., "Corona discharges on bundled conductors". IEEE PES winter meeting, paper A 78170-3 1978.

[97] Garbagnati, E., Porrino, A., Pigini, A. and Valagussa, C., "Corona and its impact on attenuation and distortion of travelling waves". Conference on Gras Dischargee, Venice, 1988.

[98] Gary, C., Cristescu, D. and Dragan, G., "Essais concernant le coefficient de couplage sous L'influence de l'effet de couronne en choc". CIGRE 33-83 (WG01) 19 IWD. Private communication, 1983.

[99] Pigini, A., Thione, L. and Brambilla, R., "Corona phenomena on high voltage electrodes in air". CIGRE 33-77 (TF03.01) 11 IWD. Private communication, 1977.

[100] Peek, F. W., "Dielectric phenomena in high voltage engineering". New York Mc Graw Hill, 1929.

[101] Steinbigler, H., "Anfangsfeldstärken and Ausnutzungsfaktoren rotationssymmetrischer Electrodenanordnungen in Luft". Theses TU Munich, 1969.

[102] Maruvada, P. S., Menemenlis, H. and Malewski, R., "Corona characteristics of conductor bundles under impulse voltages". Trans. IEEE PAS 96 (1977) 102-115.

[103] Gary, C., "Attenuation of surge propagation due to corona". CIGRE 33-81 (WG01) 22 IWD. Private communication, 1981.

[104] Weck, K. H., "Lightning performance of substations". CIGRE SC 33 Conference Rio de Janeiro, 1981.

[105] Gary, C., "Attenuation of propagation of overvoltages resulting from the corona effect". CIGRE report 1990.

[106] Harder, E. L. and Clayton, J. M., "Transmission Line Design and Performance Based on Direct Lightning Strokes", AIEE Transactions. vol. 68, pt. I, 1949, pp.439-49.

[107] AIEE Committee Report, "A Method of Estimating the Lightning Performance of Transmission Lines", AIEE Transactions, vol 69, pt. II, 1950, pp. 1187-96.

[108] Wagner, C. F., "A New Approach to the Calculation of the Lightning Performance of Transmission Lines", AIEE Transactions on Power Apparatus and Systems, vol. 75, Dec. 1956, pp. 1233-56.

[109] Lundholm, R., Finn, R. B. and Price, W. S., "Calculation of Transmission Line Lightning Voltages by Field Comcepts", AIEE Transactions on Power Appartus and Systems, Feb. 1958, pp. 1271-83.

[110] Wagner, C. F. and Hileman, A. R., "A New Approach to the Calculation of the Lightning Performance of Transmission Lines -II", AIEE Transactions on Power Apparatus and Systems, vol. 78, 1959, pp. 996-1020.

[111] Wagner, C. F. and Hileman, A. R., "A New Approach to the Calculation of the Lightning Performance of Transmission Lines III - A Simplified Method - Stroke to Tower", AIEE Transactions on Power Apparatus and Systems, pt. III, vol. 79, 1960, pp. 589-603.

[112] Wagner, C. F. and Hileman, A. R., "Surge Impedance and Its Application to the Lightning Stroke", AIEE Transactions on Power Apparatus and Systems, vol. 80, pt. III, 1961, pp. 1011-20.

[113] Wagner, C. F. and Hileman, A. R., "Effect of Predischarge Currents Upon Line Performance", AIEE Transactions on Power Apparatus and Systems, 1963, pp. 117-128.

[114] Wagner, C. F. and Hileman, A. R., "Predischarge Current Characteristics of Parallel Electrode Gaps", IEEE Transactions on Power Appartus and Systems, vol. 83, 1964, pp. 1236-42.

[115] Fisher, F. A., Anderson, J. G. and Hagenguth, J. H., "Determination of Transmission Line Performance by Geometrical Models", IEEE Transactions on Power Apparatus and Systems, vol. 78, 1960, pp. 1725-36.

[116] Anderson, J. G., "Monte Carlo Computer Calculation of Transmission Line Lightning Performance", IEEE Transactions on Power Apparatus and Systems, Aug 1961, pp.414-20.

[117] Clayton, J. M. and Young, F. S., "Estimating Lightning Performance of Transmission Lines", IEEE Transactions on Power Apparatus and Systems, vol. 83, pt. III, 1964, pp.1103-10.

[118] Anderson, J. G., Fisher, F. A. and Magnusson, E. F., "Calculation of Lightning Performance of EHV Lines", Chapter 8, EHV Transmisson Line Reference Book, Edison Electric Institute, New York, 1968

[119] Sargent, M. A. and Darveniza, M., "The Calculation of Double Circuit Outage Rate of Transmission Lines", IEEE Transactions on Power Apparatus and Systems, 1969 or 1970.

[120] Sargent, M. A. and Darveniza, M., "Lightning Performance of Double-Circuit Transmission Lines", IEEE Transactions on Power Apparatus and Systems, May/June 1970, pp.913-25.

[121] Szpor, S., "Comparison of Polish versus American Lightning Records", IEEE Transactions on Power Apparatus and Systems, May 1969, pp.646-52.

[122] Popolansky, F., "Frequency Distribution of Amplitudes of Lightning Currents", ELECTRA No.22, May 1972, pp.139-47.

[123] Ah Choy, L. and Darvenzia, M., "A Sensitivity Analysis of Lightning Performance Calculations for Transmission Lines", IEEE Transactions on Power Apparatus and Systems, 1971, pp. 1443-51.

[124] Eriksson, A. J. and Weck, K. H., "Simplified Procedures for Determining Substation Impinging Lightning Overvoltages", CIGRE Paper 33-16, 1988.

[125] Dillard, J. K. and Hileman, A. R., "UHV Transmission Tower Insulation Tests", IEEE Transactions, Nov/Dec 1970, pp. 1772-84.

[126] Lusigan, J. T. and Miller, C. J., "What Wood May Add to Primary Insulation for Withstanding Lightning", AIEE Transactions, vol. 74, 1955, pp. 534-40.

[127] Clayton, J. M. and Shankle, D. F., "Insulation Characteristics of Wood and Suspension Insulators", AIEE TRansactions, pt. III, vol. 74, 1955, pp. 1305-12.

[128] Darvenzia, M., "Electrical Properties of Wood and Line Design", University of Queensland Press, St. Lucia, Queensland, Australia, 1980.

[129] Hileman, A. R., "Weather and its Effect on Air Insulation Specifications", IEEE Transactions on Power Apparatus and Systems", Oct 1984, pp. 3104-16.

[130] Bewley, L. V., "Travelling Waves on Transmission Systems", John Wiley & Sons, New York, 1951.

[131] Devgan, S. S. and Whitehead, E. R., "Analytical Models for Distributed Grounding Systems", IEEE Transactions on Power Apparatus and Systems, Sept/Oct 1973, pp. 1763-70.

[132] Koch, R. E., Timoshenko, J. A., Anderson, J. G. and Shih, C. H., "Design of Zinc Oxide Transmission Line Arresters for Application on 138-kV Towers", IEEE Transactions on Power Apparatus and Systems, Oct 1985, pp. 2675-2680.

[133] Shih, C. H., Hayes, R. M., Nichols, D. K., Koch, R. E., Timoshenko, J. A. and Anderson, J. G., "Application of Special Arresters on 138-kV Lines of the Appalachian Power Company", IEEE Transactions on Power Apparatus and Systems, Oct 1985, pp. 2857-2863.

[134] Los, E. J., "Transmission Line Lightning Design with Surge Suppressors at Towers", IEEE Transactions on Power Apparatus and Systems, vol. 99, no. 2, 1980, pp. 720-28.

21 rue d'Artois - F-75008 PARIS

LIST OF SYMBOLS

A_T	Area in square m
A_r	Corona steepness retardation factor. General
A_{r+}	Corona steepness retardation factor. Positive
A_{r-}	Corona steepness retardation factor. Negative
BFR	Backflash rate (flashovers/100 km. Years)
C	Capacitance pu length. General (F/m)
$C_{A,B,C}$	Coupling factors per phases A,B,C
CF	Geometric coupling factor
C_f	Geometric factor, from aspect ratio
C_{dyn}	Dynamic capacitance due to corona, pu length
C_I	Initial corona capacitance, pu length
C_k	Voltage-dependent corona capacitance, pu length
C_o	Geometrical capacitance pu length
C_{tower}	Tower Capacitance to earth
ΣC	Dynamic capacitance pu length
D	Disruptive effect constant
D_c	Exposure distance in electrogeometric analysis
D_d	Horizontal distance between conductors
D_r	Diameter of ground rod
D_s	Striking distance
E	Field strength, general (kV/m)
E_i	Streamer inception field strength
E_g	Soil ionisation field strength
E_o	Minimum leader progression field strength
E_{50}	Peak of the average field strength at 50% discharge
H	Height, general (m)
$H_{A,B,C}$	Height of phases A, B, C
$H_{1,2}$	Height of conductors 1,2
H_i	Height of conductor i
H_T	Tower height
I	Stroke-current amplitude, general (kA)
I_c	Critical current above which flashover occurs
I_I	Initial peak on stroke current waveshape
$I_p = I_F$	Peak stroke current amplitude (ie, final peak)
I_g	Current required to cause soil breakdown gradient
I_R	Current through footing resistance
I_{RA}	Current through footing resistance of adjacent towers
I_m	Limiting current amplitude
I_{TRIG}	Threshhold value for lightning current measurements
I_{10}	10% intercept along the stroke current waveshape
I_{30}	30% intercept along the stroke current waveshape
I_{90}	90% intercept along the stroke current waveshape
I_1, I_2	Constants for concave stroke-front representation
K	Corona charge constant, general
K_+	Corona charge constant, positive
K_-	Corona charge constant, negative
K_g	Geometrical coupling factor (ie = CF)
K_c	Coupling factor in presence of corona
K_{ij}	Geometrical coupling factor between conductors i, j
K_{sp}	Span factor, reduces crest voltage at tower
K_{TT}	Tower-top voltage in pu stroke current
K_{TA}	Voltage at point A pu stroke current
L	Inductance pu length (H/m)
L_T	Tower inductance
L_l	Line length (km)
L_{guy}	Guy wire inductance
M	Median parameter value constant
N_c	Annual cloud-flash density (flashes/km^2 year)

N_g	Annual ground-flash density (flashes/km^2 year)
N_L	Average number of flashes to the line per 100 km. years
P(I)	Probability that the stroke current is >I
Q	Conductor charge pu length (C)
Q_I	Impulse charge in stroke current waveshape
R_a	Attractive radius (m)
R	Footing resistance (Ω)
R_o	Low-current footing resistance (measured)
R_i	Impulse (high current) footing resistance
R_e	Combination of shield-wire surge impedance and R
S	Wave-front steepness, general
S_o	Steepness of an overvoltage at point of origin (kV/μs)
S_{10}	Instantaneous rate-of-rise of current at I_{10}
S_{30}	Instantaneous rate-of-rise of current at I_{30}
S_m = TAN G	Maximum rate-of-rise of current along wavefront
$S_{10/90}$	Average steepness (through I_{10} and I_{90} intercepts)
$S_{30/90}$	Average steepness (through I_{30} and I_{90} intercepts)
SFR	Shielding failure rate per year
SFFOR	Shielding failure flashover rate per year
S_N	Normalising parameter in wavefront representation
S_g, S_{pa}, S_{pb}, S_p	Spacings in Figure 14
T_{10}	Time at which I_{10} intercept is reached on wavefront
T_{30}	Time at which I_{30} intercept is reached on wavefront
T_A	Travel time to point A on tower
T_d	Annual number of thunderstorm days
T_e	Equivalent front to obtain same BFR
T_h	Annual number of thunderstorm hours
T_T	Tower travel time
T_S	Span travel time
T_{ST}	Travel time between stroke point and tower
T_{guy}	Guy-wire travel time
ΔT	Travel time between tower top and phase conductor
ΔT_c	Time delay in overvoltage wavefront due to corona
U	Conductor voltages, general (kV)
U_i	Corona inception voltage
U_p	Operating voltage, phase to earth, general
U_{pf}	Operating voltage, peak value
U_{fo}	Flashover voltage
U_o	Minimum voltage for flashover
U_I	Voltage across the insulator
U_{50}	Standard lightning impulse, critical flashover (positive)
U_{50NS}	Non-standard critical flashover voltage
U_{TA}	Voltage on tower at point A
U_R	Final tower voltage, due only to footing resistance
U_{TT}	Voltage at top of tower
U_F	Voltage across insulator, caused by footing resistance
U_T	Voltage at t = $2T_T$
U_A	Voltage at point A, at T=$2T_T$
ΔU	Tower voltage drop, at crest voltage
V	Travelling wave velocity (with corona)
V_0	Travelling wave velocity, without corona
V_l	Leader velocity
V_1	Voltage component travelling in positive direction
V_2	Voltage component travelling in negative direction
W	Maximum tower width
X	Variable distance along lines
X_N	Normalising parameter in stroke front representation
Y	Surge admittance (Ω^{-1})
Z	Conductor surge impedance, general (Ω)
Z_c	Phase conductor surge impedance
Z_g	Shield wire surge impedance
Z_o	Conductor surge impedance without corona
Z_T	Tower surge impedance
Z_{av}	Average tower surge impedance
Z_{guy}	Guy-wire surge impedance

z_{ii}	Surge impedance of conductor i
z_{ij}	Mutual surge impedance between conductors i, j
α	Shield angle
$\alpha_p = \phi$	"Perfect" shielding angle
α_T, α_R	Reflection coefficient at tower / adjacent towers
β	Constant, or reflection coefficient in backflash analysis
β_N	Normalising parameter in electrogeometric analysis
Γ	Geometric aspect ratio
τ	Tail time constant
π_1	Normalising factor, tower footing resistance
π_2	Normalising factor, footing current
ρ	Soil resistivity
ρ_c	Correlation coefficient
Θ	Tower angle, general
ϵ_o	8.854×10^{-12} F/m
μ_o	$4\pi \times 10^{-7}$ H/m
a,b	Constants
a_{ij}	Distance between conduct i and the image of conductor j.
b_{ij}	Distance between conductors i, j
c_o	Velocity of light
d	Travel distance along line
d_g	gap clearance
f(I)	Probability density function of the stroke current I
f(I/t)	Conditional probability density function of I given t
h	Variable height along a tower
h_1	Height from base to midsection
h_2	Height from midsection to top
h_{av}	Average height of the conductor
h_t	Height of conductor at tower
i	Instantaneous current value
i_l	Leader instantaneous current
i(t)	Current variation with time
k	Leader progression constant
l_e	Earth electrode length
l_i	Insulator length
l_l	Leader length
n	Constant, exponent
pu	Per unit
q	Leader charge pu length
r	Radius general, in electrogeometric analysis
r_c	Radius to conductor, in electrogeometric analysis
r_g	Radius to conductor shield wire in electrogeometric analysis
r_s	Striking distance in electrogeometric analysis
r_t	Tower radius
r_{t1}	Tower-top radius
r_{t2}	Tower midsection radius
r_{t3}	tower-base radius
r_{av}	Average tower radius
r_i	Radius of conductor i
r_{eq}	Electrode equivalent radius for corona inception
r_1, r_2	Radii describing curvature 1, 2 of electrode
s	Variable distance, along line of highest field strength
s_{ng}	Standard deviation in N observations
t	Time variable
t_1, t_2	Constants in stroke front representation
t_c	Time to breakdown
t_d	Front duration measured between 2kA and the first current peak
t_{d10}	Equivalent stroke front time, based on I_{10} intercept
t_{d30}	Equivalent stroke front time, based on I_{30} intercept
t_f	Derived stroke front time, using $S_{30/90}$
t_m	Minimum equivalent front time (I_F/S_m)

t_h	Wavetail, time to half value		
t_l	Leader gap crossing time	$u(t)$	Gap voltage, instantaneous value
t_s	Streamer gap crossing time	$U_R(t)$	Voltage across footing resistance
t_i	Corona inception time	x, y, z	General variables
t_o	Time at which voltage reaches required minimum value		

Le CIGRÉ a apporté le plus grand soin à la réalisation de cette brochure thématique numérique afin de vous fournir une information complète et fiable.

Cependant, le CIGRÉ ne pourra en aucun cas être tenu responsable des préjudices ou dommages de quelque nature que ce soit pouvant résulter d'une mauvaise utilisation des informations contenues dans cette brochure.

Publié par le CIGRÉ
21, rue d'Artois
FR-75 008 PARIS
Tél. : +33 1 53 89 12 90
Fax : +33 1 53 89 12 99

The greatest care has been taken by CIGRE to produce this digital technical brochure so as to provide you with full and reliable information.

However, CIGRE could in any case be held responsible for any damage resulting from any misuse of the information contained therein.

Published by CIGRE
21, rue d'Artois
FR-75 008 PARIS
Tel : +33 1 53 89 12 90
Fax : +33 1 53 89 12 99